Investigating the role of viroplasm formation and calcium levels on the production of prostaglandin E_2 during rotavirus infection

By

Willem Jacobus Sander

Submitted in fulfilment of the requirements in respect of the degree
Doctor of Philosophy majoring in Microbiology

Department of Microbiology and Biochemistry
Faculty of Natural and Agriculture Sciences
University of the Free State
November 2022

Promoter: Prof. H.G. O'Neill
Co-promoter: Prof. C.H. Pohl-Albertyn

DECLARTION

I, **Willem Jacobus Sander**, declare that the PhD Degree research thesis or publishable, interrelated articles, or coursework PhD Degree mini-thesis that I herewith submit for the PhD Degree qualification at the University of the Free State is my independent work, and that I have not previously submitted it for a qualification at another institution of higher education.

I, **Willem Jacobus Sander**, hereby declare that I am aware that the copyright is vested in the University of the Free State.

I, **Willem Jacobus Sander**, hereby declare that all royalties as regards intellectual property that was developed during the course of and/or in connection with the study at the University of the Free State will accrue to the University.

I, **Willem Jacobus Sander**, hereby declare that I am aware that the research may only be published with the Dean's approval.

Signature

29/11/2002

Date

ACKNOWLEDGEMENTS

I would hereby like to express gratitude toward the following people and institutions whom without this PhD Degree research thesis would not have been possible:

My Promoter – **Prof. H.G. O'Neill**
For providing me with the opportunity to take on this very ambitious challenge. I appreciate your invaluable and skilful guidance, encouragements, and many useful discussions. I will forever be grateful for every lesson, opportunity and word of advice gifted to me by my supervisor.

My Co-promoter – **Prof C.H. Pohl-Albertyn**
For her assistance and guidance throughout this study. Her patience and words of encouragement will always be appreciated.

Units and Labs
For providing equipment and knowledge outside of my expertise. Thank you to the Next Generation Sequencing Unit, under guidance from Prof Martin Nyaga, The Microscope Unit of the University of the Free State, Prof Muriel Mering, Dr Gabré Kemp for MS analysis.

My Family
For all the support and love, your part in completing this degree does not go unnoticed. A special thank you to **Essie Gertenbach**, **Stefan Sander,** and **Lynette Sander**, I am truly blessed to have you in my life.

My Friends
To those of you who kept me motivated from outside of science. A special thank you to, Nandie Bartman, DM de Kock, Zander Raath and Calvin Watkins. Current and past colleagues from the Department of Microbiology and Biochemistry Amy Strydom, Soveij van der Schyff, Corinne Fourie, Sérgio Mendes dos Ramos, Mercy Ogunyinka, Ayanda Thusi, Nkhasi Lekena and Nikita Barron for keeping my sane.

Department of Microbiology and Biochemistry
For giving me the opportunity to broaden my mind and grow as a scientist and individual.

Research and Financial Support
Thank you to the Poliomyelitis Research Foundation (PRF) [19/82], National Research Foundation (NRF) [MND210608609361] and the Deutsche Forschungsgemeinschaft (DFG) for their financial support; this work would not have been possible without their contributions.

The University of the Free State
A very special thank you to the University of the Free State (UFS) for being the place where I could complete almost 12 years of tertiary education.

RESEACRH OUTPUTS

Conferences:

Sander, W.J., Pohl-Albertyn, C.H., O'Neill, H.G. Expression of rotavirus viroplasm-like proteins, NSP2 and NSP5, in HEK293 cells and subsequent effect on PGE_2 production. *International dsRNA symposium - 14th Conference*, Banff, 10-14 October 2022. (poster)

Sander, W.J., Pohl-Albertyn, C.H., O'Neill, H.G. Reduction in the rate of rotavirus replication by inhibition of prostaglandin E_2 biosynthetic enzymes. *ASV2021 – 40th Annual Conference*, Virtual Conference, 19-23 July 2021. (Poster)

Sander, W.J., Pohl-Albertyn, C.H., O'Neill, H.G. Rotavirus increases intracellular prostaglandin E_2 concentration during infection of MA104 cells. *SASM2020 - 21st Biennial Conference*, Virtual, 4-6 May 2021. (Oral)

Sander, W.J., Pohl-Albertyn, C.H., O'Neill, H.G. Reduction in the rate of rotavirus replication by cyclooxygenase inhibition. *Virology Africa 2020*, Cape Town, 10-14 February 2020. (Oral)

Sander, W.J., Pohl-Albertyn, C.H., O'Neill, H.G. Rotavirus infection increases PGE_2 production, leading to increased rotavirus yield and rate of replication. *African Rotavirus Symposium - 12th Conference*, Johannesburg, 30 July-01 August September 2019. (poster)

Publications:

Sander WJ, Kemp G, Hugo A, Pohl CH, O'Neill HG. Corrigendum: Rotavirus-Mediated Prostaglandin E_2 Production in MA104 Cells Promote Virus Attachment and Internalisation, Resulting in an Increased Viral Load. Front Physiol. 2022 Apr 19; 13:901082. doi: 10.3389/fphys.2022.901082. Erratum for: Front Physiol. 2022 Jan 28; 13:805565.

Sander WJ, Fourie C, Sabiu S, O'Neill FH, Pohl CH, O'Neill HG. Reactive oxygen species as potential antiviral targets. Rev Med Virol. 2022 Jan;32(1):e2240. doi: 10.1002/rmv.2240.

SUMMARY

Both *in vitro* and *in vivo* studies have shown that levels of prostaglandin E_2 (PGE_2), an immunomodulatory eicosanoid, are increased during rotavirus (RV) infection. Although it has been shown that inhibition of cyclooxygenase (COX) (PGE_2 biosynthetic enzymes) has adverse effects on viral yield, the mechanism of PGE_2 induction during replication remains unknown. Viroplasms are viral factories that consist of several viral proteins, in particular NSP2 and NSP5, and cellular lipid droplets. Lipid droplets (LDs), with their high content of neutral lipids and the proximity of PGE_2 biosynthetic enzymes, are well known sites for PGE_2 biosynthesis. In addition, during replication, RV has been shown to increase the total lipid content of infected cells, while modulating specific lipid classes during infection. Inhibitors that prevent the formations of LDs severely limit the amount of viroplasms formed and subsequently decrease viral progeny production. Another viral protein critical for viral replication is the enterotoxin, NSP4. NSP4, contains a viroporin domain that selectively conducts calcium (Ca^{2+}) from the endoplasmic reticulum to the cytosol, increasing free intracellular Ca^{2+}. Intracellular Ca^{2+} levels are crucial for the activation and function of cytoplasmic phospholipase A_2, the rate-limiting enzyme in PGE_2 biosynthesis. Both LDs and phospholipase A_2 are also essential for PGE_2 biosynthesis. Therefore, the main objective of the study was to determine when and by which mechanism(s) RV induces/amplifies the production of prostaglandin E_2.

During early infection, RV attaches to several cellular receptors and enters the cells by either clathrin-dependent or -independent endocytosis. Other viruses such as bovine ephemeral fever virus haven been shown to require the activation COX-2-mediated PGE_2/EP receptor signalling for enhanced clathrin-mediated endocytosis. To determine if PGE_2 exerts its proviral effects during internalisation we supplemented MA104 cells with γ-linolenic acid (GLA), a precursor of arachidonic acid. Infection of supplemented cells with RV SA11 led to increased production of PGE_2 as monitored by ELISA. Confocal microscopy demonstrated that PGE_2 co-localises with the viroplasm-forming proteins, NSP5 and NSP2. Due to the known association of viroplasms as well as PGE_2 with lipid droplets, our results indicate a possible role for viroplasms in the production of RV-induced PGE_2. Replication kinetics showed that inhibitors, targeting the biosynthesis of PGE_2, had negative effects on RV yield, especially during the early stages of infection. Using flow cytometry and PGE_2

addback experiments, we show that PGE_2 enhances the attachment and internalisation of rotavirus in MA104 cells, indicating a possible role for PGE_2 during clathrin-mediated RV entry.

Due to the well-known association between viroplasms and LDs, and the fact that LDs are production centres for the PGE_2, we next explored the possible role if any, of viroplasm components in the induction of PGE_2 production during RV infection. Transfection of HEK293 cells with plasmids, encoding the ORFs for NSP2 and NSP5 or both NSP2 and NSP5, showed that neither protein on their own, nor the formation of viroplasm-like structures was able to induce PGE_2 production. A MA104 cell line, stably expressing NSP5, was used to generate and characterize several SA11-based rescued rotaviruses (rSA11_aNSP5 and rSA11_aNSP5) with mutations in the α-helix within the C-terminal of NSP5. We demonstrate that a rSA11 with replaced hydrophobic amino acids in the C-terminal appeared to from less viroplasms compared to rSA11. This led to reduced replication of both rSA11_aNSP5 and rSA11_pNSP5, confirming the pivotal role of the α-helix within the C-terminal during RV replication. These mutations also affected the production of PGE_2 in HEK293 infected cells, although this is more likely due to decreased viral replication. Furthermore, we investigated how the introduced mutations affect NSP5 co-sedimentation with LD-associated protein, perilipin 2, and showed that the NSP5 mutations decreasing the hydrophobicity or abolishment of the α-helix changed the sedimentation profile. Our results indicate that individual viroplasm components or the formation of VLS do not induce PGE_2 in transfected cells, but that mutations in the C-terminal of NSP5 decrease PGE_2, most probably due to decreased replication.

After showing that viroplasms mainly indirectly induce the production of PGE_2, we switched our focus to the role of Calcium (Ca^{2+}) as it is essential for several cellular signalling and physiological processes, including the activation of cytoplasmic phospholipase A_2 ($cPLA_2$). This enzyme plays a role in lipid droplet (LD) biogenesis and is the rate-limiting enzyme in prostaglandin E_2 (PGE_2) biosynthesis. During rotavirus (RV) replication, NSP4 modulates the levels of cytoplasmic Ca^{2+} (cyto[Ca^{2+}]) by a viroporin domain, which selectively conducts Ca^{2+} from endoplasmic reticulum (ER) stores to the cytoplasm. This modulation of cyto[Ca^{2+}] is crucial for several viral process, including entry and assembly. We, therefore, investigated the role of the viroporin domain of NSP4 in the induction of PGE_2 production during RV infection. We

show that RV infection of HEK293 cells increases the activity of $cPLA_{2,}$ and that the chelation of cyto[Ca^{2+}] decreases the activity of $cPLA_2$, leading to decreases in viral progeny and RNA yield. Mutations within the viroporin domain, which decreases the conductively of Ca^{2+}, decreased the activity of $cPLA_2$ and subsequently affected PGE_2 levels as well as viral progeny and RNA yield. Our results indicate that the viroporin domain of NSP4 plays a role in the induction of PGE_2 production by increasing the activity of $cPLA_2$ in a Ca^{2+}-dependent manner.

Taken together, the data shows that PGE_2 is most likely induced in a NSP4-cyto[Ca^{2+}]-$cPLA_2$-dependent manner enhancing RV internalisation. This enhanced internalisation increases viral yield, which could contribute indirectly to PGE_2 production by increasing the numbers of LDs and thus sites of PGE_2 production.

Keywords: Rotavirus, internalisation, viroplasms, prostaglandin E_2, cytoplasmic calcium, cytoplasmic phospholipase A_2, NSP4, NSP5.

Table of Contents

LIST OF TABLES

LIST OF FIGURES

1.1. Introduction

Rotavirus (RV) is a segmented dsRNA virus that forms part of the *Sedoreoviridae* family (Matthijnssens et al., 2022)(Matthijnssens et al., 2022). These viruses have been discovered in mammals such as humans, rodents, livestock, and bats as well as in avian species and are grouped into 11 groups (A-D, F-L), based on their amino acid sequence and antigenic differences in the immunogenic middle layer capsid protein, VP6 (International Committee on Taxonomy of Viruses, 2021; Johne et al., 2022)International Committee on Taxonomy of Viruses, 2021; Johne et al., 2022). The eleven genome segments of RV encode for 6 structural proteins (VP) and 6 non-structural and within RV group A [see also p2, beginning of section 1.2.1], different strains are classified by their glycoprotein VP7 (G serotypes) and the protease-sensitive protein VP4 (P serotypes). Rotavirus is a leading cause of severe dehydrating diarrhoea in infants and children under the age of five (Estes and Greenberg, 2013)(Estes and Greenberg, 2013). According to Troeger and co-workers (2018)Troeger and co-workers (2018), RV caused approximately 128 500 deaths globally in 2016 of which 104 733 deaths occurred in sub-Saharan Africa. Although RV vaccines have been licenced since 2006, studies have shown that their efficacy in middle- and low-income countries are considerably lower when compared to high-income countries (Burnett et al., 2020; Henschke et al., 2022)(Burnett et al., 2020; Henschke et al., 2022). The reason for the difference in efficacy are not currently well-known (Desselberger, 2017)(Desselberger, 2017), but Velasquez and co-workers (2018) suggested that co-administration with live oral polio vaccine, nutritional status, microbiome composition, and maternal antibodies may be possible factors in the performance gradient and offer potential strategies to improve modest vaccine performance. In addition to the introduction of new RV vaccines (Burke et al., 2019), the development of an effective anti-viral treatment, as there is currently none (Kang, 2013), could decrease the amount of RV deaths in sub-Saharan Africa.

To aid in the development of ant-viral treatments against RV, a better understanding of RV replication is required. During replication, non-structural proteins (NSP) play essential roles in genome replication and antagonism of the innate immune response (Hu et al., 2012). NSP5 is essential for the formation of “viral factories”, termed

viroplasms (Papa et al., 2021), with several studies showing that the absence of NSP5 or modifications to the protein have negative effects on viroplasm formation and subsequent viral replication (Eichwald et al., 2004; Sen et al., 2007; Papa et al., 2020). In addition to interacting with several other viral proteins, most notably NSP2 (Eichwald et al., 2004), interaction of viroplasms with LDs is also crucial for optimal viroplasm formation and function (Crawford and Desselberger, 2016). Several studies showed that inhibition of LD formation or degradation of LDs has deleterious effects on viroplasm formation and subsequent negative effects on rotavirus replication (Gaunt et al., 2013a, 2013b). NSP4 is the first identified viral enterotoxin and selectively allows Ca^{2+} to pass from the endoplasmic reticulum (ER) into the cytosol via its viroporin domain, providing an optimal environment or rotavirus replication (Hyser et al., 2010; Pham et al., 2017).

It is important to note that both the LDs and Ca^{2+} play roles in the biosynthesis of PGE_2, an eicosanoid with well-known immunomodulatory properties (Funk, 2001). Lipid droplets are well known sites of PGE_2 production (Jarc and Petan, 2020), while intracellular Ca^{2+} is crucial for the activation of phospholipase A_2, the rate-limiting enzyme in PGE_2 biosynthesis (Bingham and Austen, 1999). Although it is known that RV is capable of increasing PGE_2 levels both *in vivo* (Yamashiro et al., 1989; Zijlstra et al., 1999) and *in vitro* (Rossen et al., 2004), the stage of replication during which these increases occur and subsequent effect on viral replication remain unknown. The aim of this work is to discuss the possible sites of PGE_2 production during replication and possible roles of viroplasm interaction with LDs and the activation of phospholipase A_2 via NSP4 induced Ca^{2+} in increased PGE_2 levels during viral replication.

1.2. Rotavirus

1.2.1. Structure and genome coding assignments

The genome segments of SA11 encode 6 structural proteins (VP) and 6 non-structural proteins and range in size from 667 to 3302 bp in length (Mlera et al., 2013). The genome-protein and protein-function assignments have been determined for several RVA strains and are summarized in **Table 1. 1**.The fully infectious RV virion (**Figure 1. 1)** is a triple-layered particle (TLP), consisting of a VP2 core shell, a middle VP6 layer and an outer layer of VP7, in which VP4 spike proteins are embedded (Settembre et al., 2011; Long and McDonald, 2017). VP4 can be cleaved into two subunits, VP5*

and VP8*, which is essential for the infectivity of rotavirus (López et al., 1985). The core shell also contains VP1-VP3 heterodimers that are tethered to VP2, along with the 11 dsRNA segments (Prasad et al., 1996). The genomic RNA segments supposedly form conical cylinders around the VP1-VP3 heterodimers, but details of the dsRNA structure remain scarce. However, data obtained with cypovirus showed the non-spooled arrangement of dsRNA in another genus of the *Reoviridae* (Liu and Cheng, 2015). The core shell, surrounded by VP6, forms the double-layered particle (DLP), with the encapsidation by VP4 and VP7 leading to the formation of TLPs (Li et al., 2009; Settembre et al., 2011).

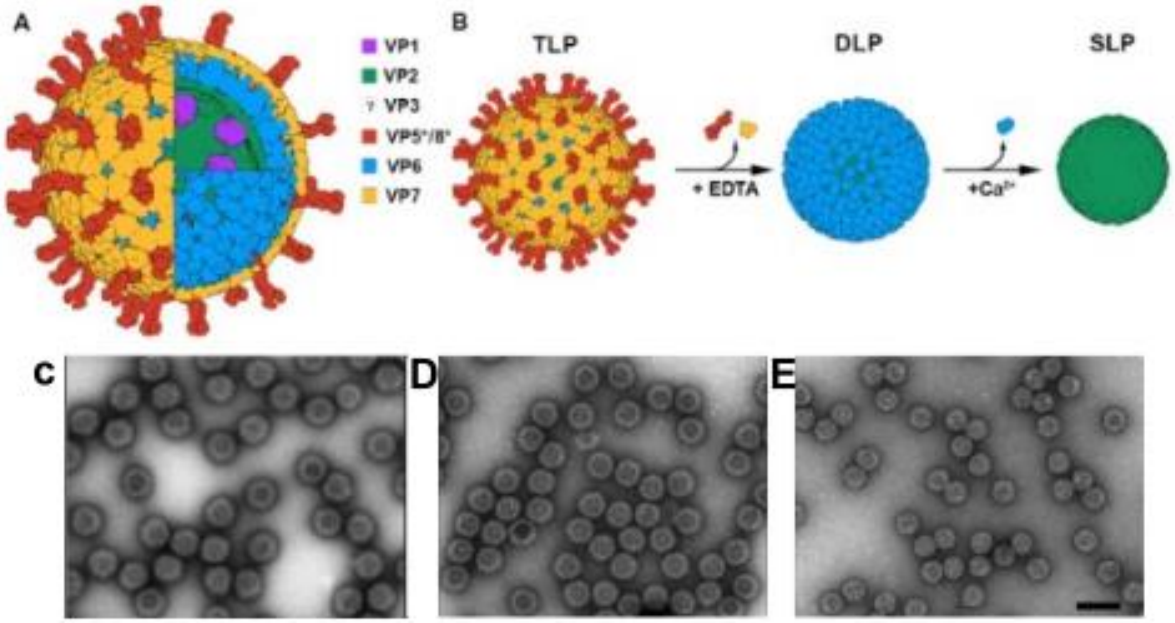

Figure 1. 1. Structure of the triple-layered rotavirus virion. A) Diagram of the fully infectious RV. (B) The formation of TLP from DLP and single-layered particle (SLP). Negative staining electron microscopy of TLP (C), DLP (D) and SLP (E). The bar represents 100 nm. Triple-layered particle (TLP), double-layered particle (DLP), single-layered particle (SLP). Modified with permission from Jiménez-Zaragoza et al., 2018.

Table 1. 1. The protein localisation, genome-protein, and protein-function assignments of rotavirus. Sizes are indicative of SA11. Modified form Mlera and co-workers (2013).

Genome segment	Size (bp)	Encoded Protein	Size (kDa)	Location	Functions	References
1	3302	VP1	125	Inner capsid	RNA-dependent RNA polymerase; ssRNA binding; transcription complex	Burns et al., 1996; Patton, 1996, 2001; Prasad et al., 1996; Zeng et al., 1996; Patton et al., 1997
2	2683	VP2	102	Inner capsid	Core shell; dsRNA binding; required for RNA-dependent RNA polymerase activity, viroplasm formation	Berois et al., 2003; Bican et al., 1982; Boyle and Holmes, 1986; Clark and Desselberger, 1988; Mitchell and Both, 1990a; Patton et al., 1997; Zeng et al., 1994
3	2591	VP3	98	Inner capsid	Guanyltransferase; methyltransferase; 2',5'-phoshodieasterase; ssRNA binding; part of transcription complex, Mitochondrial antiviral signaling protein antagonist	Liu and Estes, 1989; Pizarro et al., 1991; Liu et al., 1992; Burns et al., 1996; Prasad et al., 1996; Chen et al., 1999; Patton, 2001; Ding et al., 2018; Kumar et al., 2020
4	2362	VP4*	87	Outer capsid	Attachment protein;P type neutralization antigen; virulence factor; fusion with cell membrane	Ericson et al., 1983; Kalica et al., 1983; Hoshino et al., 1985; López et al., 1985; Offit and Blavat, 1986; Anthony et al., 1991; Fiore et al., 1991; Ruggeri and Greenberg, 1991; Shaw et al., 1993; Hoshino and Kapikian, 1996; Ludert et al., 1996; Denisova et al., 1999; Zarate et al., 2000; Dormitzer et al., 2002
5	1614	NSP1	59	Non-structural	Interferon antagonist; putative E3 ligase; dsRNA binding	Dunn et al., 1994; Graff et al., 2002; Hua et al., 1994; Kojima et al., 1996; Mitchell and Both, 1990b; Patton, 1995, 2001
6	1356	VP6	48	Middle capsid	Species determinant; intracellular neutralization;	Burns et al., 1996; Clark and Desselberger, 1988; Greenberg et al., 1983; Kalica et al., 1981; Mansell et al., 1994; Mason et al., 1980; Prasad et al., 1988; Smith et al., 1989; Tompkins et al., 1975; Yang et al., 2001
7	1105	NSP3	34	Non-structural	Binds to 3' terminus of viral ss(+)RNA; cellular eukaryotic translation initiation factor 4 G ; heat shock protein 90, displaces Poly(A)-binding protein ; inhibits host cell translation	Chizhikov and Patton, 2000; Deo et al., 2002; Groft and Burley, 2002; Mattion et al., 1992; Piron, 1998; Poncet et al., 1994; Vende et al., 2000
8	1059	NSP2	37	Non-structural	Binds ssRNA; NTPase; NDP kinase; essential for viroplasm formation	Afrikanova et al., 1998; Fabbretti et al., 1999; Jayaram et al., 2002; Kattoura et al., 1992, 1994; Patton, 2001; Petrie et al., 1984; Taraporewala et al., 1999, 2002; Taraporewala and Patton, 2001
9	1063	VP7	37	Outer capsid	G type neutralization antigen Membrane penetration	Dormitzer and Greenberg, 1992; Ericson et al., 1982, 1983; Hoshino et al., 1985; Hoshino and Kapikian, 1996; Mason et al., 1980; Michelangeli et al., 1997
10	751	NSP4	20	Non-structural	Interaction with viroplasms and autophagy pathway; modulates intracellular Ca^{2+} and RNA replication; enterotoxin; virulence factor	Au et al., 1989; Ball et al., 1996; Ericson et al., 1982, 1983; Estes et al., 2001; Jagannath et al., 2000; Meyer et al., 1989; Tian et al., 1994
11	667	NSP5	22	Non-structural	dsRNA binding; phosphoprotein; essential for viroplasm formation	Afrikanova et al., 1996, 1998; Blackhall et al., 1998; González et al., 1998; González and Burrone, 1991; Mattion et al., 1991; Patton, 2001; Poncet et al., 1997
		NSP6	11	Non-structural	Interaction with NSP5 and mitochondria; Not present in all strains	Mattion et al., 1991; González et al., 1998; Rainsford and McCrae, 2007; Holloway et al., 2015

* Cleaved by trypsin or cellular protease into VP5* and VP8Dr

1.2.2. Viral replication

The RV virions first attach to several different receptors on the surface of susceptible host cells depending on strain (Arias and López, 2021) (**Figure 1.2 and Figure 1.3**). The RV particles are then internalized by receptor-mediated endocytosis, followed by removal of the outer layer in the endosome, resulting in the release of DLPs into the cytoplasm. Release of the DLP into the cytosol triggers triggers transcription and translation of the RV genome (Abdelhakim et al., 2014).The transcriptionally active DLPs produce the 11 (+) ssRNAs, which either act as mRNAs from which viral proteins are translated or become templates for the dsRNA replication of progeny virus (Lawton et al., 1997). Several viral proteins and viral RNAs from cytoplasmic inclusion bodies called viroplasms which then interact with cellular LDs…. [See Cheung and co-workers (2010), **Figure 1.4**, where it is shown that viroplasms form earlier than their complexes with LDs.] (Papa et al., 2021). Progeny DLPs, formed in viroplasms, bud through the ER in a process that involves NSP4 as an intracellular receptor for VP6 (Silvestri et al., 2005). The nascent DLPs acquire a transient envelope, consisting of ER membrane and NSP4, which is quickly replaced with an outer layer consisting of VP7 and VP4, with VP4 being attached first (Trask and Dormitzer, 2006). The origin, function, and loss of the transitory envelope remain unknown. After formation of TLPs, RV is released from non-polarised cells by lysis, but from epithelial cells in a budding process that does not cause instant cellular death (Arias et al., 2015). Due to the importance of attachment and entry and the formation of viroplasms during RV replication and relevance to this study, these will now be discussed in greater detail.

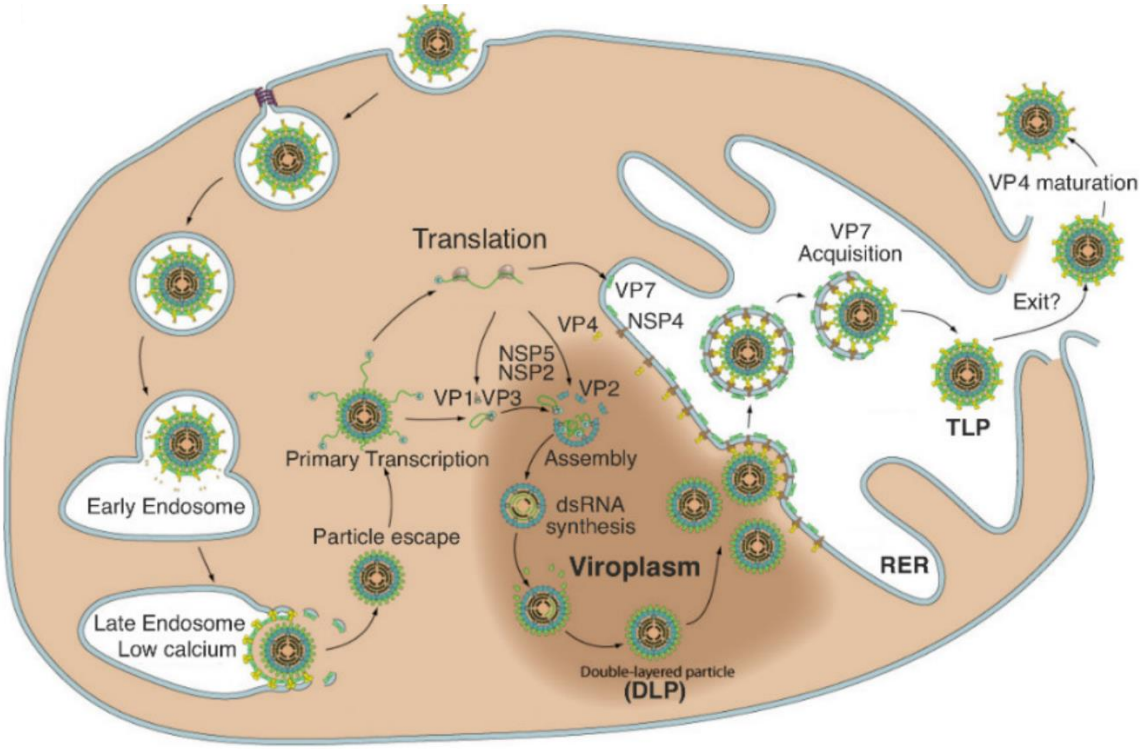

Figure 1.2. Overview of the rotavirus replication cycle. The virion loses the outer layer after entry. The DLP becomes transcriptionally active and produces capped viral mRNAs which do not have polyA tails. Viroplasms form when viral proteins and RNAs accumulate in protected sites of the cytoplasm in which particle assembly occurs. After the formation of SLP, the particle obtains its intermediate layer and becomes a DLP. Double-layered particles bud into the endoplasmic reticulum, which lead to the formation of TLPs. With permission from Arnold et al., 2013.

1.2.2.1. Viral entry

Viral entry is a complex process that involves cellular glycans for binding and several co-receptors for post attachment steps (Arias and López, 2021) (**Figure 1.3**). Initial interactions are mediated by the VP8* domain of VP4, while the VP5* domain and VP7 interact mainly with downstream co-receptors (Dormitzer et al., 2002; Venkataram Prasad et al., 2014; Ramani et al., 2016) (**Figure 1.3A**). Several glycans have been identified as receptors for RV, including terminal and sub-terminal sialic acid and histo-blood groups antigens (Hu et al., 2012a; Barbé et al., 2018). Initial binding to the cells by RV leads to subsequent interactions with integrins, α2β1, αVβ3, and αXβ2, and with the heat shock cognate protein in a strain-independent manner (Coulson et al., 1997; Arias et al., 2015) (**Figure 1.3B**). In addition, tight-junction proteins, JAM-A, occludin, and ZO-1, are also important for viral entry of some RV strains, while gangliosides play a role during virus entry at a post attachment step (Martínez et al., 2013; Torres-Flores et al., 2014). After attachment, RVs enter the cell by either clathrin-mediated endocytosis or clathrin-independent endocytosis (Gutiérrez et al.,

2010) (**Figure 1.3C**). Regardless of the endocytic pathway, all RV strains reach early endosomes, where the virus probably begins internalisation (Arias and López, 2021) (**Figure 1.3D**). The progression of early endosomes to maturing endosomes is accompanied by a progressive decrease in pH and intra-endosomal Ca^{2+} concentration through the function of the v-ATPase, leading to the formation of intraluminal vesicles (Soliman et al., 2018). Rotavirus strains RRV and SA11 subsequently reach the cytoplasm from maturing endosomes (Martínez et al., 2013) (**Figure 1.3E**). Other strains of RV reach the cytoplasm only after the formation of late endosomes in processes involving GTPase Rab7 and Rab9, cathepsins and CD-M6PR (**Figure 1.3F**)**.**

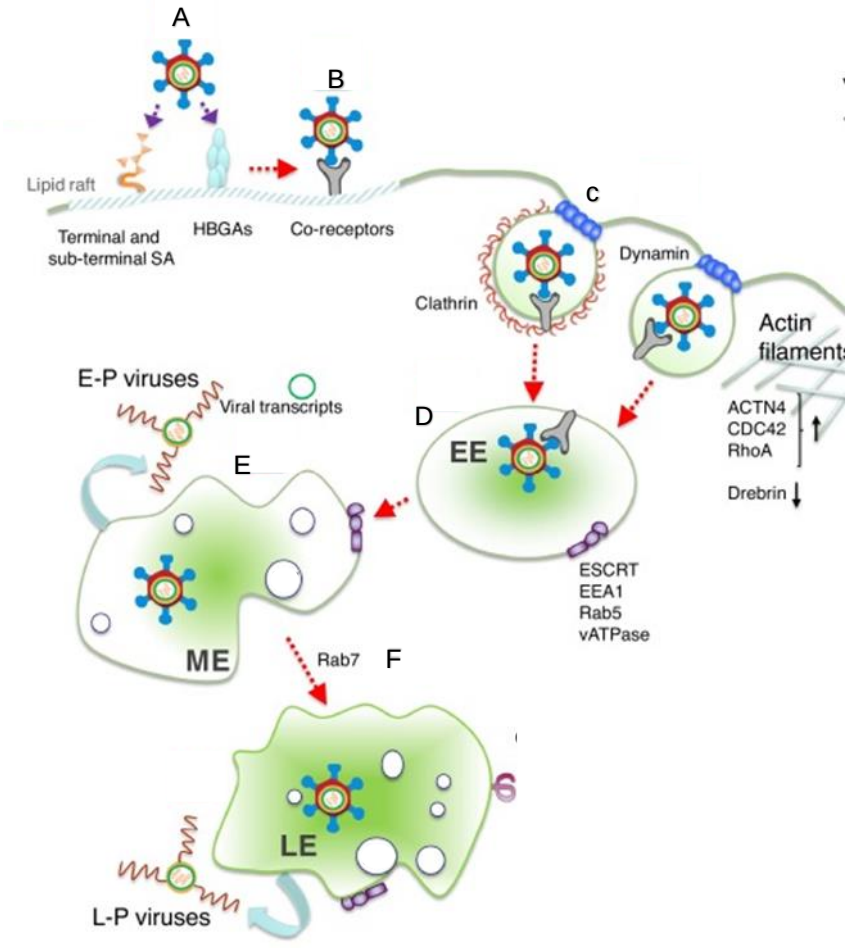

Figure 1.3. Classical endocytic pathway. A) The interaction of RV VP8* with cellular glycans initiates cell-entry. Cells have several receptors for viral attachment including terminal or subterminal SAs, as well as HBGAs. B) During post-binding RV is capable of interacting integrins α2β1, αVβ3, and αXβ2, and with hsc70 that are embedded in lipid rafts; JAM-A and occludin have also been involved at this step; a novel, human-specific post-attachment cell molecule has also been proposed. C) Several RV strains are internalized by clathrin-dependent endocytosis, in a dynamin-dependent and cholesterol-dependent process. RRV strain enters cells by an endocytic pathway that is clathrin-independent and caveolin-independent, and depends on RhoA, Cdc42, and actinin-4 (ACTN4), but is independent of

endosomal acidification. D) After internalization, all RV strains reach early endosomes (EEs), and depend on a functional ESCRT system, including the ESCRT-associated ATPase VPS4A involved in fission of intralumenal vesicles in maturating endosomes (MEs). E) Once in the MEs, different RV strains follow different routes to reach the cytosol. Early penetrating (E-P) viruses exit from ME vesicles, since their infectivity is not dependent on the GTPase Rab7. . F) Other strains depend on the expression of Rab7 and thus these viruses continue a deeper journey to reach late endosomes (LEs) that provide the environment for these—Late-penetrating (L-P) strains—to enter the cytosol. Modified with permission from Arias and López, 2021.

1.2.2.2. Viroplasm formation

Viroplasms are cytoplasmic inclusion bodies that can be detected as early as 2 h post-infection and allow for the viral RNA packaging and assembly of DLPs (Papa et al., 2021). At least seven viral proteins (NSP2/5/6 and VP1/2/3/6) have been detected in viroplasms. However, NSP2 and NSP5 are critical for the formation of viroplasms (Fabbretti et al., 1999; Vascotto et al., 2004; Cheung et al., 2010; Papa et al., 2020). Suárez and co-workers (2019) showed that VPs are found around LDs in a circular shape (**Figure 1.4A**) and by using super-resolution microscopy, were able to show that these VPs layer differently with respect to NSP2 (**Figure 1.4B-E**), while Geiger and co-workers (2021) showed that viroplasms represent protein-RNA condensates that are formed by liquid–liquid phase separation of NSP5 and NSP2 (**Figure 1.5**). Furthermore, the co-expression of NSP2 with NSP5 in cell culture is sufficient for the formation of viroplasm-like structures (VLS), In the absence of other viral proteins and mRNA (Fabbretti et al., 1999).

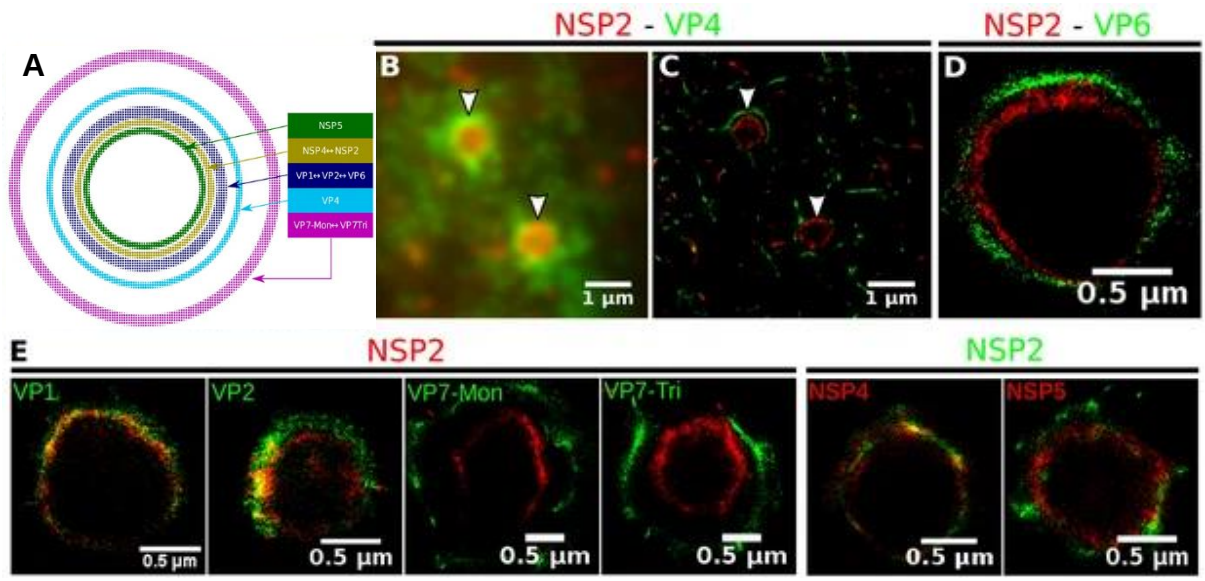

Figure 1.4. Structure of viroplasms. A) The radii of the different viral protein layers. (B) Diffraction-limited image of VPs (white arrows). (C) 3B-SRM image reconstructed from B. (D–E) 3B-SRM images of individual VPs labelled with different antibodies. Modified with permission from Suárez et al., 2019.

NSP2 forms 300 kDa octamers with many functions, including RNA-helix destabilisation, nucleoside diphosphate kinase activity, and RNA chaperone activity, while NSP5, a 22 kDa serine/threonine rich protein, is proposed to assemble into higher-order species that can become hyperphosphorylated and has ATPase activity (Papa et al., 2021). The silencing of NSP2 or NSP5 expression by RNA interference, intrabodies or in rotavirus mutants, prevent the formation of viroplasms and subsequent virion production (Fabbretti et al., 1999; Vascotto et al., 2004; Papa et al., 2020). Furthermore, deletions or mutations in the C-terminal and silencing of phosphorylation of NSP5 have adverse effects on viroplasm formation as well as VLS formation (Sen et al., 2007). In concurrence, by using the RV reverse genetic system, Papa and co-workers (2020) showed that recombinant RV [deleted C-terminal end (180 – 198)], incapable of producing NSP5, could only replicate in MA104 cells expressing the wildtype NSP5 gene in *trans*. It should also be mentioned that, in addition to NSP2, the co-expression of NSP5 and VP2 can also result in the formation of VLS, through a mechanism that remains yet to be elucidated (Contin et al., 2010; Eichwald et al., 2012; Buttafuoco et al., 2020)

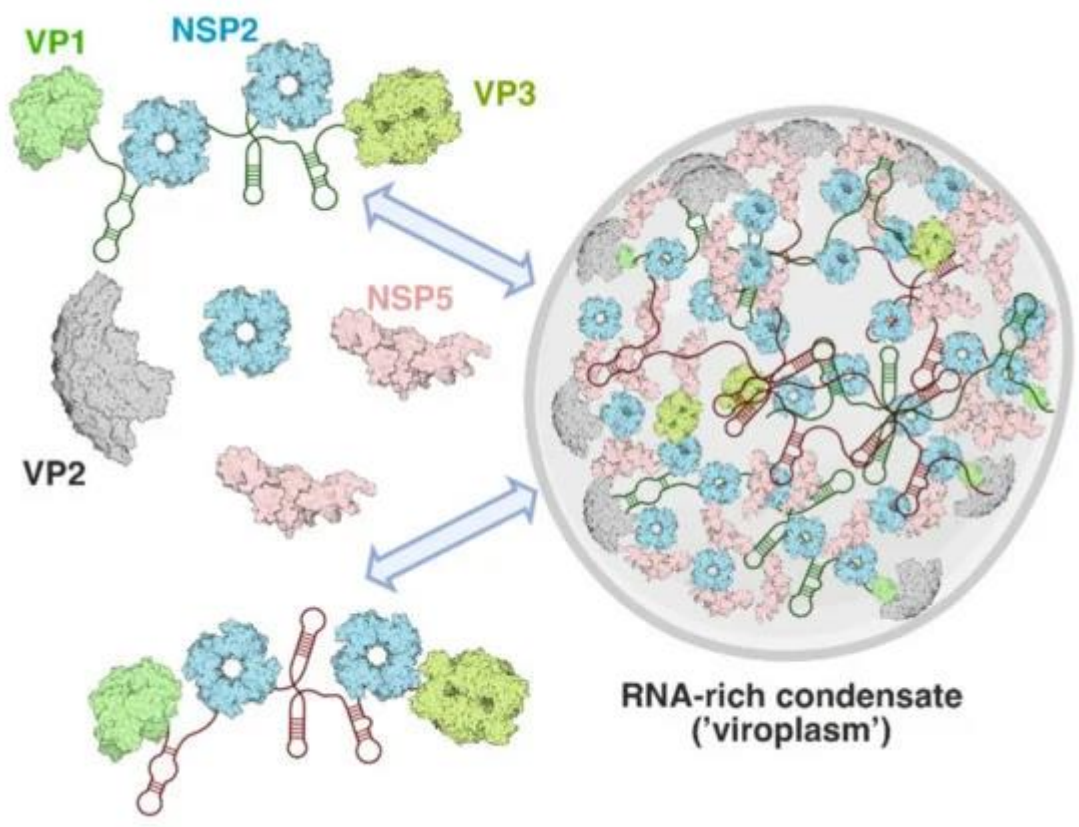

Figure 1.5. Assembly of viroplasms during rotavirus infection. NSP5 (pink) and NSP2 (cyan doughnut-shaped octamers) form protein droplets known as 'viroplasm-like structures'. Viral transcripts

are found to a high degree in these condensates and are likely recruited through protein–RNA interactions between NSP2, or VP1 and NSP5. VP1 recognizes 3′ terminal sequences of all eleven distinct (+) ssRNA transcripts, thus allowing them to enter the dense NSP5/NSP2 phase of a viroplasm. Ribonucleoprotein complexes that form due other multivalent RNA-binding proteins, such as VP3, can be absorbed into the NSP2/NSP5 condensates. The unique molecular environment is conducive to the multi-RNA genome assembly and packaging steps. With permission from Geiger et al., 2021

In addition to the requirement of NSP2 and NSP5 for viroplasm formation, viroplasms require associations with cellular LDs (Crawford and Desselberger, 2016). The first data to show an interaction between viroplasms and LDs were from studies demonstrating association between viroplasm associated proteins and LD-associated proteins, perilipin (PLIN) 1 and 2 (ADRP) (Cheung et al., 2010) (**Figure 1.6**).

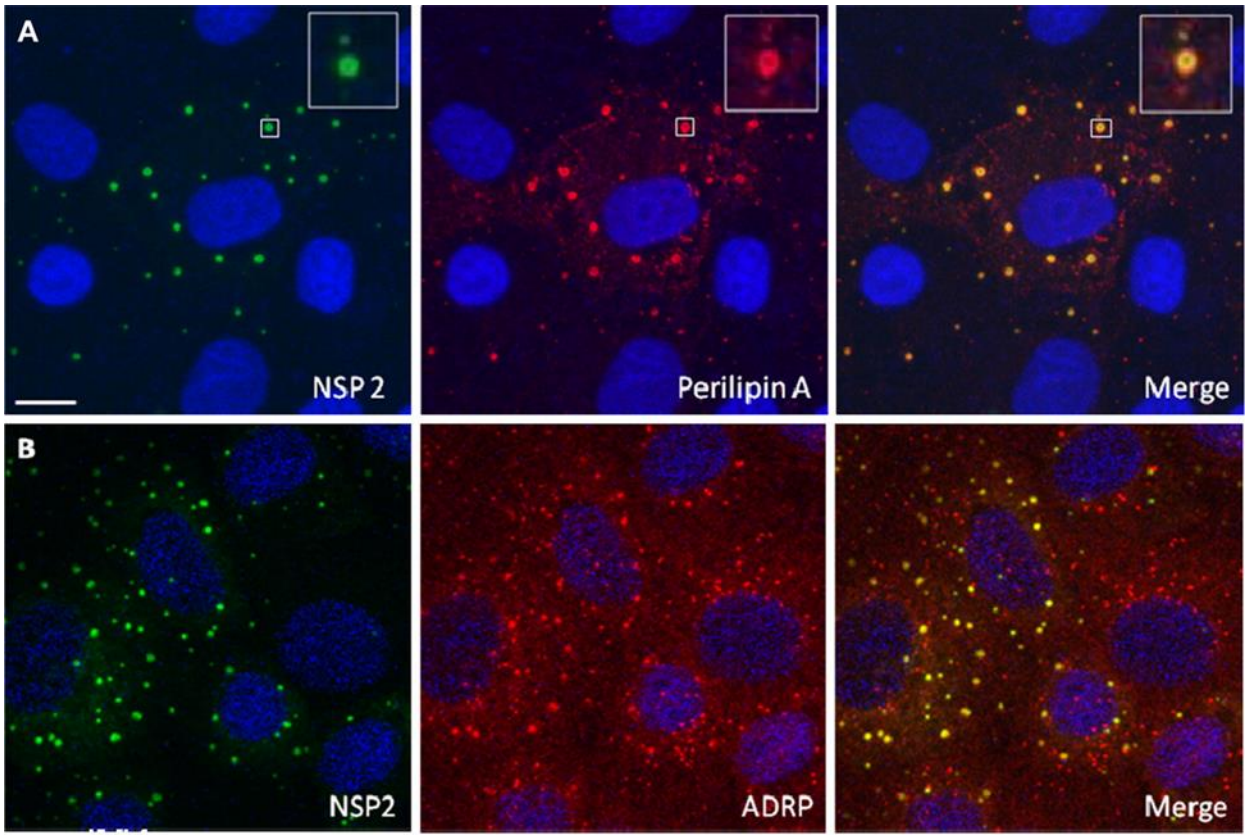

Figure 1.6. NSP2 co-localises with lipid droplet-associated proteins, perilipin A and ADRP in viroplasms. Confocal microscopy images of rotavirus infected MA104 cells at 8 h post infection were obtained. (A and B) Viroplasms were detected with anti-NSP2 antibodies, followed by visualization with Alexa Fluor 488 (green)-labelled secondary antibody, whereas LD-associated proteins were detected with anti-perilipin A (A) and anti-ADRP antibodies (B), followed by reaction with Alexa Fluor 633 (red)-labelled secondary antibody. An individual viroplasm of panel A has been magnified and is shown in the inserts. Scale bar, 10 μm. With permission from Cheung et al., 2010.

Furthermore, PLIN1 was shown to co-sediment with NSP5 and dsRNA in low-density fractions of ultracentrifugation gradients of RV-infected cell extracts (Cheung et al., 2010). Data form these observations also showed that RV could increase the amount

of lipids found within infected cells. Compounds that block LD formation or disperse LDs significantly decreases the number and size of LDs, with subsequent adverse effects on infectious progeny (Gaunt et al., 2013a, 2013b). Inhibition of acetyl-CoA carboxylase 1, responsible for regulating fatty acids synthesis, with 5-(tetradecyloxy)-2-furoic acid leads to reductions in both infectivity of progeny virus and viral dsRNA in a time- and dose-dependent manner. Although several other inhibitors of lipogenesis were also able to decrease the production of viral RNA and lower infectious progeny yield, Martínez and co-workers (2022) recently showed that the inhibition of lipogenesis by C75, a synthetic inhibitor of fatty acid synthase, does not affect the morphology of viroplasms or disrupt the LD-viroplasm association. In addition, they showed that neither lipogenesis nor lipolysis inhibition interfered with viroplasm formation, but instead affected the association of viroplasms with the ER membrane. They suggested that lipogenesis-lipolysis balance plays a crucial role during the final stages of RV replication.

1.2.3. Pathophysiology

Rotavirus infection leads to non-bloody diarrhoea which lasts for a three to eight days (Crawford et al., 2017). Rotavirus-induced diarrhoea has two proposed mechanisms: osmotic diarrhoea, due to malabsorption and secretory diarrhoea because of NSP4 and the activation of the enteric nervous system (**Figure 1. 7**).

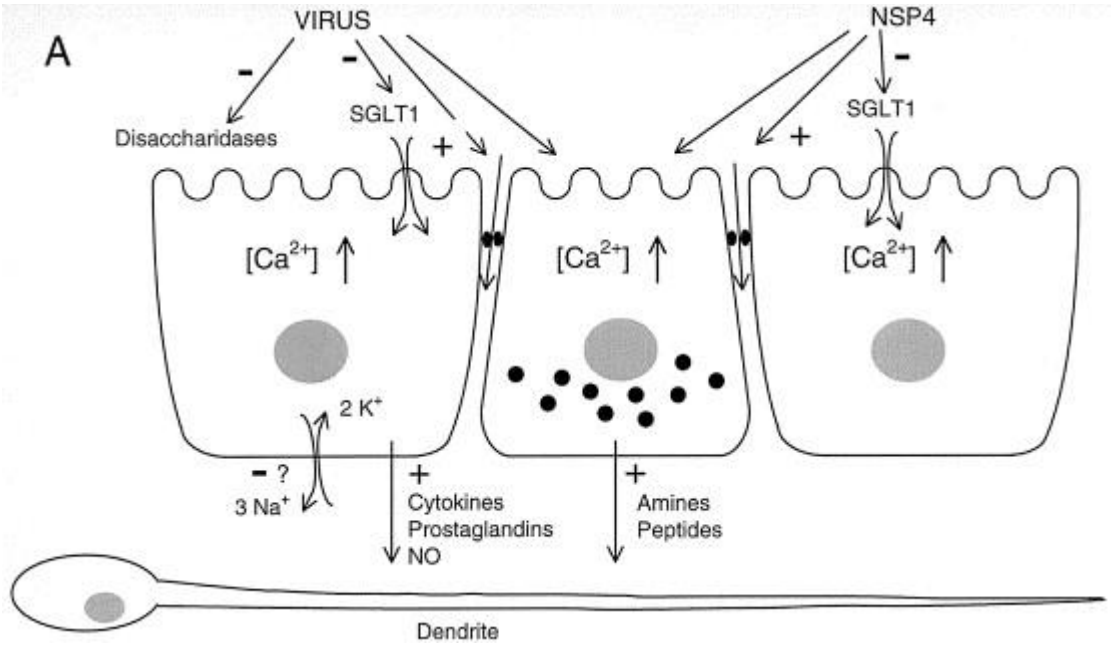

Figure 1. 7. A speculative hypothesis for rotavirus-induced diarrhoea. Rotavirus and/or its enterotoxin NSP4 inhibits fluid and electrolyte transport of the villus epithelium by attenuating the Na-

glucose symport SGLT1 and possibly also Na-amino acid symports (not shown). In addition, disaccharidase activity is also inhibited. These events will lower the rates of fluid, electrolyte, and glucose absorption. Rotavirus and NSP4 increase paracellular epithelial permeability. Intracellular calcium concentration is increased in the intestinal epithelium in response to virus/NSP4, causing the release of amines/peptides from intestinal endocrine cells. Furthermore, cytokines, prostaglandins and nitric oxide are released from the enterocytes in response to microorganisms and can activate neuronal dendrites located just underneath the intestinal epithelium and hence stimulate secretory reflexes in the enteric nervous system. With permission form Lorrot and Vasseur, 2007

Replication of RV within the duodenal mucosa of infants has been shown to disrupt normal cellular homeostasis. The disruption results in shortening and atrophy of villi, loss of microvilli, mononuclear infiltration, distended ER and mitochondrial swelling in enterocytes (Davidson and Barnes, 1979). Although the molecular mechanisms of enterocyte damage remain elusive, due to lack of human small intestine models, studies in cell culture have proposed several mechanisms, including virus-mediated apoptosis (Boshuizen et al., 2003), NSP4-mediated mislocalisation of the tight junction protein, ZO-1 (Tafazoli et al., 2001) and binding to the basement membrane extracellular matrix proteins, laminin subunit-β3 and fibronectin (Boshuizen et al., 2004). In addition to enterocyte damage and death, several mechanisms have been proposed to result in the reduction of epithelial absorptive function, contributing to RV-induced diarrhoea. Among these mechanisms are the loss of infected enterocytes and NSP4-mediated impairment of sodium-coupled solute symporters, involved in the reabsorption of large volumes of water under physiological conditions (Svensson et al., 2016). The exact contribution of reduced epithelial absorptive function to RV-induced diarrhoea remains unclear as treatment with oral rehydration therapy rapidly corrects the electrolyte imbalance and water loss in children with severe diarrhoea (Crawford et al., 2017).

NSP4 is an enterotoxin that induces diarrhoea in mice, by binding to intestinal epithelial cells and activating Ca^{2+}-dependent chloride channels (Hyser et al., 2010). Activation of these channels leads to rapid secretion of chloride ions into the lumen, resulting in an osmotic gradient that facilitates the transport of water into the lumen, resulting in secretory diarrhoea (Ball et al., 1996). Furthermore, intracellular NSP4 can cause the release of Ca^{2+} from the ER via a viroporin domain, thus increasing cytoplasmic Ca^{2+} levels. The subsequent increase in intracellular Ca^{2+} triggers several cellular processes, including disruption of the microvillar cytoskeletal network, lowered expression of disaccharidases and other enzymes at the apical surface, general inhibition of the Na^{+}-solute cotransport systems, and necrosis (Ramig, 2004).

The secretion of 5-hydroxytryptamine from enteroendocrine cells in humans and mice activates the enteric nerves that lead to increased intestinal motility and activates vagal nerves that stimulate regions in the brains associated with nausea and vomiting (Hagbom et al., 2011). Silencing of NSP4 expression and the chelation of cytoplasmic Ca^{2+} prevented the release of 5-hydroxytryptamine in RV infected enteroendocrine cells, while the treatment of RV infected mice with opioid receptor agonists and anti-muscarinic drugs decreased the severity and length of diarrhoea. In addition, Hagbom and co-workers (2012), suggested that the ability of PGE_2 to stimulate the excretion of water could contribute to RV disease progression.

1.2.4. Lipid droplets as sites of PGE_2 production

Lipid droplets are cytosolic organelles that are continuously synthesised and broken down in response to signals and cellular requirements (Cohen, 2018). They have a neutral lipid core that contains triacylglycerols and cholesteryl esters and are enveloped by a phospholipid monolayer (**Figure 1. 8**). Their functions include regulators of lipid metabolism, trafficking, and signalling. These functions are partly due to the rich proteome associated with the phospholipid membrane (Cermelli et al., 2006; Hodges and Wu, 2010). Polyunsaturated fatty acids are also stored in LDs and are well known precursors for the synthesis of various bioactive lipid mediators, such as eicosanoids (Bozza et al., 2011). The release of these lipid mediators from immune and other cell types can modulate both inflammatory and immune responses(Harizi et al., 2008).

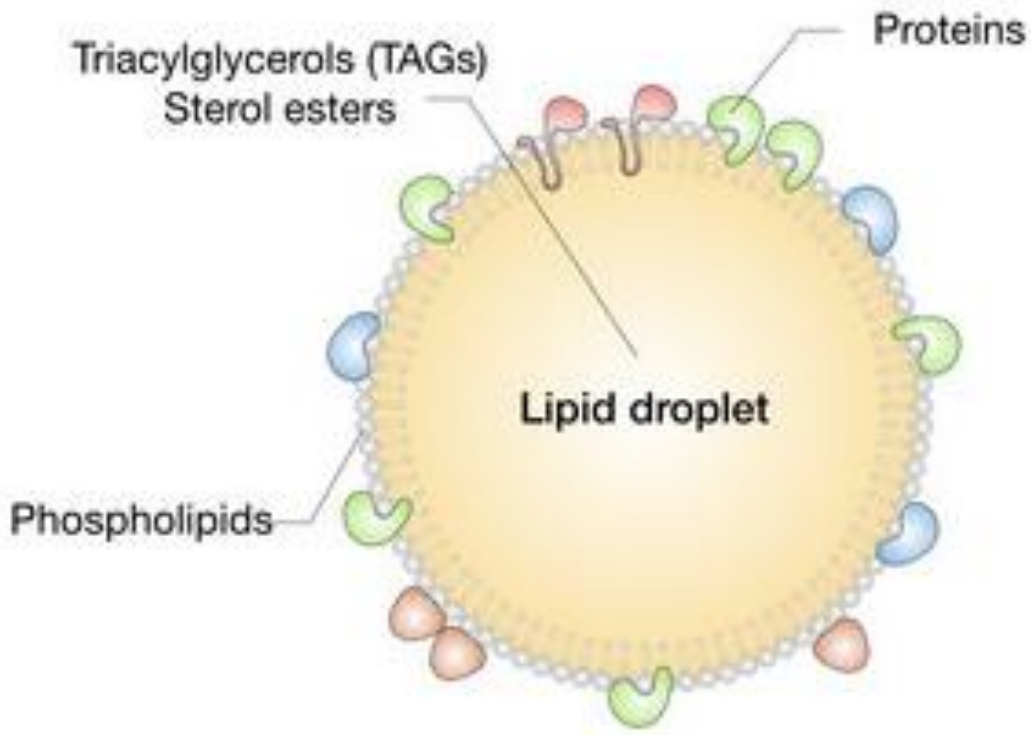

Figure 1. 8. Lipid droplet structure. Lipid droplets consist of a central hydrophobic core of neutral lipids, mostly composed of triacylglycerols and sterol esters, surrounded by a monolayer of phospholipid molecules, wherein numerous proteins are embedded. Modified with permission from Jarc and Petan, 2020Modified with permission from Jarc and Petan, 2020Modified with permission from Jarc and Petan, 2020

Eicosanoids are lipid mediators derived from arachidonic acid, an ω-6 polyunsaturated fatty acid. In mammals they are formed when arachidonic acid is oxygenated by a series of COX, lipoxygenase and cytochrome P450 epoxygenase enzymes, giving rise to prostaglandins, leukotrienes, thromboxanes, lipoxins and other related oxygenated lipid species (Hanna and Hafez, 2018). The rate of eicosanoid production is intrinsically linked to the availability of free arachidonic acid, which is released from polyunsaturated fatty acid stores (such as phospholipids and LDs) by phospholipase A_2 (PLA_2) (Leslie, 2015) (**Figure 1.9**).

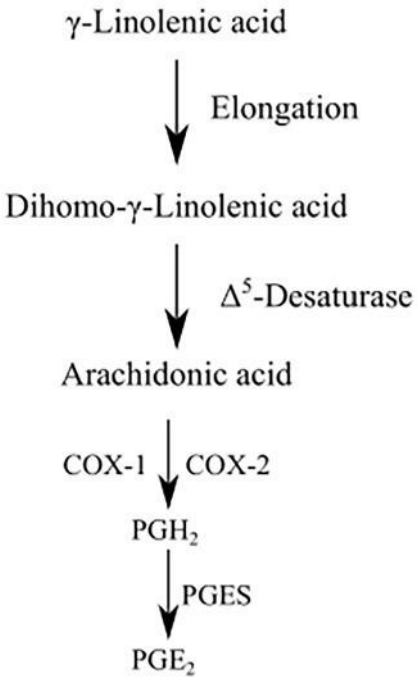

Figure 1.9. Cellular sources of precursors for lipid mediator production. γ-Linolenic acid (GLA) is converted to dihomo-γ-linolenic acid by elongases which is subsequently converted to arachidonic acid (AA) via Δ5-desaturase. Finally, AA is converted to PGE2 by either COX-1/2 and PGES. Modified with permission from Sander and co-workers (2017)

Activation of cytosolic phospholipase ($cPLA_2\alpha$) by diverse inflammatory stimuli occurs when increased intracellular Ca^{2+} levels allow for the translocation of $cPLA_2\alpha$ from the cytosol to LDs, the perinuclear membranes of the Golgi, ER and the nuclear envelope membrane (Murakami et al., 2020). This allows for immediate production of eicosanoids by COX enzymes, which are localised at LDs and the ER. In addition to regulating lipid mediator biosynthesis, $cPLA_2\alpha$ has also been implicated in LD biogenesis (Gubern et al., 2008). Together with other cellular lipases, $cPLA_2\alpha$ generates lysophospholipids which promote LD budding by reducing ER bilayer tension and increasing the positive curvature of the LD lipid monolayer (Choudhary et al., 2018).

Prostaglandin E_2 is the most abundant eicosanoid produced by a multitude of cell types and has both physiological and pathological functions (Ricciotti and FitzGerald, 2011), including pro-viral effects observed during several viral infections, including human-immunodeficiency virus, influenza A virus and RV (Sander et al., 2017). After the release of arachidonic acid from phospholipids, COX-1 and -2 convert it into prostaglandin H_2, which in turn is converted to prostaglandin E_2 by prostaglandin E_2

synthases (Park et al., 2006). It should be noted that in addition to all the PGE_2 biosynthetic enzymes localising with LDs, Bandeira-Melo and co-workers (2011) showed that PGE_2 itself localises with LDs (**Figure 1.10**).

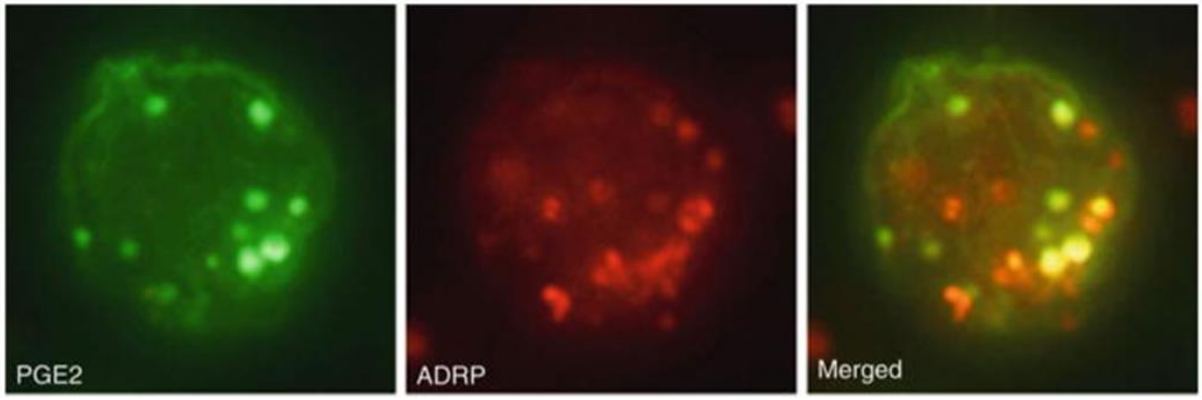

Figure 1.10. EicosaCell staining for PGE_2 immunolocalisation within BCG-infected cytospun macrophages. Macrophages from BCG-infected animals were labelled for ADRP-associated lipid bodies (red staining) and for newly formed PGE_2 (green staining). Merged image showed co-localization of PGE_2 in ADRP-associated lipid bodies (yellow staining). Modified with permission from Bandeira-Melo et al., 2011

Calcium is not only essential during RV replication but can also modify the production of PGE_2. As mentioned above, the biosynthesis of PGE_2 is dependent on the rate at which arachidonic is released from phospholipids by $cPLA_2$ (Tithof et al., 2007). Cytosolic PLA_2 is a Ca^{2+}-dependent enzyme and, together with Ca^{2+}-independent- and secretory PLA_2, forms part of the PLA_2 family (Burke and Dennis, 2009). Although all these enzymes cleave fatty acids from phospholipids by hydrolysing the ester bond at position sn2 , $cPLA_2$ has a higher specify for arachidonic acid. Several stimuli have been shown to activate $cPLA_2$ via many types of receptors, indicating that arachidonic acid release is a common response to cell stimulation (Leslie, 2015). Cytosolic PLA_2 is rapidly activated via posttranslational processes including increased intracellular levels of Ca^{2+} (Clark et al., 1995). Structural studies show that $cPLA_2$ contains both a C-terminal catalytic domain and N-terminal Ca^{2+}-dependent lipid binding domain (C2), with the latter having high affinity for Ca^{2+} (Nalefski and Falke, 1996). Increases in Ca^{2+} allow for the translocation of $cPLA_2$ from the cytosol to intracellular membranes, where Ca^{2+} binds to the C-domain of $cPLA_2$ increasing the hydrophobicity of the Ca^{2+} binding loops, resulting in membrane penetration (Ward et al., 2012). Evans and co-workers (2001) showed that sustained intracellular Ca^{2+} levels between 100 – 125 nM allowed for the translocation of $cPLA_2$ to the Golgi and ER, while translocation to the

perinuclear membranes occurred at levels between 210 – 280 nM. In addition, they showed that short increases in intracellular Ca^{2+} levels were enough for the translocation to membranes and that decreases in intracellular Ca^{2+} levels resulted in the quick dissociation of C2 from the membranes. Although translocation of $cPLA_2$ to intracellular membranes is essential, it is not sufficient for arachidonic acid release (Leslie, 2015). The catalytic activity of $cPLA_2$ is enhanced by phosphorylation of S505 by mitogen-activated protein kinases, extracellular regulated protein kinases, and p38 (Lin et al., 1993).

It should however be noted that studies indicating a $cPLA_2$ activation due to intracellular Ca^{2+} levels resulting in increased PGE_2 production are scarce. Studies in Chinese hamster ovary cells showed more PGE_2 was released in response to the modulation of intracellular Ca^{2+} resulting in the phosphorylation of $cPLA_2$ and its translocation to membranes subsequently increasing PGE_2 production (Kuda et al., 2011). In addition, Bonventre and Swidler (1988) showed that enhanced PLA_2 activity was observed with both protein kinase C activation and increases in intracellular Ca^{2+}, leading to increased PGE_2 production in stimulated glomerular mesangial cells. Importantly, they also showed that the increase in PGE_2 production was not dependent on extracellular Ca^{2+}. Studies have also shown that extracellular PGE_2 can increase intracellular Ca^{2+} by several mechanisms, including in a PGE_2 receptor 1 and 3 dependent-manner (Asbóth et al., 1996).

1.2.5. Rotavirus and prostaglandin E_2

Prostaglandin E_2 is modulated by several viruses to the detriment of the host (Sander et al., 2017), and RV is no exception. Increased PGE_2 was observed in the stool of both RV infected children and piglets. Yamashiro and co-workers (1989) showed that treatment of RV-infected children with aspirin (a non-specific inhibitor of COX) caused diarrhoea to end earlier, while Zijlstra and co-workers (1999) showed that PGE_2 was elevated in piglets early after infection, irrespective of nutritional state, but remained elevated for longer in malnourished piglets subsequently prolonging duration of diarrhoea.

Inhibition of PGE_2 biosynthesis by classical inhibitors such as indomethacin (a non-specific inhibitor of cyclooxygenases), SC-560 (cyclooxygenase-1 specific inhibitor) and NS-398 (cyclooxygenase-2 specific inhibitor) restrict RV replication *in vitro* (Rossen et al., 2004). Infection of human colorectal adenocarcinoma (Caco-2) cells at an MOI of 1 with either SA11 or WA rotavirus strains resulted in an increase of both COX-2 expression and secreted levels of PGE_2. Importantly, the treatment of RV infected Caco-2 cells with these inhibitors decreased viral yield and lead the authors to propose that PGE_2 is necessary early during infection and is most likely involved in viral protein synthesis and production of virus progeny, while they found no effect on viral RNA production.

Recently, Kim and co-workers (2020) showed that both pre- and post- treatment of RV-infected MA104 cells with genipin (extracted from gardenia fruit, an iridoid monoterpenoid with protein inhibitor, hepatotoxic agent, apoptosis inhibitor, antioxidant, anti-inflammatory and cross-linking reagent properties) decreased levels of PGE_2 and other inflammatory markers (IL-6, IL-10, IL-1β, and TNF-α). Treatment of SA11 and WA infected MA104 and Caco-2 cells with indomethacin showed significant decreases in plaque numbers and quantification of viral titre via real-time PCR, in contrast to Rossen and co-workers (2004) which showed no effect on viral RNA. Interestingly, they also showed that, dependent on time of treatment, either attachment/entry (pre-treatment) or assembly/release (post-treatment) was impacted. Furthermore, the treatment of EDIM strain infected mice showed significantly reduced diarrhoeal incidence and faecal viral shedding compared to the untreated group (Kim et al., 2020).

1.3. Problem statement

Rotavirus is a leading cause of severe dehydrating diarrhoea in infants and children under the age of five. Although great strides have been made in reducing the burden of RV by introduction of several vaccines, relatively low efficacy contributes to the high burden still experienced in the developing world. In addition, other than oral rehydration therapy, no treatment exists for children infected with RV. Currently, we know that PGE_2 is increased during RV infection, both *in vivo* and *in vitro,* and the inhibition of COX reduces viral yield and decreases the duration and severity of diarrhoea. Although, the stimulation of PGE_2 during RV replication is an attractive target for anti-viral development, we currently lack knowledge as to when and during which stage of RV replication PGE_2 exerts pro-viral effects and by which mechanism(s) RV induces the production of PGE_2.

1.4. Aim and objectives

The study aims to determine when and by which mechanism(s) RV induces/amplifies the production of prostaglandin E_2.

This will be achieved through the following objectives:

1. To determine during which stage of viral replication PGE_2 exerts pro-viral effects.
2. To identify if the viroplasm/viroplasm-like structures or individual viroplasm proteins play a role in the induction of PGE_2 during RV infection.
3. To determine if increased cytoplasmic Ca^{2+} levels, induced by NSP4, amplify the effect of PGE_2 on RV replication.

1.5. Ethics

Ethical approval was obtained from the Environmental & Biosafety Research Ethics Committee under: UFS-ESD2019/0170 (**Appendix A**)

CHAPTER 2: Rotavirus mediated prostaglandin E_2 production in MA104 cells promote virus attachment and internalisation, resulting in an increased viral load[1]

2.1. Introduction

Although RV attachment and internalisation is not well understood, it is known that RV binds to several cell receptors, whereafter internalisation occurs rapidly by either clathrin-dependent or -independent endocytosis, depending on viral strain (Arias and López, 2021). During viral replication, RV forms cytoplasmic inclusion bodies, termed viroplasms, which are required for assortment, genome replication and formation of progeny viral particles (Papa et al., 2021). Once viroplasms have been synthesized they form complexes with lipid droplets (LDs) and several viral proteins, specifically NSP2 and NSP5 (Cheung et al., 2010; Kim et al., 2012; Gaunt et al., 2013a; Crawford and Desselberger, 2016).

Lipid droplets are organelles that play diverse roles in the physiology and pathophysiology of cells (Guo et al., 2009; Walther et al., 2017). The major components, making up the neutral core of LDs, are triacylglycerols and sterol esters, which serve as energy stores mobilized during nutrient deprivation (Jackson et al., 2016). This core is surrounded by a phospholipid monolayer that contains diverse membrane-bound proteins (Bartz et al., 2007). Some of these proteins, such as viperin, immunity-related GTPases, lipoxygenases and cyclooxygenases (COX), are involved in the production of lipid mediators, which play crucial roles during the immune response to viral infections (Accioly et al., 2008; Bozza et al., 2011; Monson et al., 2021). Important examples of such lipid mediators are the eicosanoids belonging to the prostaglandins, which modulate inflammation (Ricciotti and FitzGerald, 2011).

Prostaglandins are bioactive molecules that are derived from arachidonic acid (AA) (Phipps et al., 1991; Ricciotti and FitzGerald, 2011). The most common prostaglandin, prostaglandin E_2 (PGE_2), is produced by all mammalian cell types and regulates several physiological processes, including blood pressure, fertility, gastrointestinal integrity, immunity and inflammation (Ricciotti and FitzGerald, 2011). During viral

[1] Parts of chapter has been published in Sander WJ, Kemp G, Hugo A, Pohl CH, O'Neill HG. Rotavirus-Mediated Prostaglandin E_2 Production in MA104 Cells Promotes Virus Attachment and Internalisation, Resulting in an Increased Viral Load. Front Physiol. 2022 Apr 19;13:901082. See **Appendix** B.

infections, the production of PGE_2 can be modulated to benefit the virus (Sander et al., 2017). During previous work we showed that the supplementation of MA104 cells with γ-linolenic acid (GLA), a known precursor to AA, significantly increased the rate of RV replication (Sander, 2019).

To elucidate when and where PGE_2 is produced during RV infection, we supplemented MA104 cells with GLA or treated them with PGE_2 biosynthetic inhibitors and subjected the infected cells to ELISA, confocal microscopy, viral growth kinetics, and flow cytometry.

2.2. Materials and Methods

2.2.1. Cells, virus, and inhibitors

The African Green Monkey kidney (MA104) cell line was maintained in Dulbecco's modified Eagle medium (DMEM) (Gibco), supplemented with 5 % (v/v) foetal bovine serum (FBS) (Gibco), 1 % (v/v) Penicillin-Streptomycin-Amphotericin B Mixture (10 000 U, 10 000 µg and 25 µg per ml) (Lonza), and 1 % (v/v) nonessential amino acids (NEAA) (Lonza) at 37°C and 5 % CO_2. Sub-confluent cells were supplemented with 50 µM GLA (Thermo Fischer Scientific) for 24 h according to Tanaka and co-workers (2001). Rotavirus simian agent 11 strain, SA11 (Mlera et al., 2013) was used to infect MA104 cells and viral yield was determined using 50 % tissue culture infectious doses, $TCID_{50}$ (Reed and Muench, 1938). To facilitate infection, pancreatic porcine trypsin type IX (1 µg/ml; Sigma Aldrich) was added during all viral replication experiments.

The non-specific cyclooxygenase inhibitor, indomethacin; the COX-1-specific inhibitor, SC-560; the COX-2-specific inhibitor, Celecoxib; cytoplasmic phospholipase A_2 inhibitor, CAY10502 and PGE_2 were obtained from Sigma-Aldrich and resuspended in 100 % (v/v) dimethyl sulfoxide (DMSO; Sigma-Aldrich).

2.2.2. Cytotoxicity of inhibitors

The tetrazolium salt XTT (2,3-bis(2-metoxy-4-nitro-5-sulphophenyl(-2H-tetra-zolium-5-carboxanilide inner salt) (Sigma Aldrich) assay was used to determine cell viability after treatment with inhibitors. Briefly, XTT and N-methyl dibenzopyrazine methyl sulfate (PMS) (Sigma Aldrich) were dissolved in phosphate buffered saline (PBS) at a concentration of 1 mg/ml and 10 mM, respectively. Afterwards PMS was added to the

XTT solution immediately before use to a final concentration of 25 µM. MA104 cells were seeded in 96-well plate (5×10^3 cells/ml) and incubated for 24 h in 37 °C with 5 % CO_2. The cells were subsequently treated with different drugs in various concentrations and incubated further for 16 h. For indomethacin, celecoxib and SC-560 the concentrations ranged from 2.5 µM to 150 nM, while concentrations ranging from 25 nM to 500 nM were used for CAY10502. After drug exposure, the cell culture medium was removed and replaced with the XTT-PMS solution and incubated 2 h at 37 °C in 5 % CO_2. The optical density (OD) of the solution was determined using a test wavelength of 450 nm, and a reference wavelength of 650 nm, subtracting blank control values.

2.2.3. Prostaglandin E_2 quantification and authentication

MA014 cells (0.3 x 10^6 cells/ml) were seeded into 6-well plates (Thermo Fischer Scientific) and allowed to grow to 100 % confluence. To determine the effect of viral load on PGE_2 production, PGE_2 was measured at different multiplicity of infection (MOIs: 0.1; 1; 10). In order to prevent free radical catalysed lipid peroxidation, citric acid (Sigma-Aldrich) and butylated hydroxytoluene (Sigma-Aldrich, USA) were added to a final concentration of 80 mM and 0.1 % (v/v), respectively. Prostaglandins were extracted by addition of 2 ml hexane/ethyl acetate (1:1, v/v), followed by vortex mixing for 1 min. After centrifugation for 5 min at 1000 x g at 4 °C, the upper, organic phase was removed (Caoa et al., 2008). The extraction procedure was repeated, and the organic phases were combined and evaporated to dryness under a stream of nitrogen gas. The amount of secreted PGE_2 in the supernatants of mock- or RV-infected (MOI = 5) cells, both in the presence and absence of inhibitors, were determined at 2 and 4 h post infection using an enzyme-linked immunosorbent assay (ELISA; Cayman Chemicals) according to the manufacturer's protocol. LC-MS/MS was used for authentication of PGE_2 production. Briefly, the supernatant of each infection was divided into two 500 µl aliquots. One of the 500µl aliquots was spiked with PGE_2 to a final concentration of 100ng/mL). Twenty microliters of each sample were separated on a C18 column (Luna 3µm C18, 150x3mm, Phenomenex) at a flow rate of 200 µl/min, using 0.1 % (v/v) formic acid (mobile phase A) and acetonitrile with 0.1 % formic acid (mobile phase B). The column was equilibrated and loaded at 20 % of mobile phase B, increasing to 42.5 % B over 50 minutes, 95 % B for 10 minutes, followed by re-equilibration at 20 % B for a total run time of 70 minutes. Ion spray voltage was set

at 4500V, nebuliser gas (GS1) was at 40 psi and heater gas (GS2) at 30 psi with the heater temperature set at 400 °C. Samples were analysed using a 4000 QTRAP hybrid triple quadrupole ion trap mass spectrometer (AB Sciex) and Shimadzu UFLC stack with LC-20AB binary pump and SIL-20A HT autosampler as front end. All data acquisition and processing were performed using Analyst 1.5.2 (AB SCIEX) software. To analyse the sample a targeted Multiple Reaction Monitoring (MRM) workflow was followed on the instrument. All compound and source dependent parameters were optimised using compound optimization in Analyst 1.5.2. The targeted analysis for the extracted PGE_2 used 5 MRM transitions: 351.17 > 315.2; 351.17 > 271.2; 351.17 > 333.3; 351.17 > 189.0; 351.17 > 235.1. Only if all 5 transitions were recorded at the same retention time would the presence of PGE_2 be confirmed.

2.2.4. Confocal-laser scanning microscopy (CLSM)

To determine the co-localization between viroplasms and PGE_2, MA104 cells (0.1 x 10^6 cells/ml) were seeded onto coverslips in 24-well plates (Thermo Fischer Scientific) and allowed to grow to 80 % confluence before being infected at a MOI of 5. The cells were then processed according to Bandeira-Melo and co-workers (2011) with slight modifications, 2 and 4 h post infection. Briefly, MA104 cells were fixed and permeabilised with a mixture of 0.5 % (w/v) 1-ethyl-3-(3-dimethylamino-propyl) carbodiimide hydrochloride (Sigma-Aldrich) and 1 % (v/v) paraformaldehyde in PBS, for 1 h at 37°C. In addition to cross-linking the carboxyl groups of eicosanoids to the amines of adjacent proteins localized at eicosanoid-synthesizing sites, 1-ethyl-3-(3-dimethylamino-propyl) carbodiimide hydrochloride is also able to both fix and permeabilise cells (Bandeira-Melo et al., 2011). After fixation and permeabilisation, the cells were blocked with 1 % (w/v) bovine serum albumin (BSA) plus 0.1 % (v/v) Triton X-100 in PBS and washed with PBS before overnight incubation (4 °C) with PBS containing 1 % BSA and 1:100 anti-PGE_2 monoclonal antibody (Cayman Chemicals). The cells were washed three times and then incubated in PBS containing 1 % BSA and 1:500 rabbit anti-NSP2 (kind gift from Prof. Potgieter, Deltamune, South Africa) and/or rabbit anti-NSP5 peptide [KSPEDIGPSDSASNC] (Genscript) for 1 h at 37 °C. The cells were then washed three times and incubated with 1:500 anti-mouse Alexa Flour 488 (Thermo Fischer Scientific) and 1:500 anti-rabbit Alexa-Flour 647 (Thermo Fischer Scientific) for 1 h at 37 °C. Cells were extensively washed and incubated with 300 nM DAPI (Thermo Fischer Scientific) for 5 min at room temperature. After three

washes, the coverslips were mounted on glass slides with 90 % (v/v) glycerol in PBS. The samples were analysed by CLSM, using a Zeiss LSM 900 instrument, Zen Blue software and ImageJ (Schneider et al., 2012).

2.2.5. Replication Kinetics

MA104 cells (0.7 x 10^6 cells/ml) were seeded in 25-cm^3 flasks (Thermo Fischer Scientific) and allowed to grow to 80 % confluence before being supplemented with 50 µM GLA 24 h prior to infection. The cells were rinsed three times with PBS and incubated with either 25 µM indomethacin, 5 µM celecoxib, 2.5 µM SC-560 or 25 nM CAY10502 in serum-free DMEM for 1 h prior to infection. The addition of inhibitors was repeated every 4 hours until the completion of the experiment. For addback experiments, 0.1 µM of exogenous PGE_2 was added to the cells directly after addition of inhibitors. SA11 was activated for 1 h at 37°C with 10 µg of trypsin/ml and diluted in serum free DMEM. Subsequently, MA104 cells were infected with SA11 at a MOI of 5, both in the presence and absence of GLA or the inhibitors. For the replication studies, time-point 00:00 is defined as the initial viral inoculum, while time-point 00:30 are cells that were washed with PBS and subsequently freeze-thawed. After infection for 1h at 37 °C the inoculum was removed and replaced with serum-free DMEM containing 1 µg of trypsin/ml. SA11 was harvested from MA104 cells by three cycles of freeze-thawing, whereafter cellular debris was removed by centrifugation for 10 min at 4000 x g. The supernatant was used to determine viral RNA yield (qRT-PCR) and infectious viral yield ($TCID_{50}$).

2.2.6. RNA isolation and RT-qPCR

In order to evaluate the production of VP6 transcripts, the VP6 coding sequence was inserted into the pTZ57R/T cloning vector (Thermo Fischer Scientific). Positive-sense single-stranded RNA was transcribed using the TranscriptAid T7 High Yield Transcription Kit (Thermo Fischer Scientific), with 1 µg Xba I -linearized (Thermo Fischer Scientific) plasmid DNA as template, followed by incubation with DNaseI (Thermo Fischer Scientific) at 37 °C for 20 min. *In vitro* synthesized RNA was purified using Trizol reagent (Thermo Fischer), according to the manufacturer's instructions, and quantified with a Qubit RNA BR kit (Thermo Fischer Scientific). RNA from RV-infected MA104 cells, in the presence or absence of PGE_2 biosynthesis inhibitors, were semi-purified by ultracentrifugation through a 35% sucrose cushion, at 6 h post

infection (Arnold et al., 2009). RNA was extracted from the semi-purified virus by using Trizol reagent according to the manufacturer's instructions.

Transcribed RNA was used in 2-fold serial dilutions to generate standard curves for determination of the assay efficiency. The Qiagen Rotor-Gene Q System with the Luna® Universal Probe One-Step RT-qPCR Kit (New England Biolabs) was used for RT-qPCR, according to the manufacturers protocol, using the following primers: cDNA primer (5'- AGGAACGGAATTGCACCT-3'), qPCR forward (5'- CTGGATTTGACTACTCATG -3') reverse (5'- CGTCTGGTAGAAGAGTTA -3') and probe (5'- /56-FAM/AACGCACCAGCCAATATACAA -3') (Integrated DNA Technologies). Cycling conditions were 55 °C for 10 min, then 95 °C for 1 min, followed by 40 cycles of 95 °C for 10 s and 60 °C for 30 s. Data were analysed with Q-Rex Software Version 1.1.

2.2.7. Attachment and internalisation assay

The effect of PGE_2 on RV attachment and internalisation was determined using a modified protocol for influenza A virus (Pohl and Stertz, 2015). Twenty-four well plates were seeded with MA104 cells (0.2×10^6 cells/ml) and supplemented and/or treated with exogenous PGE_2/inhibitors as previously described. To determine if the inhibitors of PGE_2 production affected attachment, RV infected MA104 cells were tagged with FITC anti-RV (Abcam) and anti-DLP (rabbit polyclonal antibody raised against RV double-layered particle; a kind gift from Prof. Potgieter, Deltamune, South Africa) at time 0 min. The experimental set consisted of 2 groups: '0 min' and '0 min + anti-DLP'. Rotavirus (MOI = 10) was allowed to cold-bind to MA104 cells for 1 h on ice and then washed 3 times with ice-cold PBS. The samples were fixed in 4 % (v/v) paraformaldehyde for 10 min at room temperature, washed 3 times and stored at 4 °C until analysis.

To determine whether the inhibitors of PGE_2 affected internalisation, RV-infected MA104 cells were again tagged with FITC anti-RV and anti-DLP at 30 min. Rotavirus (MOI = 10) was allowed to cold-bind to MA104 cells for 1 h on ice and then washed 3 times with ice-cold PBS. After the incubation on ice the '30 min' and '30 min + anti-DLP' samples were washed and PBS containing 2 % (w/v) BSA and 1 µg/ml trypsin was added to the MA104 cells, which were then incubated for 30 min at 37°C, fixed

and washed three times. Following fixation, all samples were permeabilised with PBS containing 0.5 % (v/v) Triton X-100 for 5 min at room temperature.

Cells were again washed and incubated with 1:500 Alexa Fluor 532 (Thermo Fischer Scientific). Cells were extensively washed and detached with StemPro™ Accutase™ (Thermo Fischer Scientific) for 30 min at 37 °C before fluorescent analyses on the BD Accuri C6 Plus instrument.

2.2.8. Statistical analysis

Each assay was carried out at least in triplicate (biological/independent replicates) on separate days. Each repeat was analysed in triplicate (n = 3). Data are presented as means ± standard deviation of the mean. For statistical analysis, two-way analysis of variance (ANOVA) was performed using a Tukey-Kramer test in GraphPad Prism version 3.00 for Windows (GraphPad Software, San Diego, Calif.). In all tests, $p < 0.05$ was considered statistically significant. Co-localisation in CLSM experiments were verified using Pearson:Pearson correlation coefficients in ImageJ.

2.3. Results

2.3.1. Cytotoxicity of PGE_2 biosynthesis inhibitors

To determine the optimal concentration of inhibitors, XXT cell viability assays were performed. For the inhibitors that were dissolved in DMSO, it was determined that no more that 1 % DMSO (93.66 %± 3.74) could be added to the cells (**Figure 2. 1A**). Data from the XTT viability assays showed that concentrations to be used for the different inhibitors were as follows: indomethacin 25 µM (84 %±0.19), celecoxib 5 µM (85 %±0.85), SC-560 2.5 µM (83 %±1.5), CAY10502 25 nM (93 %±2.8) (**Figure 2. 1B**).

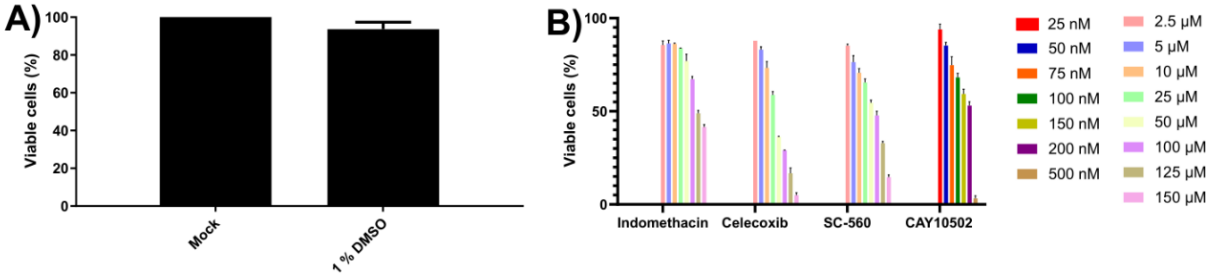

Figure 2. 1. Cellular toxicity of the inhibitors and DMSO were evaluated with the XTT assay. MA104 cells (4 x 10^4 cells/ml) were seeded into 96 well plates and allowed to grow to 100 % confluence. The inhibitors were added 1 h prior to infection and subsequently every 4 hours till the completion of the experiment. A) All inhibitors were added to MA104 cells containing a final concentration of 1 % DMSO to ensure the vehicle had no detrimental effect on the cells. Results indicate that 1 % decreases cell viability to approximately 92±3 %.
The following specific indices were calculated for the inhibitors:

Indomethacin	Celecoxib	SC-560	CAY10502	
CC_{50}	125 uM	25uM	100 uM	200 nM
Conc used	25 uM	5uM	2.5 uM	25 nM

2.3.2. Rotavirus infection stimulates PGE_2 production in a dose-dependent manner

The concentration of PGE_2 produced by cells during viral infection was determined. The supplementation of MA104 cells with GLA in the absence of virus caused an increase in PGE_2, as measured by ELISA, at both two and four hours post infection, indicating a shift in the baseline production of PGE_2 in GLA-supplemented cells **Figure 2. 2**. Rotavirus infection of unsupplemented cells also caused a significant increase in PGE_2 production at both time points (p= 0,00004; p= 0,00008, respectively). It should also be noted that the concentration of PGE_2 increased from two to four hours post infection regardless of supplementation, but the effect is more significant in supplemented MA104 cells (increase of ~ 38 pg/ml vs. ~ 18,5 pg/ml increase in unsupplemented cells (p = 0.047). **Figure 2. 2A** indicates where each of the inhibitors act in the PGE_2 biosynthesis pathway. Treatment of infected MA104 cells with inhibitors of PGE_2 biosynthesis, decreased the levels on PGE_2, with the indomethacin (p= 0.0008) and CAY10502 (p= 0,0004) having the biggest effect, followed by celecoxib (p = 0,00009) and SC560 (p= 0,0007) (**Figure 2. 2B**). To evaluate if PGE_2 production is viral load dependent, PGE_2 production was evaluated at different MOIs **(Figure 2. 2C).** The production of PGE_2 by mock-infected cells remained constant from 2 to 4 h post infection, while there was a steady increase in the amount of PGE_2 produced in cells infected at a MOI of 0.1 and 1. Interestingly, the production of PGE_2 increased rapidly in cells infected with a MOI of 10, appearing to peak at two hours

post infection. The difference in PGE_2 levels at different MOIs shows that SA11 modulates PGE_2 concentration in a time- and viral dose-dependent manner.

Chromatograms obtained from LC-MS/MS showed that all 5 transitions of PGE_2 were present in all the infected samples, thus authenticating its presence (**Figure 2. 3**). During multiple reaction monitoring, PGE_2 were measured by recording the signal for the transition of the deprotonated molecules of m/z 351 to the most abundant fragment ion of m/z 271. The discrepancy between ELISA and LC-MS/MS data for the mock control could be due to the ability of the ELISA to cross-react with PGE_2-ethanolamide and/or PGE_2-1-glycerylester or the inherently low concentration of PGE_2 in unstimulated cells (Funk, 2001). In addition, the discrepancy could also be attributed to the higher sensitivity of the ELISA compared to LC-MS.

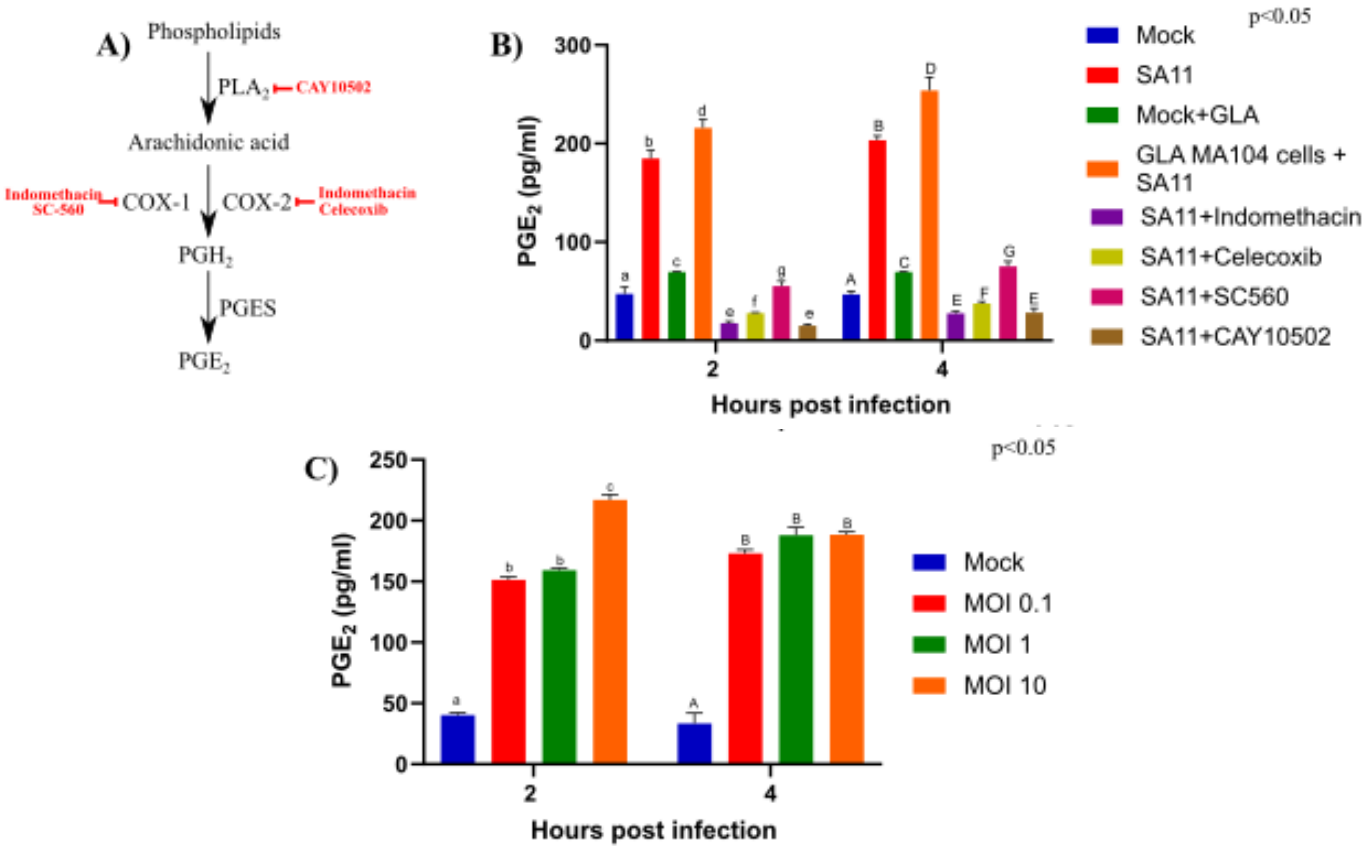

Figure 2. 2. Rotavirus increases the concentration of prostaglandin E_2 in MA104 cells in a dose- and time-dependent manner. A) CAY10502 inhibits the releases of AA from phospholipids, while indomethacin non-specifically inhibits both COX-1 and COX-2. In contrast SC-560 specifically inhibits COX-1 and celecoxib specifically inhibits COX-2. B) The amount of PGE_2 produced during rotavirus (SA11) infection (MOI = 5) as determined by ELISA was compared to uninfected MA104 cells (mock), in the presence and absence of γ-linolenic acid (GLA) and inhibitors of the PGE_2-biosynthetic pathway at two and four hours post infection). C) The amount of PGE_2 produced at increasing multiplicities of infection (MOI) at two and four hours post infection. Error bars indicate the standard error of the mean (n = 3). Lowercase and uppercase letters indicate a significant difference ($p<0.05$) compared to the control. Cyclooxygenases (COX1/2), phospholipaseA_2 (PLA_2), prostaglandin E_2 synthase (PGES), Prostaglandin H_2 (PGH_2), prostaglandin E_2 (PGE_2).,

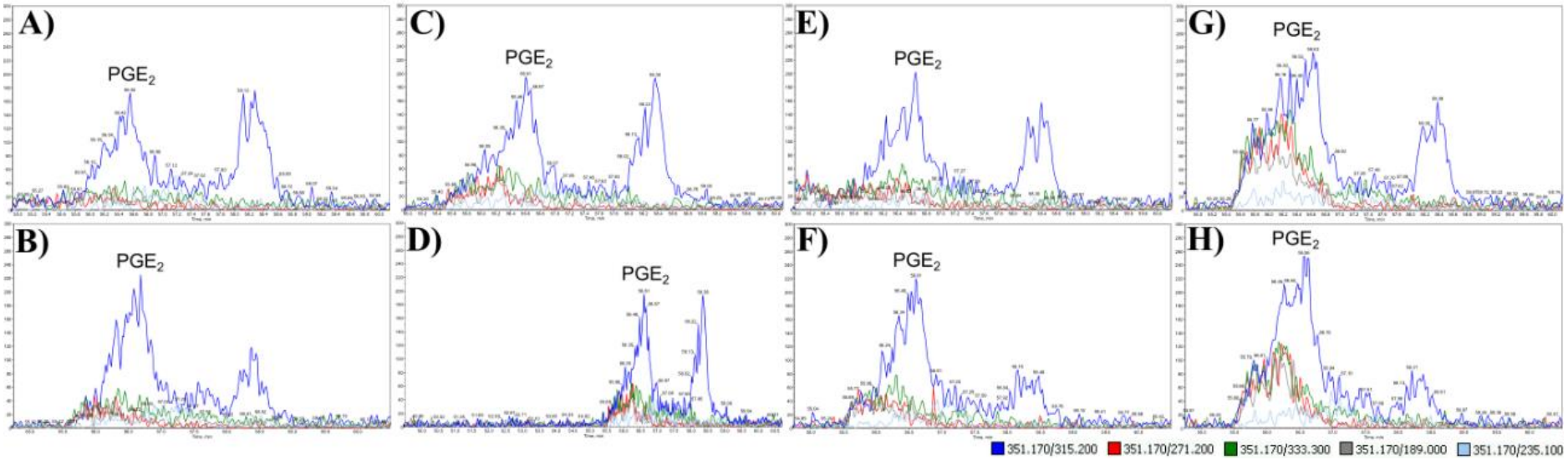

Figure 2. 3. Mass spectra showing the five transitions Multiple reaction monitoring (MRM) for each of the samples. Only one transition of PGE_2 is present in the mock infections at A) 2 h and B) 4 h and. All five the transitions of PGE_2 are present in cells infected at a MOI 0.1 (C and D) and 1 (E and F) at 2 h (C and E) and 4 h (D and F) post infection, respectively. Furthermore, all five the transitions of PGE_2 are present in cells infected at a MOI of 10 t G) 2 h and H) 4 hours post infection. Due to very low signal to noise ratios the LC-MS/MS data was only used to verify the presence of PGE_2. Peaks show the relevant transitions 351.17 > 315.2; 351.17 > 271.2; 351.17 > 333.3; 351.17 > 189.0; 351.17 > 235.1. Prostaglandin E_2 (PGE_2).

2.3.3. Prostaglandin E_2 and rotavirus co-localise

Lipid droplets are known sites for PGE_2 synthesis (Accioly et al., 2008; Bozza et al., 2011) and RV viroplasms are known to associate with LDs (Cheung et al., 2010). Therefore, to assess if there is co-localisation between viroplasms and PGE_2, we targeted NSP5 and NSP2 to visualise viroplasms. Both anti-NSP2 and anti-NSP5 antibodies were able to independently detect viroplasms (**Figure 2. 4B&C**). As expected, cells treated with indomethacin showed no co-localisation due to reduced PGE_2 production (**Figure 2. 4D**). Indomethacin is a non-specific inhibitor of both COX-1 and COX-2 (Mitchell et al., 1993) and is included in the EicosaCell procedure as negative control to inhibit PGE_2 production (Bandeira-Melo et al., 2011). Co-localisation, albeit at a relativly low level, was observed 2 hours post infection in unsupplemented (**Figure 2. 4E**) and GLA supplemented cells (**Figure 2. 4F**)**.** This observation is confirmed by the Pearson:Pearson correlation coefficient (0.40; **Figure 2. 4**). An increase in co-localisation was observed 4 hours post infection (**Figure 2. 4G&H**) with the Pearson:Pearson correlation coefficient reaching a maximum of 0.81 (**Figure 2. 4**)**.**

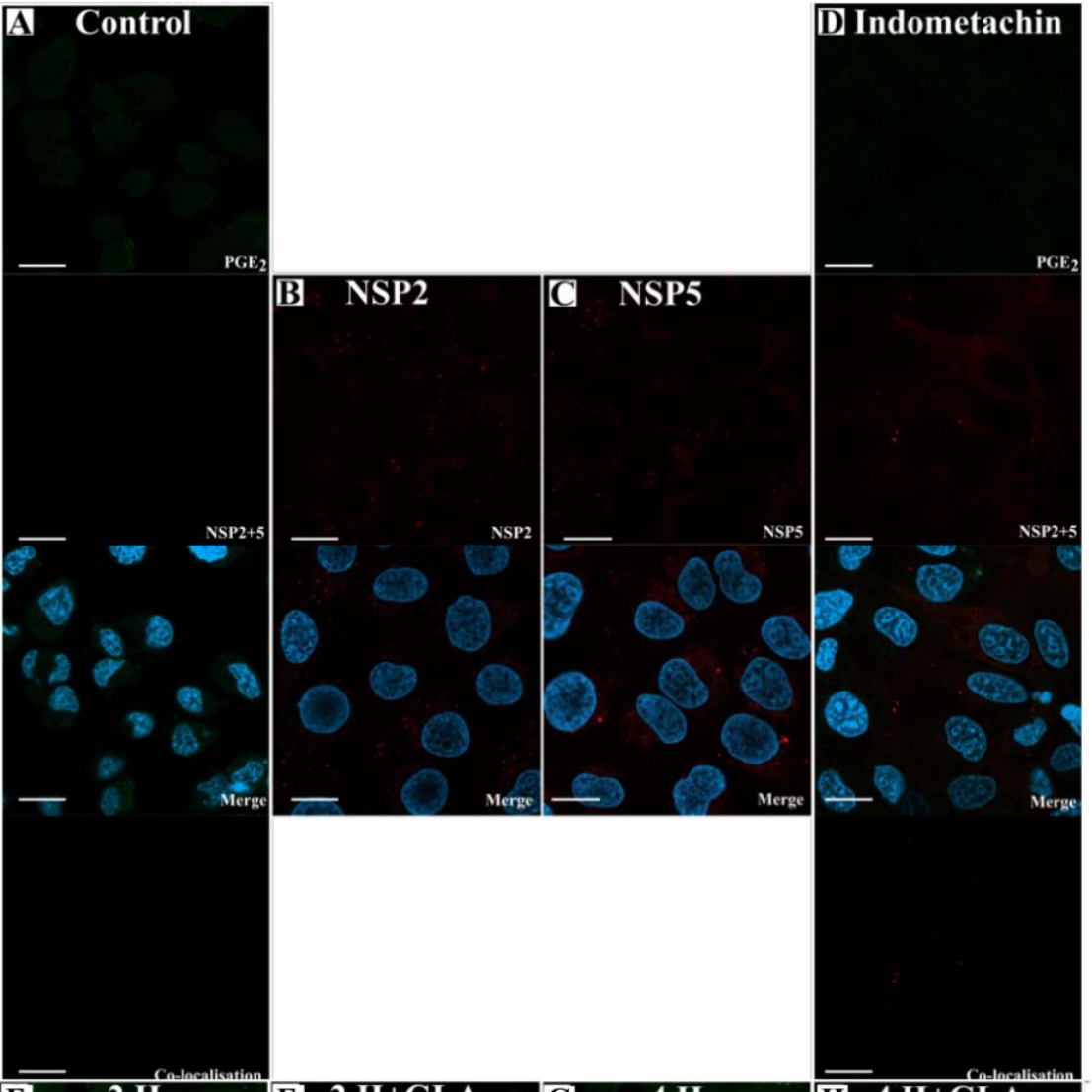
A Control
PGE2
NSP2+5
Merge
Co-localisation
B NSP2
NSP2
Merge
C NSP5
NSP5
Merge
D Indometachin
PGE2
NSP2+5
Merge
Co-localisation

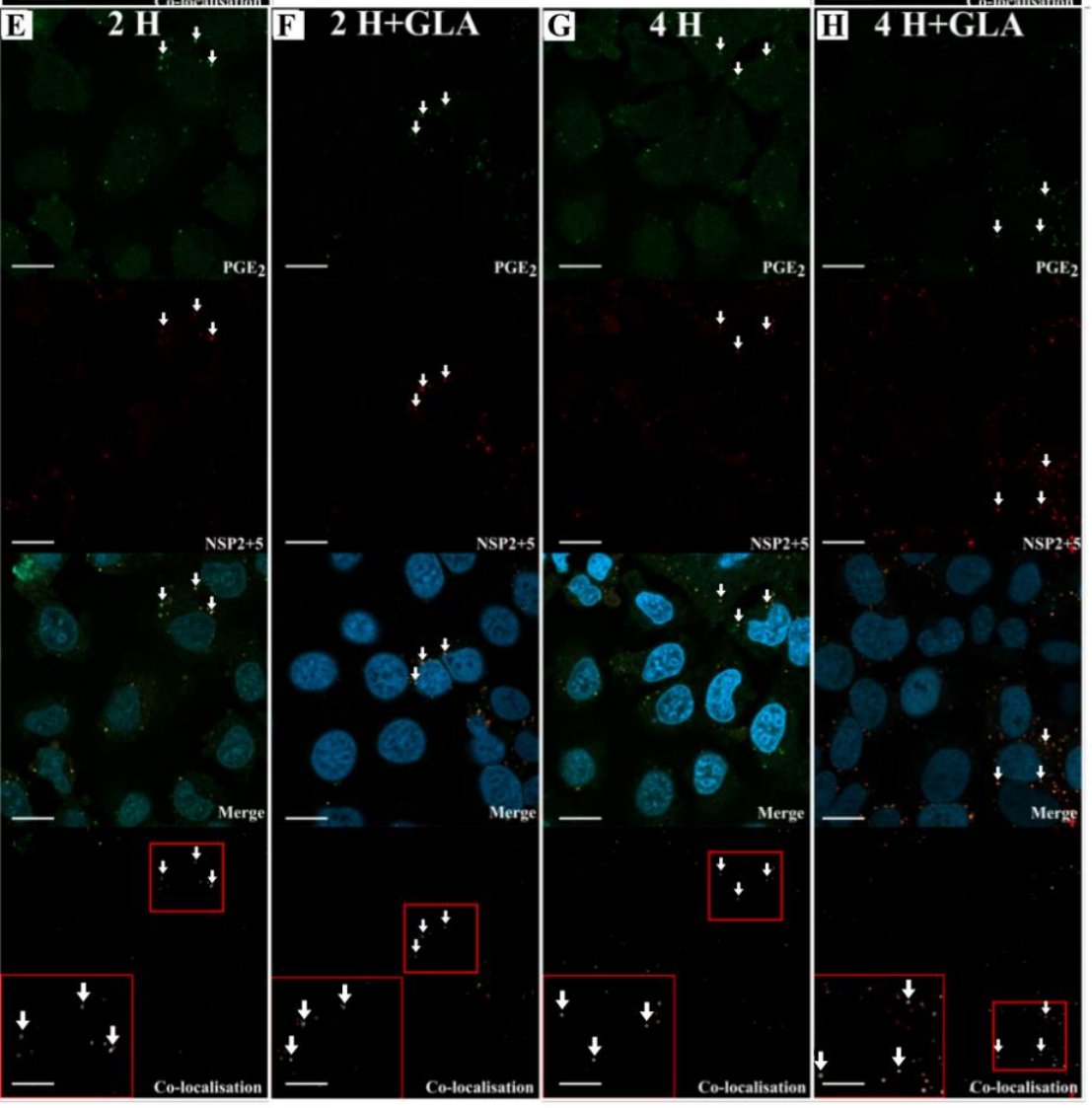
E 2 H
F 2 H+GLA
G 4 H
H 4 H+GLA
PGE2
NSP2+5
Merge
Co-localisation

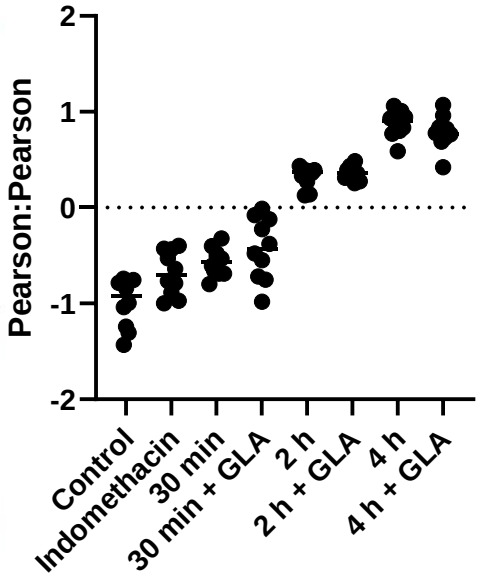
Pearson:Pearson
2
1
0
-1
-2
Control
Indomethacin
30 min
30 min + GLA
2 h
2 h + GLA
4 h
4 h + GLA

Figure 2. 4. Laser scanning microscopy images showing co-localisation between RV and PGE_2. The presence of co-localisation (white arrows) between PGE_2 (green) and RV NSP2 and NSP5 (red) was evaluated using Coloc2 in ImageJ. Blue DAPI-staining indicates cell nuclei. A) The no-virus control showed no detection of RV. The ability of the B) anti-NSP2 and C) anti-NSP5 antibodies to detect RV were independently assessed. D) The required inclusion of indomethacin shows no detection of PGE_2. After 2 hours post infection, NSP2 and NSP5 were detected in both E) GLA unsupplemented and F) supplemented cells, with co-localisation with PGE_2 first detected as suggested in the merge and confirmed in the co-localisation panels. Co-localisation increases at 4 hours post infection both in the G) absence or H) presence of GLA. Small red squares in the co-localisation panels indicate the area that was magnified and shown in the large red square in the same panel. Pearson:Pearson correlation coefficients of confocal microscopy images as determined by ImageJ are shown in the adjacent table (Schneider et al., 2012). Values close to -1 indicate no co-localisation with values close to 0 indicating random co-localisation, while values close to 1 indicate co-localisation with a (very) high degree of certainty. prostaglandin E2 (PGE_2). White arrows indicate co-localisation. Scale bar 10 µm.

2.3.4. Rotavirus replication is enhanced by changes in cellular lipids

In order to determine if the modulation of AA and GLA and the subsequent increase in PGE_2 had any effect on viral replication, we employed replication kinetics to determine the effect of GLA supplementation on the replication of SA11. The supplementation of MA104 cells with GLA increased the viral yield at 30 min (**Figure 2. 5*A*)**. This initial effect caused an approximate 1 log increase in the overall viral yield after the 16-hour period, compared to the unsupplemented MA104 cells. The addition of several PGE_2 biosynthetic inhibitors affected the yield of SA11 during the 16-hour period (**Figure 2. 5B**). Treatment of MA104 cells with indomethacin (non-specific COX inhibitor) caused the largest decrease in viral yield at 30 min, followed by CAY10502 ($cPLA_2$ inhibitor), celecoxib (COX-2 specific inhibitor) and SC-560 (COX-1 specific inhibitor). The rate of replication between different time-points is shown in **Figure 2. 5C**. Interestingly, the supplementation of MA104 cells with GLA only significantly increased the rate of replication between two and eight hours post infection, while the rate of replication remained comparable to the control at 30 minutes to two hours as well as between eight and 16 hours post infection. Similarly, the treatment of MA104 cells with PGE_2 biosynthesis inhibitors significantly decreased the rate of replication between 30 minutes to two hours, while no significant difference was observed at the other time points.

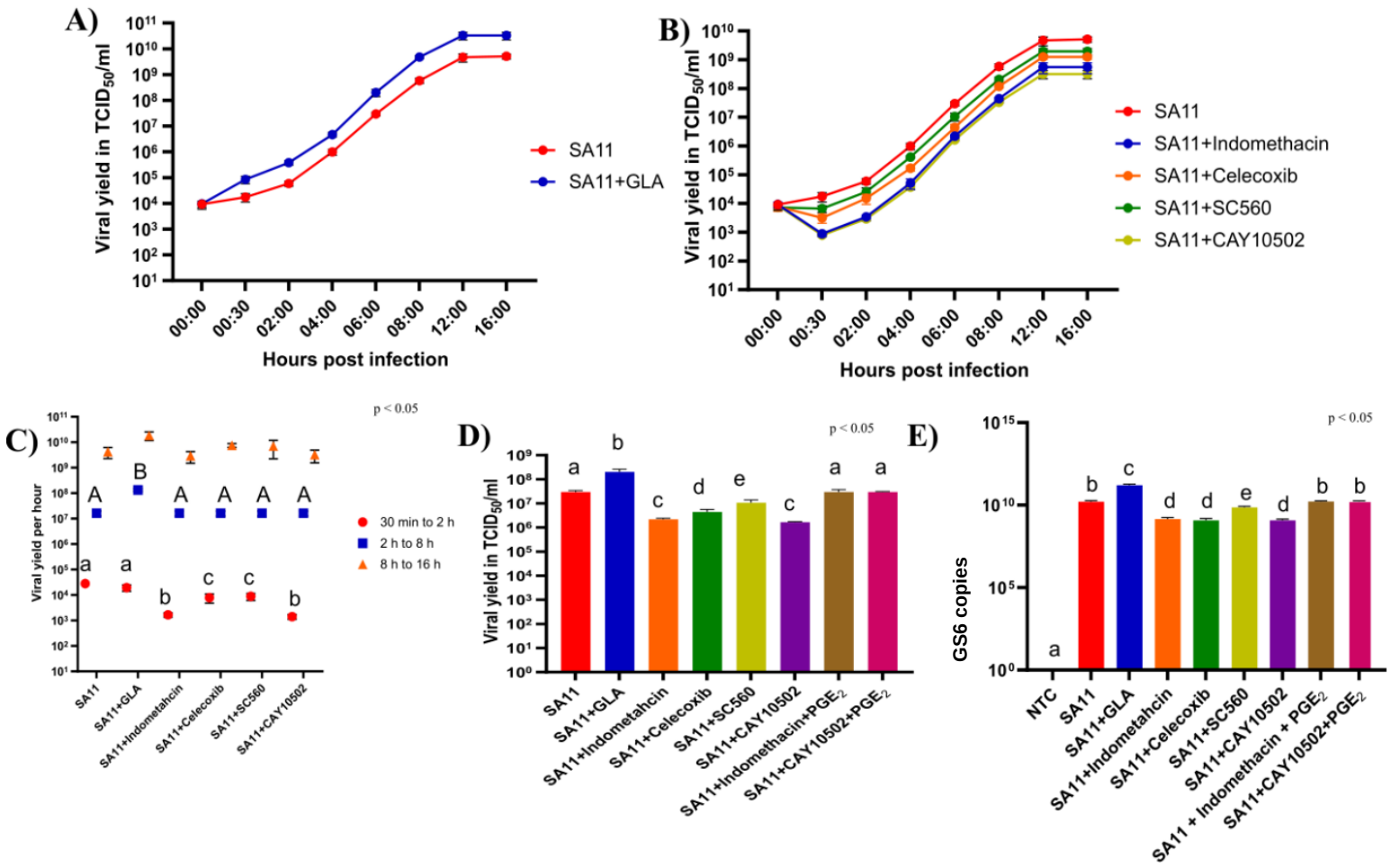

Figure 2. 5. GLA supplementation and treatment with inhibitors of PGE2 biosynthesis affect RV replication. A) Rotavirus yield determined by $TCID_{50}$ was compared to SA11-infected MA104 cells, in the presence and absence of γ-linolenic acid (GLA) and B) inhibitors of the PGE_2-biosynthetic pathway at several time points post infection. C) The replication rate of rotavirus as determined by calculating the slope between 30 min and 2 hours (red), 2 hours and 8 hours (blue) or 8 hours and 16 hours (orange), was compared to SA11-infected MA104 cells, in the presence and absence of γ-linolenic acid (GLA) and inhibitors of the PGE_2-biosynthetic pathway. D) Rotavirus yield as determined by $TCID_{50}$ and E) copy number of VP6 as determined by RT-qPCR was compared to SA11-infected MA104 cells, in the presence and absence of γ-linolenic acid (GLA) and inhibitors of the PGE_2-biosynthetic pathway at 6 hours post infection. Error bars indicate the standard error of the mean (n = 3). Lowercase and uppercase letters indicate significant difference ($p<0.05$) compared to the control. For further details see Table 2. 1.

To ensure that the effect of the inhibitors on viral yield was due to their inhibitory effect on PGE_2 biosynthesis, viral yield was determined with indomethacin in the presence of 0.1 µM PGE_2 at 6 h post infection (**Figure 2. 5D**). In addition, RNA production was determined with RT-qPCR, targeting the genome segment encoding VP6, and calculating the relative copy number in GLA supplemented MA104 cells and in cells treated with the different PGE_2 biosynthesis inhibitors (**Figure 2. 5E**). GLA supplementation of MA104 cells and subsequent infection with SA11, significantly increased both viral yield and the copy number of the VP6 genome segment. In contrast, treatment of SA11 infected MA104 cells with COX inhibitors significantly decreased the viral yield and copies of the VP6 genome segment. The viral yield was most affected by indomethacin and CAY10502, followed by celecoxib and SC-560. Interestingly, indomethacin, CAY10502 and celecoxib appear to have the same decreasing effect on the copy number of the VP6 genome segment, while SC-560 has the least potent effect. The addition of PGE_2 to MA104 cells treated with indomethacin or CAY10502, restored both the viral yield and copies of VP6 to control levels, indicating that PGE_2 is important for SA11 replication in MA104 cells.

2.3.4. Cyclooxygenase inhibition and GLA supplementation affect rotavirus internalisation

Due to the effect of GLA supplementation and inhibition of PGE_2 biosynthesis observed during the initial stages on SA11 replication, we used flow cytometry to determine if PGE_2 and GLA supplementation play a role during the attachment and/or internalisation of SA11. **Figure 2. 6A** shows the principle of the internalisation and attachment assay. Briefly, RV was allowed to cold-bind to MA104 cells. The virus was then subsequently tagged with anti-RV-FITC, which detects the outer capsid protein VP7, indicating the percentage of attached virus. When RV is internalised and released from the endosomes, the shedding of the outer layer exposes VP6 and allows for tagging with anti-DLP (targeting the outer VP6-layer of the DLP) and Alexa Fluor 532, quantifying intracellular RV.

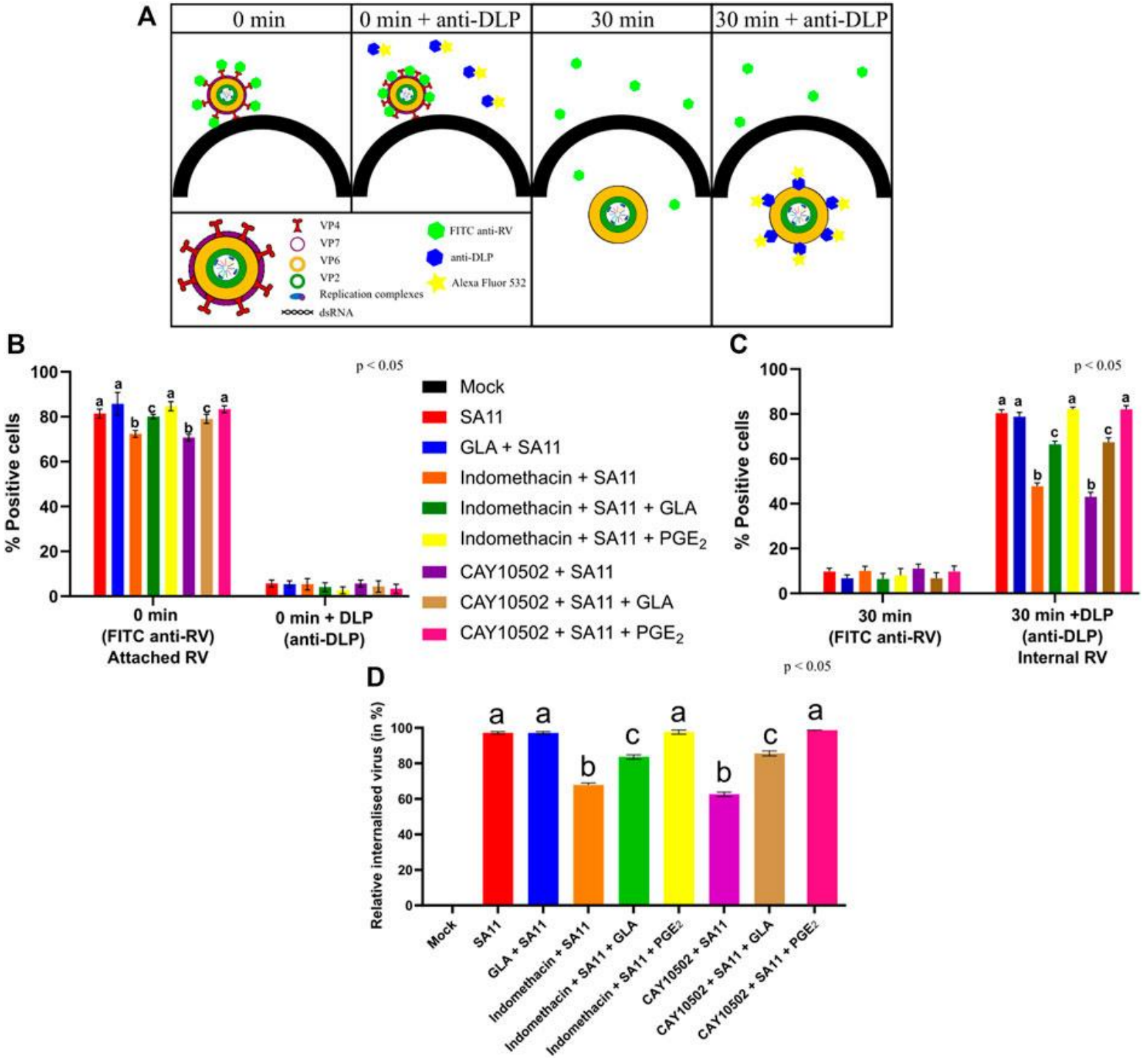

Figure 2. 6. Inhibition of PGE_2 biosynthesis affects RV attachment and internalisation. A) At time zero, RV at an MOI = 10, is cold-bound to MA104 cells and is visualized by anti-RV-FITC labelling, which detected the outer capsid protein VP7. When labelling with anti-double layered particle (DLP) is applied, virus at the cell surface cannot be detected as the antibodies target the middle-layer protein, VP6, which is only accessible after the outer layer has been shed. Thus, the signal intensity of 0 min + anti-DLP is strongly reduced compared to 0 min + anti-RV due to the inability to detect VP6. When the temperature is increased form storage on ice to 37 °C, RV is internalized and the loss of the outer capsid allows for the detection of VP6, i.e., DLPs, to be accessible for staining. B) Graph showing a higher positive detection of anti-RV-FITC compared to anti-DLP at 0 min. C) Graph showing a higher positive detection of anti-DLP compared to anti-RV-FITC at 30 min. D) Relative percentage of internalized virus from untreated and inhibitor-treated cells at 30 min post infection is calculated by dividing the relative internalised RV (30 min; C) by relative attached RV (0 min; B). Error bars indicate the standard error of the mean (n = 3). Lowercase letters indicate significant differences ($p<0.05$) compared to the control. **F**or further details **see** Table 2. 2**.**

Internalisation was calculated by dividing the relative percentage intracellular RV (30 min + DLP) by the relative percentage attached RV (0 min). Results compiled from raw flow cytometry data (**Figure 2. 6B**) indicate that the supplementation of MA104 cells with GLA had no significant effect (p= 0.067) on SA11 attachment, but the treatment of MA104 cells with indomethacin (p =0.008) and CAY10502 significantly decreased (p= 0.019) the percentage of attached SA11. The addition of exogenous PGE_2 to the inhibitor-treated cells fully restored the percentage of attached SA11. Interestingly, the supplementation of inhibitor-treated cells with GLA only partially restored the percentage of attached SA11, indicating that the amount of PGE_2 produced from GLA may not be sufficient to completely restore attachment. **Figure 2. 6C** shows the amount of RV that was internalised after 30 min. Although the effect of PGE_2 inhibition on attachment is significant, the effect on internalisation is much more pronounced (**Figure 2. 6D**). Treatment of MA104 cells with either indomethacin (p= 0.0014) or CAY10502 (p= 0.003) decreased the percentage of internalised SA11, while the addition of exogenous PGE_2 fully restored the percentage of internalised SA11 and GLA supplementation only partially restored the percentage of internalised SA11. This shows a role of PGE_2 during both the attachment and internalisation of SA11.

2.4. Discussion

Lipids and in particular LDs are crucial for RV replication, as chemical compounds affecting the integrity of LDs can disrupt viroplasms and subsequently, viral RNA replication and progeny production (Cheung et al., 2010; Crawford and Desselberger, 2016). Previously it was shown that supplementation of cells with saturated fatty acids increased RV yield (Superti et al., 1995).

Prostaglandin E_2 is the most abundant prostanoid and exerts homeostatic, pro- and, in certain cases, anti-inflammatory effects in host cells (Park et al., 2006). Thus, it is not surprising that PGE_2 plays a role in the pathogenesis of several viruses, including human immunodeficient virus, influenza A and herpes simplex virus (Sander et al., 2017). Along with the aforementioned viruses, RV infection has been shown to increase PGE_2 levels in both *in vitro* (Rossen et al., 2004) and *in vivo* studies (Zijlstra et al., 1999), while increased levels of PGE_2 have also been found in the stool of children infected with RV (Yamashiro et al., 1989). In these studies, an increase in

PGE_2 was accompanied by an increase in RV yield as well as severity and longevity of gastroenteritis, while the inhibition of PGE_2 biosynthesis decreasing the duration of diarrhoea (Yamashiro et al., 1989).

In concurrence with previous studies (Yamashiro et al., 1989; Zijlstra et al., 1999; Rossen et al., 2004), we have also shown that SA11 increases the concentration of PGE_2 and that the GLA supplementation of MA104 cells leads to a further increase in the concentration of PGE_2. These increases in PGE_2 levels are time- and viral dose-dependent and coincide with the decrease in AA and GLA during RV infection (Sander, 2019). Supplementation of MA104 cells with GLA significantly increased the rate of RV replication between two and eight hours post infection, with no significant effect on the rate of replication earlier (30 minutes to 2 h) or later (8 to 16 h) during infection. This indicates that GLA has no effect on early replication, but may play a role later during replication, probably during the formation of viroplasms, as these occur approximately two hours post infection (Carreño-Torres et al., 2010), by increasing the amount of LD available as scaffolds (Exner et al., 2019).

It is well-known that PGE_2 is produced in LDs in response to external stimuli, such as viral infections (Accioly et al., 2008; Bozza et al., 2011). Furthermore, during RV replication, LDs serve as scaffolds for viroplasms (Cheung et al., 2010). Viroplasms consist of several viral proteins, with NSP2 and NSP5 being essential for their formation. Viroplasms start to form at 2 hours post infection and increase in number as infection progresses (Carreño-Torres et al., 2010; Contin et al., 2010). We show that co-localisation does occur between NSP2 and NSP5 and PGE_2 at two and four hours post infection. Interestingly, we show that co-localisation between NSP2 and NSP5 and PGE_2 increases as infection progresses and could be due to an increase in both the number of viroplasms that are formed and the increase in PGE_2 levels as shown by ELISA.

The inhibition of COXs have shown that these enzymes are essential during replication of several viruses (Steer and Corbett, 2003). Although, indomethacin is a well-known non-selective inhibitor of COX-1 (IC_{50}= 1,67 µM) and COX-2 (IC_{50}= 24,6 µM) it has several off-targets effects, including the inhibition of phospholipase A_2 (Kaplan et al., 1978). We therefore employed more specific inhibitors for COX-1 (SC-560, IC_{50}= 9

nM) (Smith et al., 1998), COX-2 (celecoxib, IC_{50}= 5 nM) (Uddin et al., 2003) and phospholipase A_2 (CAY10502, IC_{50}= 4,3 nM) (Ludwig et al., 2006). It should however be noted that celecoxib can also inhibit several other enzymes, such as carbonic anhydrases (IC_{50}= 16 nM), phosphoinositide-dependent kinase-1 (IC_{50}= 48 µM) and sarcoplasmic/ER calcium ATPase (Schönthal, 2007). It is therefore possible that at the concentration of celecoxib (5 µM) used in this study, carbonic anhydrases could also have been inhibited. However, the results for indomethacin and celecoxib correlate with that for the COX-1 (SC-560) and phospholipase A_2 (CAY10502) inhibitors. Phospholipase A_2 is also the rate-limiting enzyme during the biosynthesis of PGE_2 (Funk, 2001). In addition, the effects on RV replication and entry were neutralised when exogenous PGE_2 was added.

Treatment of MA104 cells with inhibitors of PGE_2 biosynthesis has negative effects on viral yield and on the rate of replication between 30 minutes and 2 hours post infection. This is in concurrence with Rossen and co-workers (2004), who determined that RV replication is negatively affected by treatment with PGE_2 biosynthesis inhibitors and indicated a role of PGE_2 during early RV replication. However, in contrast to their results, showing no effect on total RNA levels from RV GS10 and GS4 or on the (+) ssRNA and dsRNA derived from VP4, our results show that all the inhibitors had a negative effect on the RNA levels of the VP6 encoding genome segment. The discrepancy could be due to differences in experimental procedures used as well as the time point measured. In the current study, purified viral dsRNA was used in a RT-qPCR analysis, compared to a semiquantitative RT-PCR evaluation of total, single-stranded and double-stranded RNA by Rossen and co-workers (2004). The authors also determined dsRNA levels at 15 hours post infection, while we determined RNA levels at six hours post infection. The addition of exogenous PGE_2 to inhibitor treated cells, restored both the viral yield and RNA levels of GS6. Similar to the findings by Rossen and co-workers (2004), we show that there is no significant effect of PGE_2 biosynthetic inhibitors on late stage (8 – 16 hours) RV replication.

Due to the effect of PGE_2 biosynthesis inhibitors during early infection (0 min to 30 min) and in concurrence with previous data (Rossen et al., 2004), which show that the inhibitors are most potent when added at time-point zero, we investigated RV attachment and internalisation in the presence of PGE_2 biosynthesis inhibitors and

GLA supplementation. We show that the treatment of MA104 cells with inhibitors of PGE_2 significantly decreases the amount of RV that is internalised. The effect of early and non-specific inhibition of PGE_2 production suggests a role for PGE_2 during the early phase of SA11 infection. In addition, the significant difference ($p < 0.05$) in viral yield with cells treated with celecoxib and SC560 possibly indicates a more pronounced role for induced PGE_2 (via COX-2), consistent with previous data (Rossen et al., 2004). While the addition of exogenous PGE_2 restored the levels of RV that is internalised, supplementation with GLA only partially restored internalisation. In addition, the supplementation of MA104 cells with GLA does not significantly affect RV attachment, which is in concurrence with Superti and co-workers (1995) that showed the effect of fatty acid supplementation on viral replication did not affect attachment.

To conclude, we show that supplementation of MA104 cells with GLA increases rotavirus rate of replication during early infection, with no significant effect during later stages of replication. The observed increase in PGE_2 occurs irrespective of supplementation and could potentially enhance clathrin-dependent endocytosis of RV, as Cheng and co-workers (2015) showed that elevated levels of PGE_2 enhanced clathrin-mediated bovine ephemeral fever virus endocytosis via Cox-2-mediated PGE_2/PGE_2 receptor signalling. Furthermore, Robb and co-workers (2020) speculated that PGE_2 could affect the attachment of SARS-CoV-2 by modulating the expression of ACE2 and TMPRSS2, enhancing virus endocytosis by regulating lipid vesicle fusion. Although we show that there is co-localisation between PGE_2 and viroplasm associated proteins, further work needs to be done to determine if viroplasms play any role in the induction of PGE_2 production. In addition, it should also be pointed out that cytoplasmic calcium that is increased by NSP4 could lead to the translocation and activation of cytoplasmic phospholipase A_2, the rate-limiting enzyme in PGE_2 biosynthesis.

3.1. Introduction

During rotavirus (RV) replication, several viral proteins, together with cellular lipid droplets (LDs) form viral replication factories, called viroplasms (Papa et al., 2021). During replication, (+) single stranded RNAs (ssRNAs) of all 11 genome segments, as well as VP1, VP3, VP2 and VP6, which are all key players in the replication and production of new progeny virus can be found within viroplasm (Settembre et al., 2011; Estes and Greenberg, 2013). In addition, viroplasms also interact with cellular lipids and proteins(Cheung et al., 2010; Gaunt et al., 2013b, 2013a). This allows for packaging, assembly and subsequent release of DLPs into the cytosol. Interactions between NSP2 and NSP5 are essential for the formation of viroplasms, with the co-expression of both leading to the formation of viroplasm-like structures (VLS) (Eichwald et al., 2004; Contin et al., 2010). In addition, the inhibition of either NSP2 or NSP5 during RV replication has a deleterious impact on the production of infectious viral progeny (Silvestri et al., 2004; Vascotto et al., 2004; Campagna et al., 2005). In fact, recent modifications to the plasmid-only-based reverse genetics system for RVs, allowed for the generation of a rescued RV (rRV) unable to produce NSP5 but rescuable in cells expressing native NSP5 *in trans* (Papa et al., 2020).

Although it is well-known that NSP2 forms large octamers that have RNA-helix destabilizing, nucleoside diphosphate kinase and RNA chaperone activities the complete structure of NSP5 remains unknown (Taraporewala et al., 1999; Kumar et al., 2007; Borodavka et al., 2017; Bravo et al., 2018). During replication, NSP5 is hyperphosphorylated, and recombinant RV with Ser to Ala mutations, lead to the formation of aberrant spindle-like viroplasms and impaired viral replication (Poncet et al., 2000; Papa et al., 2020)(Poncet et al., 2000; Papa et al., 2020)(Poncet et al., 2000; Papa et al., 2020). In concurrence, work by Sen and co-workers (2007), showed that the 21 amino acids in the C-terminal of NSP5 are essential for VLS formation and play a role in the hyperphosphorylation of NSP5. Computer models of the C-terminal region predicted the presence of an amphipathic α-helix, that is highly conserved among RVs. Mutating hydrophobic amino acids in the hydrophobic face of the α-helix to proline, disrupted the formation of VLS (Sen et al 2007). Interestingly, the authors also identified a potential calcium switch, formed by two tandem pseudo-EF-hand motifs

(DxDxD). Removal of the DxDxD resulted in punctate VLS, leading the authors to propose calcium as trigger for the formation of VLS.

In addition to viral proteins, cellular LDs are essential for the formation of functioning viroplasms (Cheung et al., 2010). Lipid droplets are now considered fully functioning organelles with several functions including biosynthesis of eicosanoids such as prostaglandin E_2 (PGE_2)(Jarc and Petan, 2020). Prostaglandin E_2 is a well-known immunodulatory eicosanoid that has proviral effects on several viruses, including RV (Sander et al., 2017).

The aim of the study is to determine the role of viroplasm associated proteins (NSP2 and NSP5) or formation of VLSs in the induction of PGE_2 production during infection. In addition, the study aims to determine if viroplasms themselves play any role in the induction of PGE_2 production during infection.

3.2. Materials and Methods

3.2.1. Cells and virus

Human embryonic kidney 293 (HEK293) and MA104 cells were maintained in Dulbecco's modified Eagle medium (DMEM) (Gibco), supplemented with 5 % (v/v) foetal bovine serum (FBS) (Gibco, USA), 1 % (v/v) Penicillin-Streptomycin-Amphotericin B Mixture (10 000 U, 10 000 µg and 25 µg per ml) (Gibco, USA), and 1 % (v/v) nonessential amino acids (NEAA) (Gibco, USA) at 37°C and 5 % CO_2. MA104-NSP5 was maintained under the same conditions with the addition of 500 µg/ml Geneticin™ (G-418) (Gibco, USA). Rotavirus simian agent 11 strain, SA11 (Mlera et al., 2013) was used to infect MA104 cells and viral yield was determined using 50 % tissue culture infectious doses, $TCID_{50}$ (Reed and Muench, 1938). To facilitate infection, pancreatic porcine trypsin type IX (1 µg/ml; Sigma Aldrich) was added during all viral replication experiments.

3.2.2. Expression and co-expression of NSP2 and NSP5

Using the mammalian dual expression vector, pBudCE4.1 (Invitrogen, USA), expression plasmids were previously engineered to contain the open reading frame (ORF) for pBudNSP2, pBudNSP5 or pBudDual (NSP2 and NSP5). Since coding sequences for either V5 and 6x His tags or *myc* and 6x His tags were included at the 3’ ends of the ORFs, stop codons were inserted to exclude these tags during

expression using the primers listed in **Table 3. 1**. Each reaction contained 1 x Phusion HF Buffer, 10 µM dNTPs (Thermo Fisher Scientific, USA), 0.3 µM each for forward and reverse primers, 0.02 U Phusion DNA polymerase and nuclease-free H_2O (Sigma-Aldrich, USA). PCR amplicons were then phosphorylated with 10U of T4 polynucleotide kinase (Thermo Fisher Scientific, USA) for 30 min at 37°C and subsequently ligated with 1U of T4 DNA ligase (Thermo Fisher Scientific, USA) overnight and transformed into DH5-α™ *Escherichia coli*. The integrity of the mutant plasmids after cloning was confirmed by digestion with the corresponding restriction enzyme and Sanger sequencing.

Table 3. 1. Mutagenic primers designed for pBudCE4.1-NSP2 and pBudCE4.1-NSP5.

	PRIMER	**PRIMER SEQUENCE**
Amplification of NSP2	pBudNSP2_F	TCTCAAGTTGGCGTTTAATAAGGTAAGCC
	pBudNSP2_R	AGGGATAGGCTTACCTTATTAAACGCCA
Amplification of NSP5	pBudNSP5_F	TTGATTGAAGATTTGTGATAAGAACAAA
	pBudNSP5_R	GATGAGTTTTTGTTCTTATCACAAATCT

HEK293 cells were seeded in 6-well plates (7×10^5 cells per well) and incubated for 24 hours at 37°C and 5 % CO_2. At 90 % confluency, the cells were transfected with the pBudNSP2, pBudNSP5 or pBudDual (2.5 µg) using 5 µL of P3000™ reagent and 3.75 µL Lipofectamine™ 3000 Reagent (Thermo Fisher Scientific, USA). The cells were incubated with the transfection mixture for 48 h at 37˚C and 5 % CO_2 before the supernatant was harvested for PGE_2 analysis, while the cells were either lysed to determine protein expression or subjected to immunofluorescent staining.

3.2.3. Generation of mutant viruses

3.2.3.1. Generation of stable cell line

The plasmid encoding mutant pcDNA™3.1$^{(+)}$-NSP5 was generated using NEBuilder® HiFi DNA Assembly Cloning Kit (NEB, USA). Briefly, fragments were amplified from their respective sources (**Appendix C**) using the primers in **Table 3. 2** and using Phusion DNA polymerase as previously described. After digestion with DpnI, the insert and vector fragments were added to the NEBuilder® HiFi DNA Assembly Master Mix and nuclease-free H_2O at a ratio of 2:1 and allowed to assemble for 30 min at 50°C. The assembled fractions were then transformed into DH5-α™ *Escherichia coli*. The integrity of the mutant plasmids after cloning was confirmed by digestion with the corresponding restriction enzyme and Sanger sequencing.

Table 3. 2. List of primers used in the construction of pcDNA™3.1(+)-NSP5

	PRIMER	PRIMER SEQUENCE
Amplification of NSP5	pcDNANSP2_F	TAGAGGGCCCATGTCTCTCAGTATTGACG
	pcDNANSP2_R	ATCAGCGGGTCTTATCACAAATCTTCAATCAATTG
Amplification of pcDNA™3.1$^{(+)}$ vector backbone	NSP5_F	TTGTGATAAGACCCGCTGATCAGCCTCG
	NSP5_R	TGAGAGACATGGGCCCTCTAGACTCGAG

MA104-NSP5 cells were generated using pcDNA™3.1$^{(+)}$ containing the open reading frame for NSP5. Briefly, MA104 cells were maintained in DMEM supplemented with 5 % FBS. Approximately 7 x 10^6 MA104 cells were seeded in 6 well culture plates 24 h before transfection. For each well, 2.5 µg of pcDNA™3.1$^{(+)}$-NSP5 was transfected with Lipofectamine 3000 (Sigma-Aldrich, USA) according to the manufacturer's instructions. After 48 h, the MA104 cells were selected for NSP5 expression for 14 days by replacing the media with DMEM containing 2 % Geneticin. After 14 days the MA104 cells were diluted (10^{-3} to 10^{-8}) in 24 well culture plates to further ensure the selection of MA104 cells stably expressing NSP5. The surviving cells were upscaled to 25 cm^2 tissue culture flasks, whereafter the expression of NSP5 was determined by western blot analysis and immunofluorescent microscopy.

3.2.3.2. Construction of transcription plasmids pT7SA11_aNSP5 and pT7SA11_pNSP5

An overview of all unmodified NSP5-encoding genome segments is provided in **Figure 3. 1A**. **Figure 3. 1B** indicates the exact location of the amino acid substitutions for each plasmid encoding rSA11_aNSP5 and rSA11_pNSP5. To determine what effect the mutations would have on the hydrophobicity and structure of NSP5 C-terminal region, we used a helical wheel program (Pepwheel; available online at https://www.bioinformatics.nl/cgi-bin/emboss/pepwheel) and a protein prediction program [Phyre version 2, (Kelley et al., 2015)].

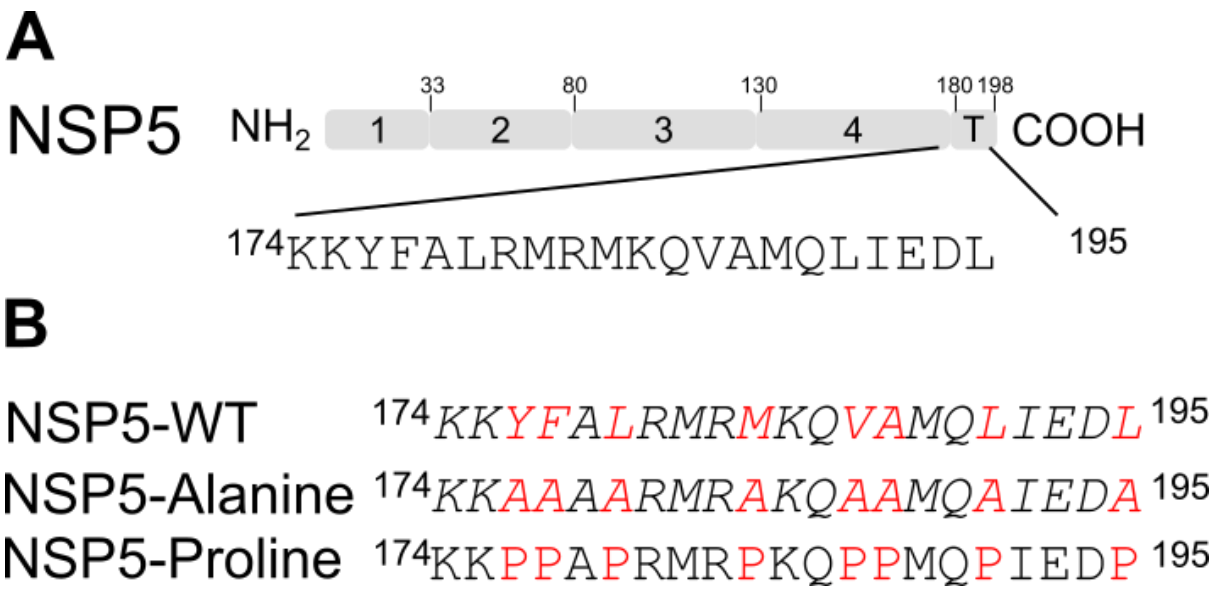

Figure 3. 1. Schematic representation of NSP5 and alanine- and proline-directed NSP5 peptides. (A) Linear schematic of NSP5 and unmutated SA11 sequence of the amphipathic tail region (T, aa180–198) (B) Linear schematic of the two NSP5 proteins corresponding to wild-type (NSP5-WT) alanine mutated (NSP5-Alanine), or proline mutated (NSP5-Proline) sequences. The primary sequence of the NSP5-WT peptide details the mutations (italicized and in red) in the amphipathic domain.

The transcription plasmids encoding the eleven simian SA11 genome segments (Kanai et al., 2017) as well as the two helper plasmids (phCMVdream-C3P3 and pCAG-FAST-p10) were a kind gift from Prof. Albie van Djik (North-West University). The plasmids encoding mutant rSA11_aNSP5 and rSA11_pNSP5 were generated using NEBuilder® HiFi DNA Assembly Cloning Kit (NEB, USA). Briefly, fragments were amplified from their respective sources (**Appendix C**) using the primers in **Table 3. 3** and using Phusion DNA polymerase as previously described. The mutated encoding region of NSP5 was amplified from plasmids purchased from GenScript (USA), while the backbone was amplified from the T7 plasmid, excluding the region encoding NSP5. After digestion with DpnI, the insert and vector fragments were added to the NEBuilder® HiFi DNA Assembly Master Mix and nuclease-free H_2O at a ratio of 2:1 and allowed to assemble for 30 min at 50°C. The assembled fractions were then transformed into DH5-α™ *Escherichia coli*. The integrity of the mutant plasmids after cloning was confirmed by digestion with the corresponding restriction enzyme and Sanger sequencing.

Table 3. 3. List of primers used in the construction of pT7-aNSP5, pT7-aNSP5 and pcDNA™3.1(+)-NSP5

	PRIMER	PRIMER SEQUENCE
Amplification of NSP5	pT7aNSP5_F	GTTCCCAGGTCAGACTTACGCGTCCTCGATGGCCTG
	pT7aNSP5_R	CTTTTAAAGCGCTACAGTGATGAGCCTGAGCATCGATG
	pT7pNSP5_F	GTTCCCAGGTCAGACTTACGGGTCTTCGATCGGCTG
	pT7pNSP5_F	CTTTTAAAGCGCTACAGTGATGAGCCTGAGCATCGATG
Amplification of pT7 vector backbone	aNSP5_F	ATCGATGCTCAGGCTCATCACTGTAGCGCTTTAAAAG
	aNSP5_R	CAGCCGATCGAAGACCCGTAAATCTAGATGCATTCG
	pNSP5_F	ATCGATGCTCAGGCTCATCACTGTAGCGCTTTAAAAG
	pNSP5_R	CAGCCGATCGAAGACCCGTAAATCTAGATGCATTCG

3.2.3.3. Transfection of pT7SA11 transcription plasmids

BSR T7/5 cells were seeded in 6-well plates (7×10^5 cell per well) and incubated for 24 hours at 37°C and 5 % CO_2. At 90 % confluency, the cells were rinsed and serum-free DMEM was added to the cells, afterwards the cells were co-transfected with 11 plasmids encoding the individual RV genome segments (2250 ng for the plasmids encoding NSP2 and NSP5 or rSA11_aNSP5, rSA11_pNSP5; 750 ng for the remaining plasmids) and two helper expression plasmids encoding African swine fever virus capping enzyme (750 ng each) as well as a small membrane fusion protein (Duncan, 2019) (15 ng) using 30µL of TransIT-LT1transfection reagent (Mirus Bio, USA). The cells were incubated with the transfection mix for 48 h DMEM at 37°C and 5 % CO_2. Forty-eight hours later, 1×10^5 MA104/MA104-NSP5 cells were added to the transfected BSR T7/5 cells, and trypsin was added to a final concentration of 1 µg/mL. After three days at 37°C and 5 % CO_2, the co-cultured cells were frozen and thawed three times before passaging on MA104/MA104-NSP5 cells.

3.2.3.4. Passaging

Pancreatic porcine trypsin type IX solution was added to the entire freeze/thaw supernatants (2 mL, 1µg/mL trypsin final concentration), and the mixture was incubated for 1 hour at 37°C. Confluent MA104/MA105-NSP5 cells grown in 6 well plates were washed three times with PBS, after which the infection mixture was added to the cells. After 1 hour at 37°C and 5 % CO_2, the mixture was removed, and the cells were washed once with unsupplemented media. Infection media (DMEM without serum, containing 1µg/mL trypsin) was added, and the cells were incubated for 7 days before they were passaged again following the same protocol. Negative and positive rescue results for mutant constructs were confirmed using PCR amplification and restriction digestion analyses as described below.

3.2.3.5. Confirmation of rescued viruses

Once the cell monolayer showed ~ 60 % cytopathic effect (CPE), the supernatant was removed and TRIzol® reagent (Invitrogen, USA) was added directly onto the remaining cells to facilitate RNA extraction as described by Potgieter and co-workers (2009).

To distinguish wild type SA11 (wt-SA11) from rescued SA11 (rSA11) virus and ensure mutants (rSA11_aNSP5 and rSA11_pNSP5) were correct, cDNA synthesis, PCR and restriction enzyme digestions were performed. Genome segments encoding NSP2 and NSP4 were amplified for all rescued viruses to identify genetic markers (Kanai et al., 2017), which were previously added to these encoding segments to allow for screening of rescued viruses (van der Schyff, 2021), using primers listed in **Table 3. 4**. cDNA synthesis was performed using the AMV First Strand cDNA Synthesis Manual (Promega, USA). Briefly each reaction, contained up to 1 µg RNA, 12 µM Primer mix, 1 x AMV Buffer, 2 U AMV reverse transcriptase, 0.5 mM dNTP mix, and Nuclease-free H_2O. The RNA and primer mix was incubated together at for 5 min at 95°C and subsequently chilled on iced for 5 min. The rest of the components were added and incubated for 2 h at 42°C, after which the AMV reverse transcriptase was inactivated at 85°C for 5 min.

Table 3. 4. List of primers for the amplification of RVA genome segments.

	PRIMER	**PRIMER SEQUENCE**
Amplification of NSP2	rNSP2_F	GGTCACATAAGCGCTTTCTA
	rNSP2_R	GCWYACRYTAACACCRTTCC
Amplification of NSP4	rNSP4_F	AGTTCTGTTCCGAGAGACC
	rNSP4_R	GGWYACRYTAAGACCRTTCC

The cDNA templates were amplified using primers listed in **Table 3. 4** and using Phusion DNA polymerase as previously described. The cycling parameters were as follows: 95°C for 2 min; 25 cycles of 98°C for 10 s, 55°C for 15 s and 72°C for 30 s; 72°C for 5 min. PCR products were cleaned using the Zymogen Gel DNA Recovery Kit (Zymo Research, USA) to remove residual PCR components that could interfere with downstream DNA analysis. The amplified genome segments were evaluated using restriction digestion analysis. rNSP4 was digested overnight at 37°C with XbaI (Thermo Fisher Scientific, USA), while rNSP2 was digested with BstUI (Thermo Fisher Scientific, USA). Digestions were analysed on 2 % agarose gel.

To obtain full-length sequences, an anchor primer (PC3-T7loop; Integrated DNA Technologies) was ligated to the dsRNA as previously described (Potgieter et al., 2009) and next generation sequencing and analysis of CLCbio was done as described by Strydom and co-workers (2019).

3.2.4. Prostaglandin E_2 quantification

Quantification of PGE_2 production in HEK293 cells transfected with a plasmid encoding for NSP5 only or co-transfected with a plasmid encoding for NSP2, or infected with rSA11, rSA11_aNSP5 or rSA11_pNSP5 were determined as previously described in Section 2.2.3.

3.2.5. Confocal-laser scanning microscopy (CLSM)

Co-localisation of PGE_2 with NSP5 in HEK293 cells transfected with a plasmid encoding for NSP5 only or co-transfected with a plasmid encoding for NSP2, or infected with rSA11, rSA11_aNSP5 or rSA11_pNSP5 were determined as previously described in section 2.2.4. In addition to co-localisation with PGE_2, co-localisation in cells infected with rSA11, rSA11_aNSP5 or rSA11_pNSP5 with LDs were also determined. After infection, the cells were sequentially stained for LDs and NSP5. Briefly, cells were fixed in 4 % paraformaldehyde at room temperature for 10 min. The cells were then stained for NSP5 as previously described and LDs were stained using BODIPY 493/503 (4,4-difluoro-1,3,5,7,8 pentamethyl-4-bora 3a,4a-diaza-s-indacene; 1 µg/ml, diluted from 1-mg/ml stock in dimethyl sulfoxide; Thermo Scientific, USA).

3.2.6. Replication kinetics, RNA isolation and RT-qPCR

The yield of GS6 in HEK293 cells infected with rSA11, rSA11_aNSP5 or rSA11_pNSP5 were determined at 2 and 6 hours post infection as previously described in section 2.2.6.

3.2.7. Co-sedimentation of Lipid droplets and NSP5

HEK293 cells were seeded (1 x 10^7 cells/ml) in 175 cm^2 tissue culture flasks and incubated for 24 hours at 37°C and 5 % CO_2. The cells were then either transfected with 45 µg plasmid containing the ORF for NSP5 or both NSP2 and NSP5 with Lipofectamine 3000 (Sigma-Aldrich) according to the manufacturer's instructions and incubated for 48 h or infected with rSA11, rSA11_aNSP5, rSA11_pNSP5 at a MOI of

5 for 2 and 6 h. The HEK293 cells were scraped off and washed twice with PBS whereafter LDs were isolated from 200 mg wet weight, using the LD isolation kit from Abcam (UK), as indicated by the manufacturer. A gradient is then created with the homogenate, and the material is centrifuged at 3000 x g for 3 h. The lipid droplets float to the top of the gradient and are recovered by carefully pipetting from the top of the gradient. Five fractions of 270µL were sequentially removed from the top of the gradient and the proteins were precipitated by the addition of 4 volumes of 100 % EtOH and incubated overnight at -20°C. After overnight incubation, the solution was centrifuged for 15 000 x g for 15 min at 4°C, the supernatant discarded, the protein resuspended in Laemmli sample buffer, containing β-mercaptoethanol, and used in western blot analysis. For immunoblotting, membranes were incubated with the following primary antibodies: anti-rabbit NSP5 (1:1,000) and anti-rabbit ADRP (1:5,000; Thermo Scientific, USA). The membranes were then incubated with the corresponding horseradish peroxidase (HRP)-conjugated goat anti-rabbit sera (1:10,000; Thermo Scientific, USA). Signals were detected using the enhanced chemiluminescence system (Pierce ECL Western blotting substrate; Thermo Scientific).

3.2.8. Statistical analysis

Each assay was carried out at least in triplicate (biological/independent replicates) on separate days. Each repeat was analysed in triplicate (n = 3). Data are presented as means ± standard error of the mean. For statistical analysis, two-way analysis of variance (ANOVA) was performed using a Tukey-Kramer test in R studio software (2022.7.1.554) for Windows (R studio, USA). In all tests, $p < 0.05$ was considered statistically significant. Co-localisation in CLSM experiments were verified using Pearson:Pearson correlation coefficients in ImageJ.

3.3. Results

3.3.1. Design of mutated SA11-based NSP5 viruses

Sen and co-workers (2007) showed that mutating the hydrophobic amino acids in the C-terminal of NSP5 to proline or alanine affected the formation of VLS when co-expressed with NSP2. We decided to investigate the role of both hydrophobicity and the amphiphilicity in the α-helix found within the C-terminal of NSP5. To determine the effect of the mutations (**Figure 3. 1**) on structure of the α-helix, we employed Phyre2 (Kelley et al., 2015). The C-terminal of wildtype NSP5 forms a predicted α-helix (

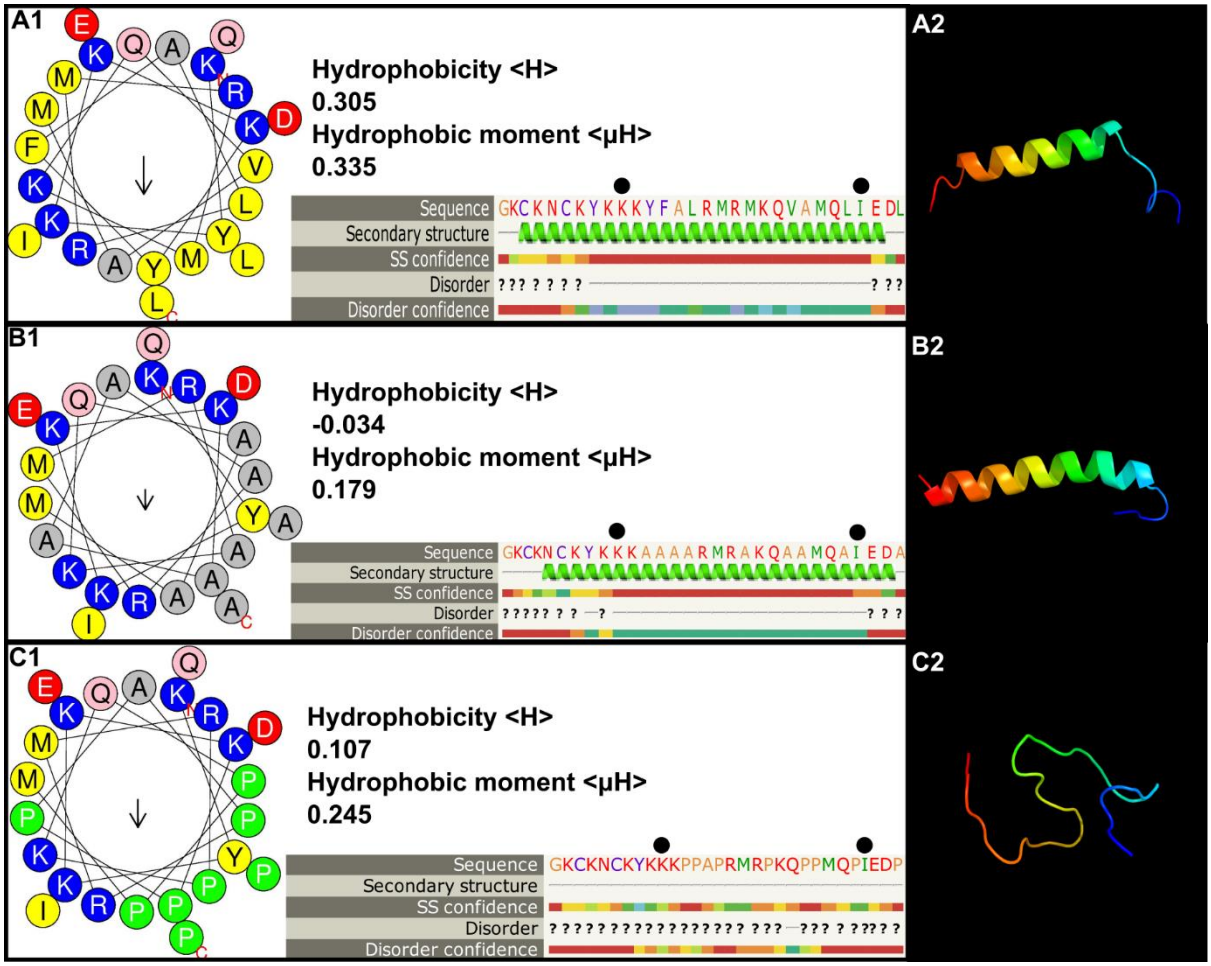

Figure 3. 2A1), with a hydrophobicity (provides a measure of hydrophobicity) and hydrophobic moment (provides a measure of amphiphilicity) score of 0.305 and 0.335, respectively. The predicted structure of the C-terminal of wildtype NSP5 also confirms an α-helix with high SS confidence (indicates the confidence in the prediction from PSI-Pred) between amino acids K117 and I195 (

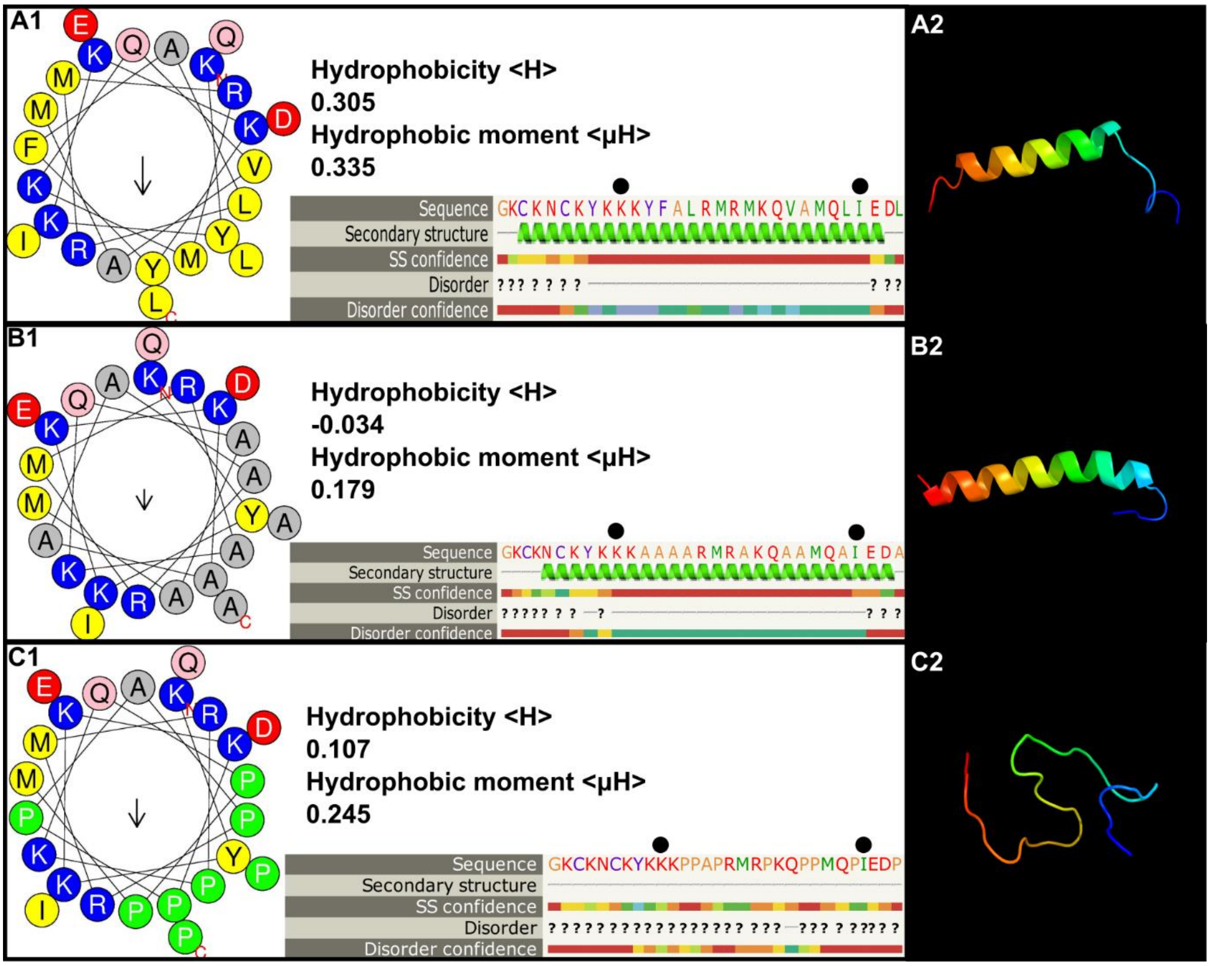

Figure 3. 2A2). The mutation of several hydrophobic amino acids to either alanine (

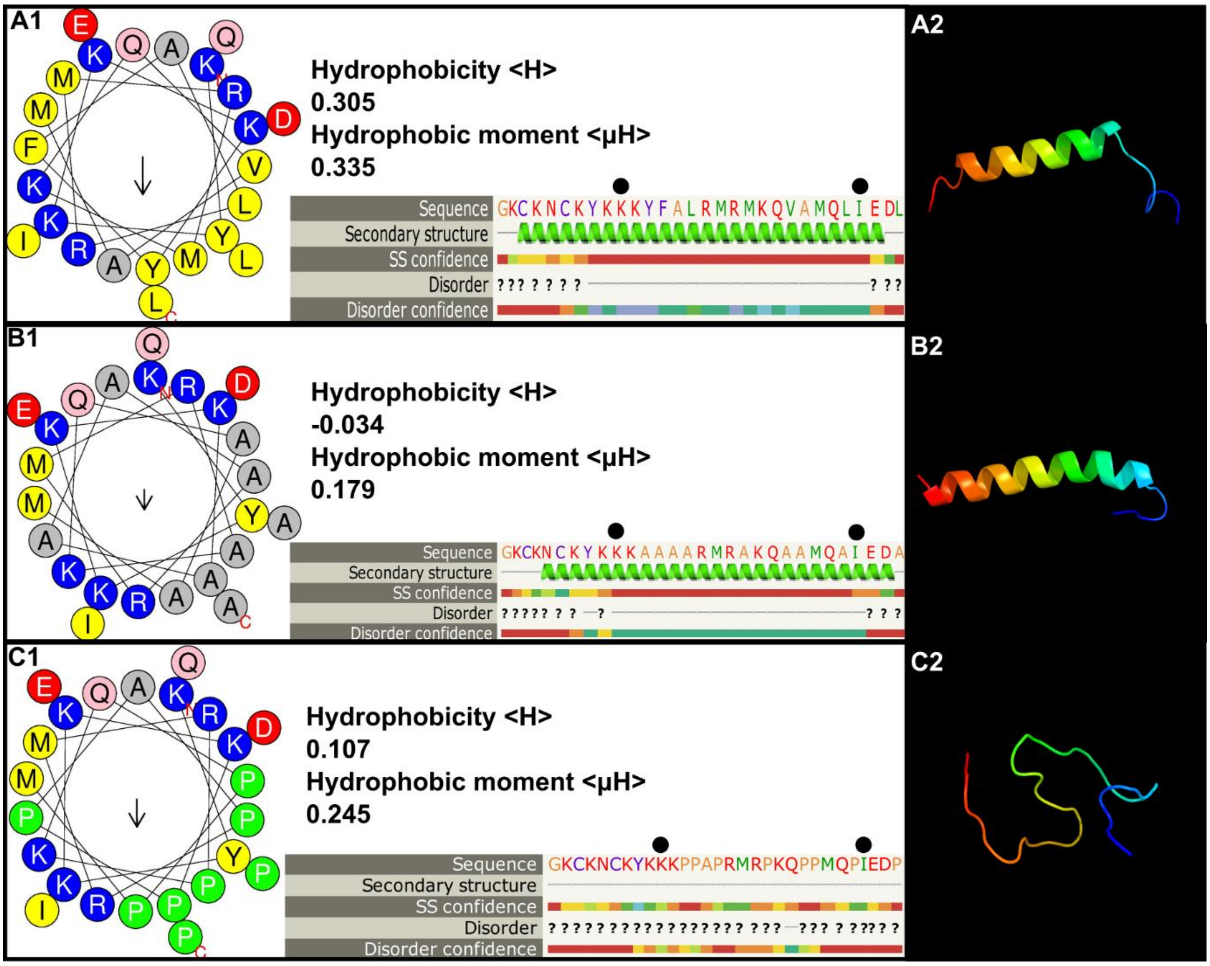

Figure 3. **2A2**) or proline (

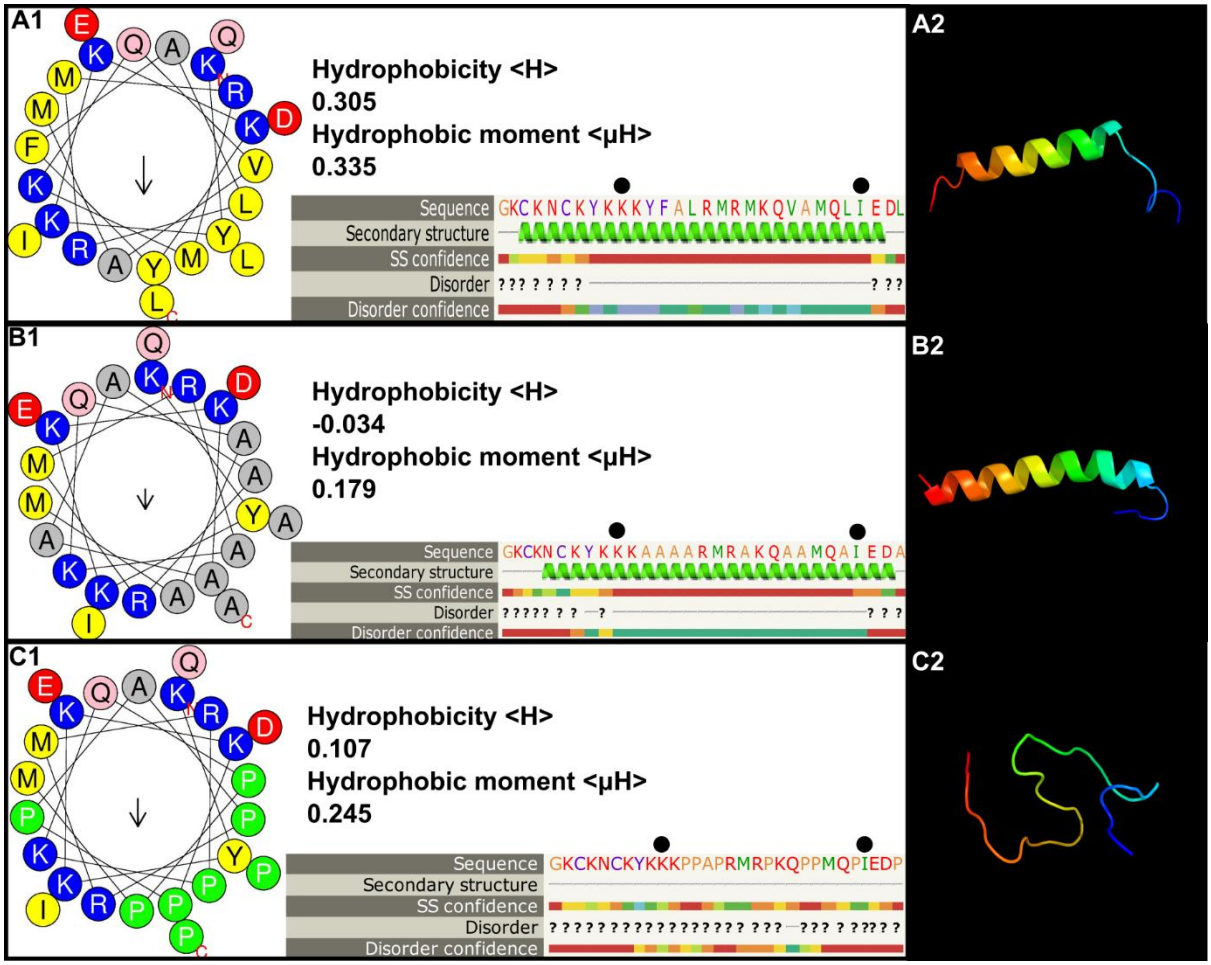

Figure 3. 2**A3**) resulted in a decrease of both hydrophobicity (-0.034 and 0.107) and hydrophobic moment (1.79 and 0.245). Furthermore, although the alanine mutations appear to have minimal effect on the predicated C-terminal α-helix (high SS

confidence between K119 and I194), the proline mutations completely abolished the C-terminal α-helix replacing it with a highly disordered structure.

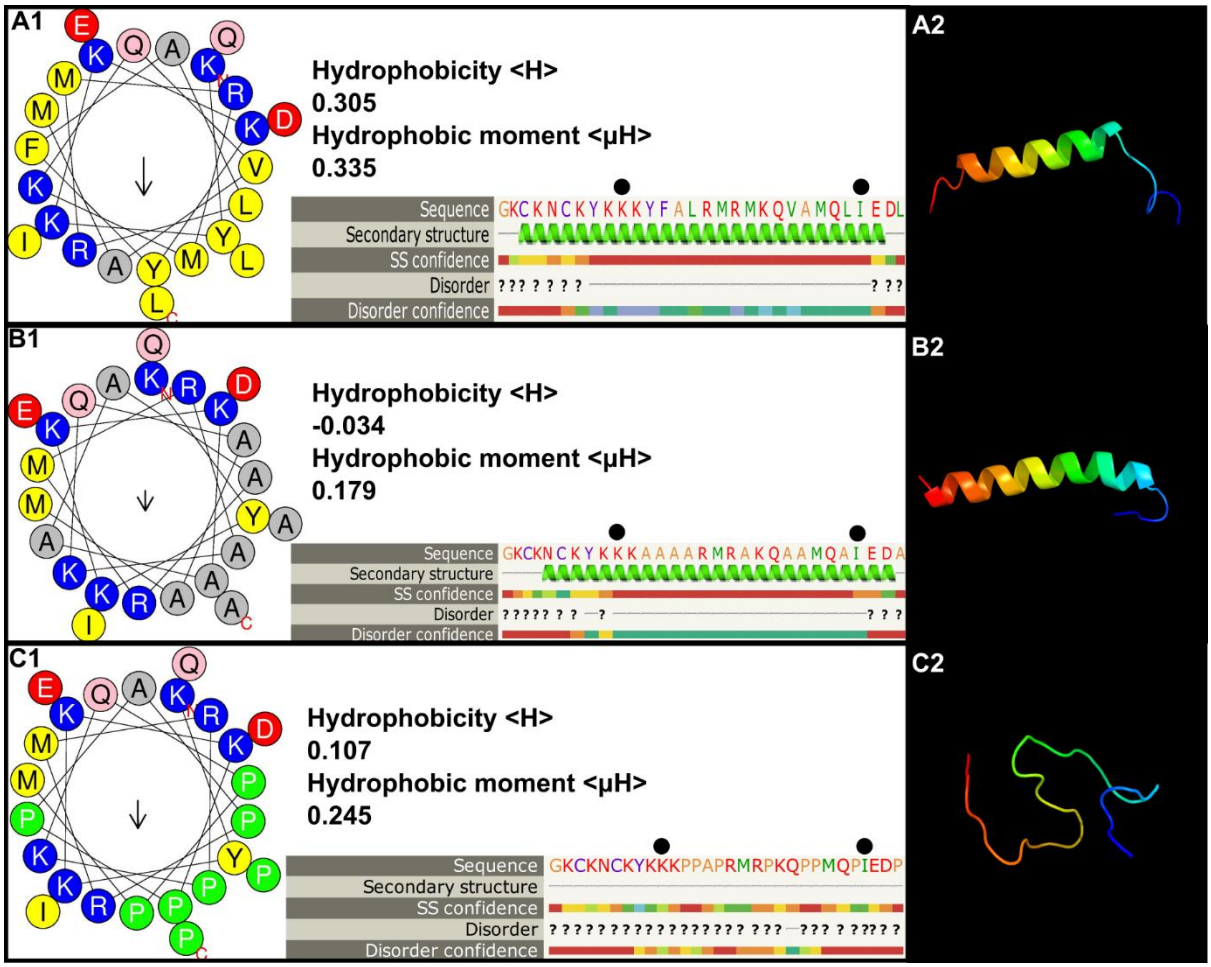

Figure 3. 2. α-Helical wheel prediction and protein modelling of wild type NSP5, aNSP5 and pNSP5. 1) Helical wheel diagrams for A) wildtype NSP5, B) ala-NSP5 and C) pro-NSP5 C termini as constructed by Pepwheel. Grey - aliphatic, Blue – amphipathic, Green - cyclic, Yellow - hydrophibic, Red – hydrophilic. 2) Predicted structure C termini using a fold recognition algorithm. rainbow N → C terminus Circles indicate amino acids K174 and I195.

To successfully rescue the mutant NSP5 viruses, a MA104 cell line, stably expressing NSP5, was generated. Analysis by both western blot and immunofluorescence showed that four clones stably express NSP5 (**Figure 3. 3**).

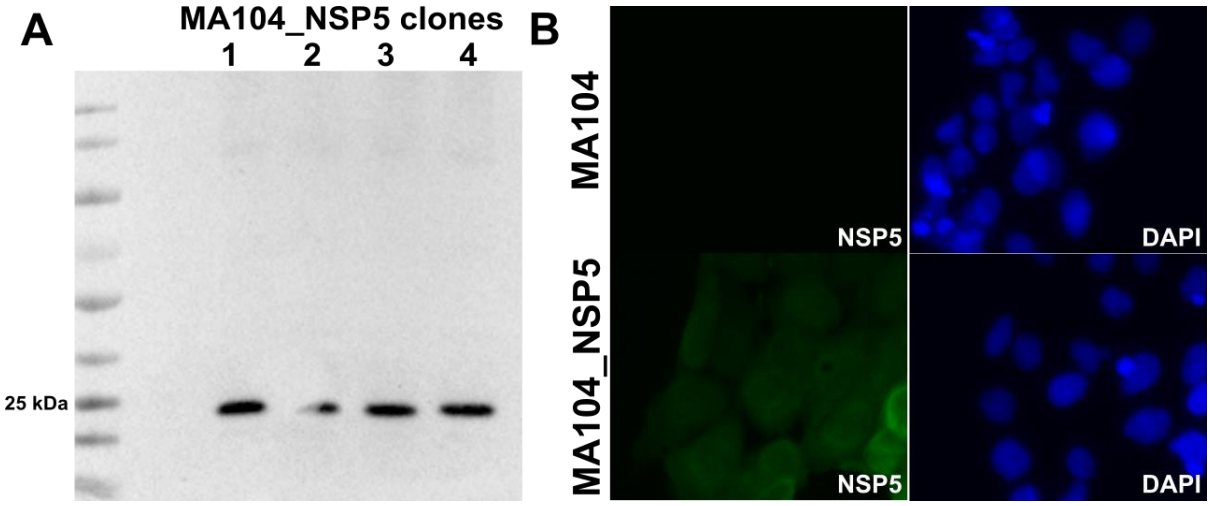

Figure 3. 3. Western blot and Immunofluorescent analysis of MA104 cells expressing NSP5. NSP5 expression was detected by A) western blot analysis B) immunofluorescence showing the expression of NSP5 in MA104 cells.

3.3.2. Rescue and confirmation of mutant viruses

After transfection and co-seeding (P0), the mutant and rescued viruses were harvested and confluent monolayers of MA104 or MA104-NSP5 cells were freeze-thawed to release any possible virus. The subsequent viral supernatant was activated and added to fresh monolayers of MA104 or MA104-NSP5 cells (P1). As indicated in **Table 3. 5**, first signs of cytopathic effect were observed for rSA11 one day post infection with complete CPE observed at three days post infection (**Figure 3. 4).** In contrast, both rSA11_aNSP5 and rSA11_pNSP5 only started showing sign of CPE at two days post infection with partial CPE on three days post infection.

Table 3. 5. Cytopathic effect score chart of mutant viruses compared to rSA11 and associated MA104 cells**.**

			Day 1	Day 2	Day 3
P1	**MA104 cells**		-	-	-
	w/o pT7-VP1SA11		-	-	-
	rSA11		-	+	+++
	rSA11_aNSP5		-	-/+	++
	rSA11_pNSP5		-	-/+	++

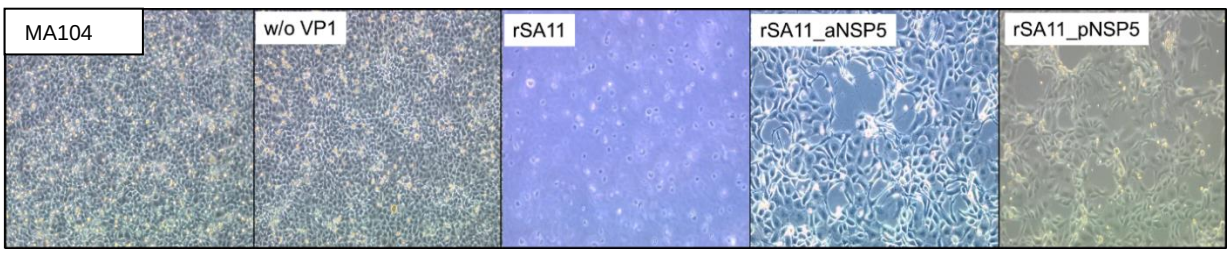

Figure 3. 4. Light microscope images showing cytopathic effect of rSA11, rSA11_aNSP5 and rSA11_pNSP5 at three days post infection. MA104 cells were mocked infected, while w/o VP1 was

infected with supernatant from HEK293 cells transfected with plasmids containing all the genome segments, except for the plasmid encoding VP1.

The viral RNA that was extracted from the viruses (**Figure 3. 5**), was subjected to cDNA synthesis and both restriction enzyme digestion and whole genome characterisation using Illumina MiSeq was used to ensure the viruses contained the inserted mutations.

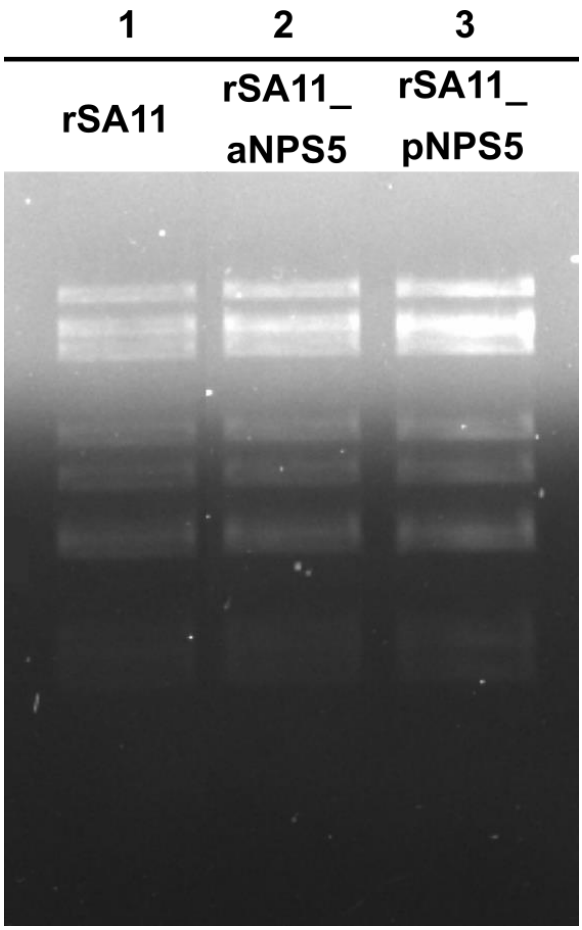

Figure 3. 5. Viral RNA extraction. Extracted RNA from cellular pellets and supernatant collected fromm 75 cm^3-infected monolayers at 16 hours post infection.

Figure 3. 6 shows the successful digestion of genome segment 8 confirming the successful rescue of rSA11, rSA11_aNSP5 and rSA11_pNSP5. Restriction enzyme digestion of genome segment 10 with XbaI is also shown in **Figure 3. 6**, confirming the successful rescue of rSA11, rSA11_aNSP5 and rSA11_pNSP5. Next generation sequencing data can be seen in **Appendix C** and shows that rSA11_aNSP5 and rSA11_pNSP5 was successfully rescued.

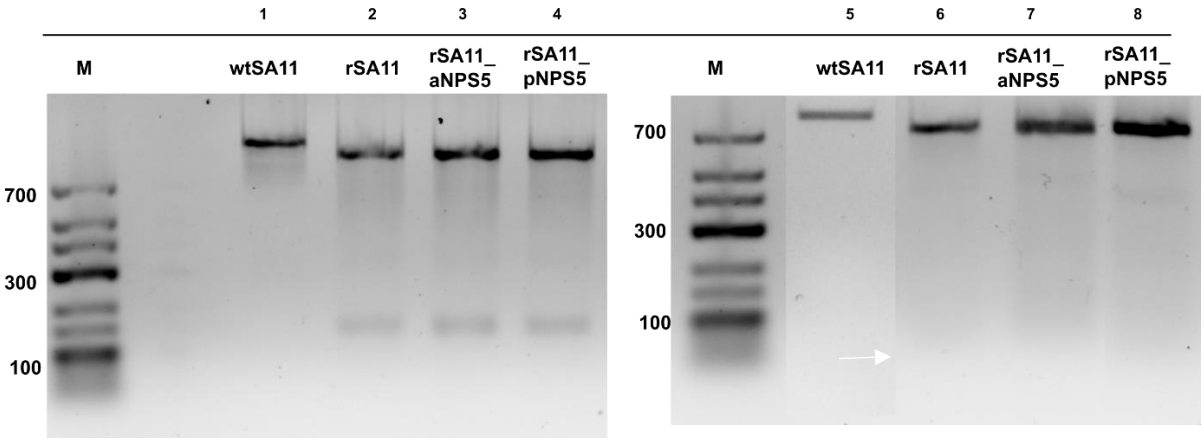

Figure 3. 6. Restriction enzyme digestion analysis for amplified genome segments 8 and 10. A 2.0 % agarose gel indicating the restriction enzyme digestion. Lane 1 shows an uncut genome segment 8 and lanes 2-4 shows the respective mutant genome segment 8 cut with BstUI resulting in two products – 800bp and 150bp. Lane 5 shows an uncut genome segment 10 and lanes 6-8 shows the respective mutant genome segment 10 cut with XbaI resulting in two products – 638bp and 100 bp (indicated by arrow).

3.3.3. Expression of NSP2, NSP5 and the formation of viroplasm-like structures (VLS)

To determine the role of NSP2, NSP5 and VLS on PGE_2 production, we first had to determine expression of the proteins and the formation of VLS in HEK293 cells. **Figure 3. 7** shows successful expression of NSP2 and NSP5 and that the co-expression of NSP2 and NSP5 resulted in the formation of VLS as indicated by the distinct round structures within transfected HEK293 cells.

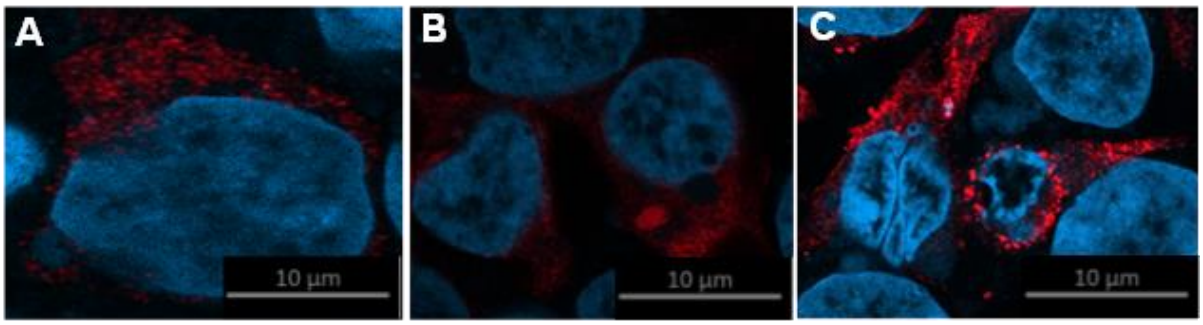

Figure 3. 7. Expression of viral proteins in HEK293 cells. Successful expression of A) NSP2, B) NSP5 and C) NSP2 and NSP5 and subsequent formation of VLS. Scale bar 10 µm.

3.3.4. Replication of mutant viruses

Here, we show the role of the NSP5 C-terminal α-helix in RV replication, using rSA11_aNSP5 and rSA11_pNSP5 mutant viruses and employed replication kinetics. Copies of genome segment 6 appear to be unaffected by the introduced mutations at 2 hours post infection (rSA11: $1.58x10^3 \pm 4.10x10^2$ molecules/g; rSA11_aNSP5:

$1.42x10^3 \pm 4.65x10^2$ molecules/g; rSA11_pNSP5: $1.40x10^3 \pm 6.65x10^2$ molecules/g), while decreasing significantly ($p = 0.00038$, $p = 0.000311$) when compared to rSA11 at 6 hours post infection (rSA11: $1.63x10^6 \pm 5.01x10^5$ molecules/g; rSA11_aNSP5: $1.32x10^4 \pm 3.39x10^3$ molecules/g; rSA11_pNSP5: $1.15x10^3 \pm 4.44x10^2$ molecules/g) (**Figure 3. 8A**). Although both mutant viruses (rSA11_aNSP5: $1.56x10^3 \pm 4.01x10^2$ $TCID_{50}$/ml; rSA11_pNSP5: $1.44x10^3 \pm 3.79x10^2$ $TCID_{50}$/ml) showed no significant difference in viral yield at 2 h post infection compared to rSA11 ($1.44x10^3 \pm 2.55x10^2$ $TCID_{50}$/ml), both mutant viruses (rSA11_aNSP5: $6.63x10^4 \pm 2.46x10^4$ $TCID_{50}$/ml; rSA11_pNSP5: $7.21x10^2 \pm 3.13x10^2$ $TCID_{50}$/ml) showed significantly ($p = 0.0025$, $p = 0.0024$) lower yield at 6 h post infection compared to rSA11 ($1.44x10^6 \pm 2.55x10^2$ $TCID_{50}$/ml) (**Figure 3. 8C**).

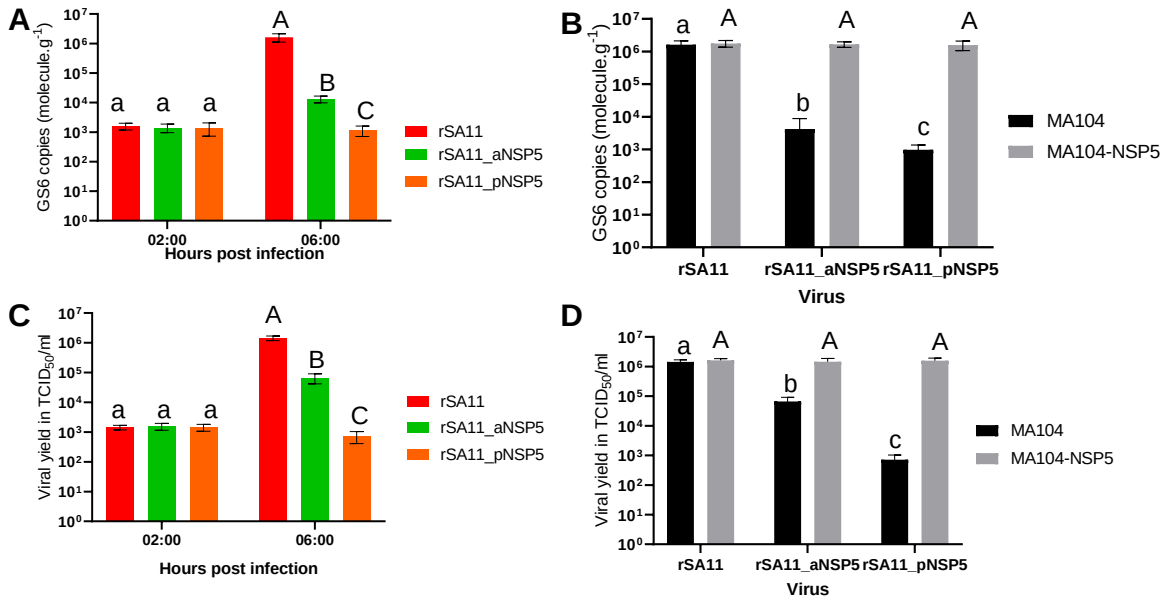

Figure 3. 8. Viral titre and copies of genome segment 6 at 2 and 6 h post infection. A) Copy number of genome segment 6 (GS6) for the respective mutant viruses as determined by RT-qPCR was compared to rSA11-infected HEK293 cells and C) rotavirus yield as determined by $TCID_{50}$ at two and six hours post infection. B) Copy numbers of GS6 and D) viral yield of rSA11, rSA11_aNSP5 and rSA11_pNSP5 in MA104 and MA104-NSP5 cells at 6 hours post infection. Error bars indicate the standard error of the mean (n = 3). Lowercase and uppercase letters indicate significant difference ($p<0.05$) compared to rSA11. For further details see Table 3. 6.

To determine if the mutations were the cause of the lower levels of genome segment 6 (VP6) copy numbers and viral yield, we infected both MA104 and MA104-NSP5 with rSA11, rSA11_aNSP5 and rSA11_aNSP5 (**Figure 3. 8B & D**). Although comparable results were seen in MA104 cells compared to HEK293 cells, both GS6 copy numbers and viral yield was restored when MA104-NSP5 cells were infected with

rSA11_aNSP5 and rSA11_pNSP5. Taken together, these data confirm that the NSP5 C-terminal α-helix is essential for RV replication.

3.3.5. Prostaglandin E_2 production is only induced during rotavirus infection

HEK293 cells transfected with plasmids encoding the open reading frame (ORF) for NSP2, pBudNSP2 (55.37±6.44 pg/ml) or NSP5, pBudNSP5 (54.02±9.74 pg/ml) and encoding the ORFs for both NSP2 and NSP5, pBudDual(73.86±14.46 pg/ml), showed no significant difference in the production of PGE_2 compared to the mock transfected HEK293 cells when measured 48 hours after transfection (**Figure 3. 9A**). There was no significant difference in the production of PGE_2 in HEK293 cells infected with rSA11 (94.42±11.50 pg/ml), rSA11_aNSP5 (88.37±7.78 pg/ml) or rSA11_pNSP5 (81.56±10.31 pg/ml) at two hours post infection (**Figure 3. 9B**). However significant decreases (p = 0.00008, p = 0.00005) in PGE_2 production were observed in HEK293 cells infected with rSA11_aNSP5 (145.40±6.65 pg/ml) or rSA11_pNSP5 (116.83±9.60 pg/ml) when compared to rSA11 at six hours post infection (209.37±4.67 pg/ml). The results thus indicate that neither the proteins involved in viroplasm formation (NSP2 and NPS5) nor the formation of viroplasms-like structure is sufficient to induced PGE_2 production. In addition, we show that both rSA11_aNSP5 and rSA11_pNSP5 are capable of inducing PGE_2 during both early and later stages of replication although the levels during later stages are significantly lowered compared to rSA11.

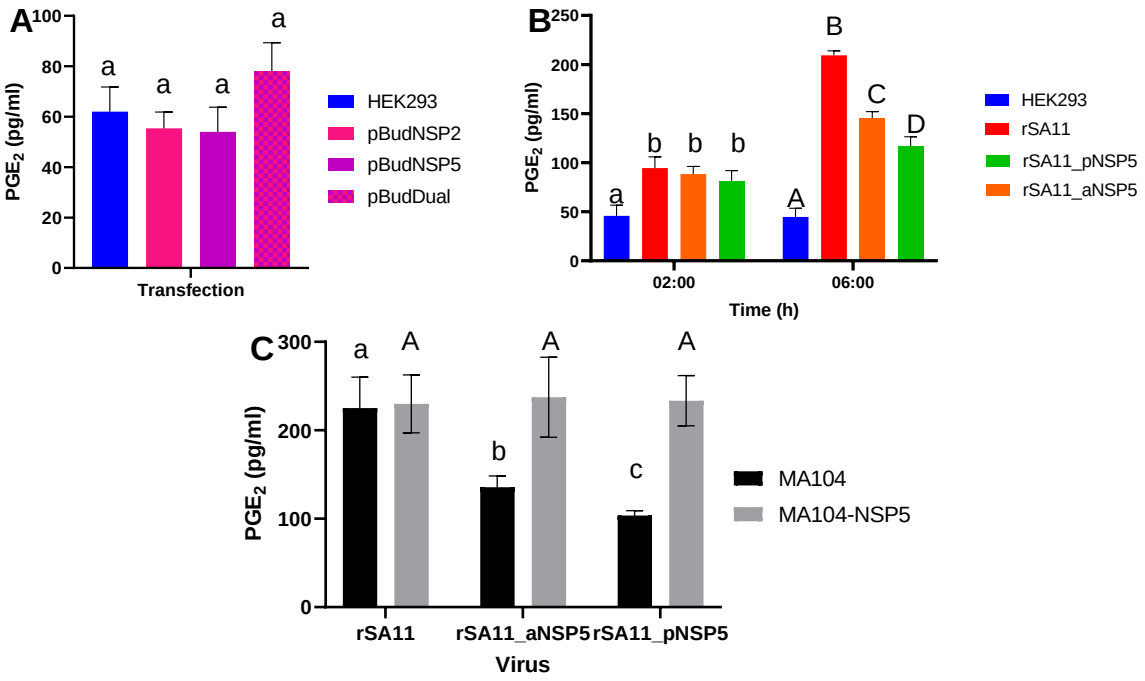

Figure 3. 9. Rotavirus increases the concentration of prostaglandin E_2 in HEK293. A) The amount of PGE_2 produced during the transfection of HEK293 cells with plasmids containing the ORFs for NSP2, NSP5 or both (dual) determined by ELISA was compared to transfection reagent only transfected HEK293 cells. B) The amount of PGE_2 produced during rSA11_aNSP5 and rSA11_pNSP5 infection (MOI = 5) as determined by ELISA was compared to rSA11 infected HEK293 cells at two and six hours post infection. C) The amount of PGE_2 produced during infection of MA104 and MA104-NSP5 cells with rSA11, rSA11_aNSP5 or rSA11_pNSP5 at 6 hours post infection lowercase and uppercase letters indicate a significant difference ($p<0.05$) compared to rSA11. Error bars indicate the standard error of the mean (n = 3).

To determine if the mutations were the cause of the decreased of PGE_2, we infected both MA104 and MA104-NSP5 with rSA11, rSA11_aNSP5 and rSA11_aNSP5 **Figure 3. 9C**). Although results were comparable between MA104 cells and HEK293 cells, production of PGE_2 was restored when MA104-NSP5 cells were infected with rSA11_aNSP5 and rSA11_pNSP5.

3.3.6. Co-localisation between LDs/PGE_2 and NSP5

Confocal laser scanning microscopy was employed to determine the co-localisation of PGE_2 (**Figure 3. 10**) with viroplasms or VLS in either transfected or infected HEK293 cells. HEK293 cells that were transfected with pBudNSP2, pBudNSP5 or pBudDual showed no co-localisation between viral proteins or VLS (**Figure 3. 10A**), which is also shown by Pearson:Pearson correlation coefficients (**Figure 3. 10C**). This is in concurrence with PGE_2 ELISA data that showed no significant increase of PGE_2 during transfection (**Figure 3. 9**). In contrast, HEK293 cells that were infected with rSA11

showed co-localisation between PGE_2 and viroplasms (**Figure 3. 10B & C**). Although rSA11_aNSP5 and rSA11_pNSP5 also showed co-localisation between PGE_2 and viroplasms, the number of viroplasm formed during these infections appeared less compared to rSA11 infection. Taken together, the data indicate that neither expression of NSP2 and NSP5 or dual expression were able to induce PGE_2 production.

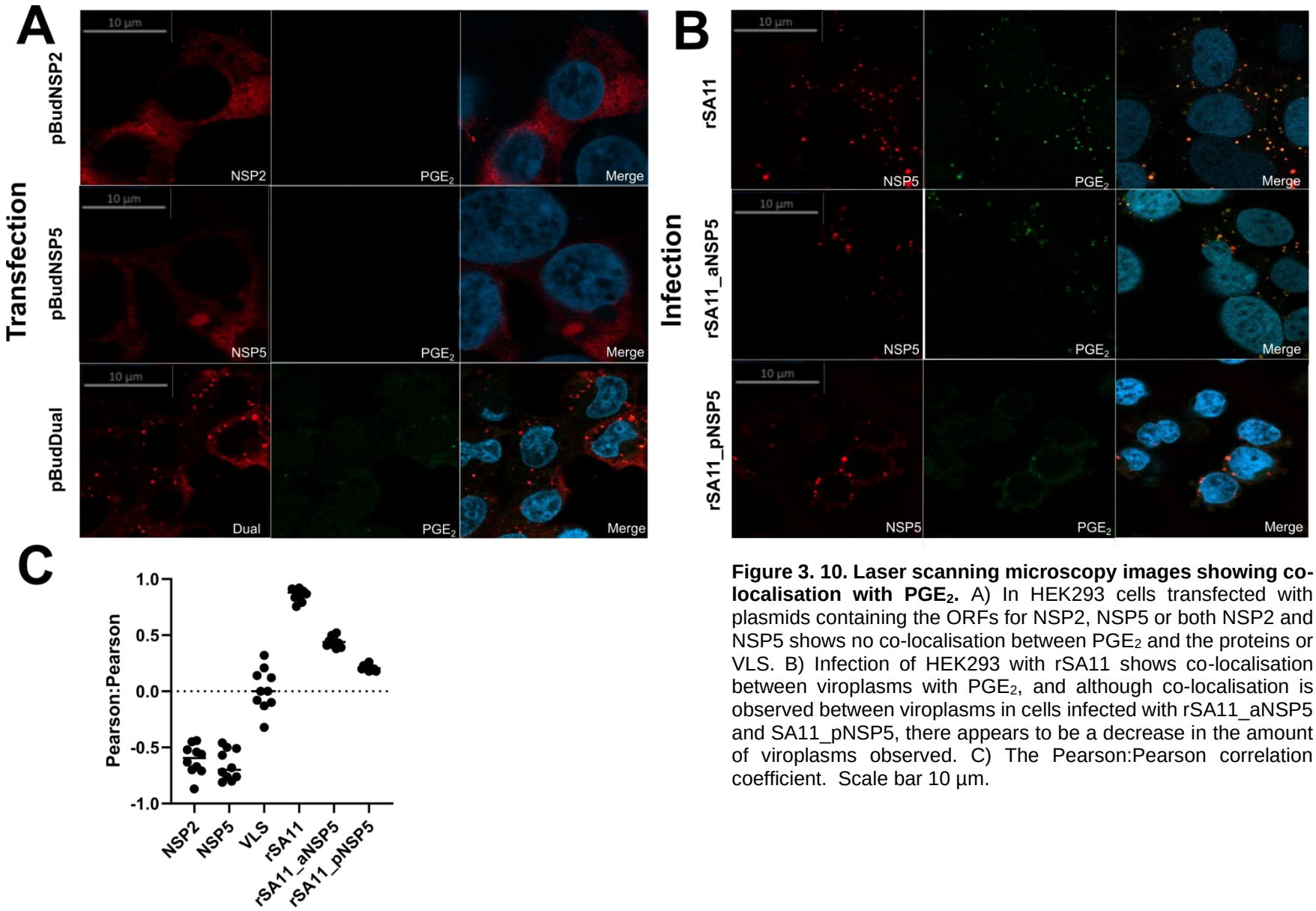

Figure 3. 10. Laser scanning microscopy images showing co-localisation with PGE_2. A) In HEK293 cells transfected with plasmids containing the ORFs for NSP2, NSP5 or both NSP2 and NSP5 shows no co-localisation between PGE_2 and the proteins or VLS. B) Infection of HEK293 with rSA11 shows co-localisation between viroplasms with PGE_2, and although co-localisation is observed between viroplasms in cells infected with rSA11_aNSP5 and SA11_pNSP5, there appears to be a decrease in the amount of viroplasms observed. C) The Pearson:Pearson correlation coefficient. Scale bar 10 µm.

In addition to determining co-localisation of viroplasms with PGE_2 we also determined the co-localisation of viroplasm with LDs in infected HEK293 cells (**Figure 3. 11)**. In **Figure 3. 11A** a decrease in co-localisation can be observed when comparing rSA11 to both rSA11_aNSP5 and rSA11_pNSP5, with rSA11_pNSP5 showing the least co-localisation. These observations are supported by Pearson:Pearson correlation coefficients which shows that viroplasms in rSA11-infected cells have a correlation coefficient of 0.86±0.054 with LDs, while viroplasms in both rSA11_aNSP5- and rSA11_pNSP5-infected cells have a correlation coefficient of 0.44±0.044 and 0.21±0.025 with LDs, respectively. This means that there is low to random co-localisation between the mutant NSP5 proteins and LDs.

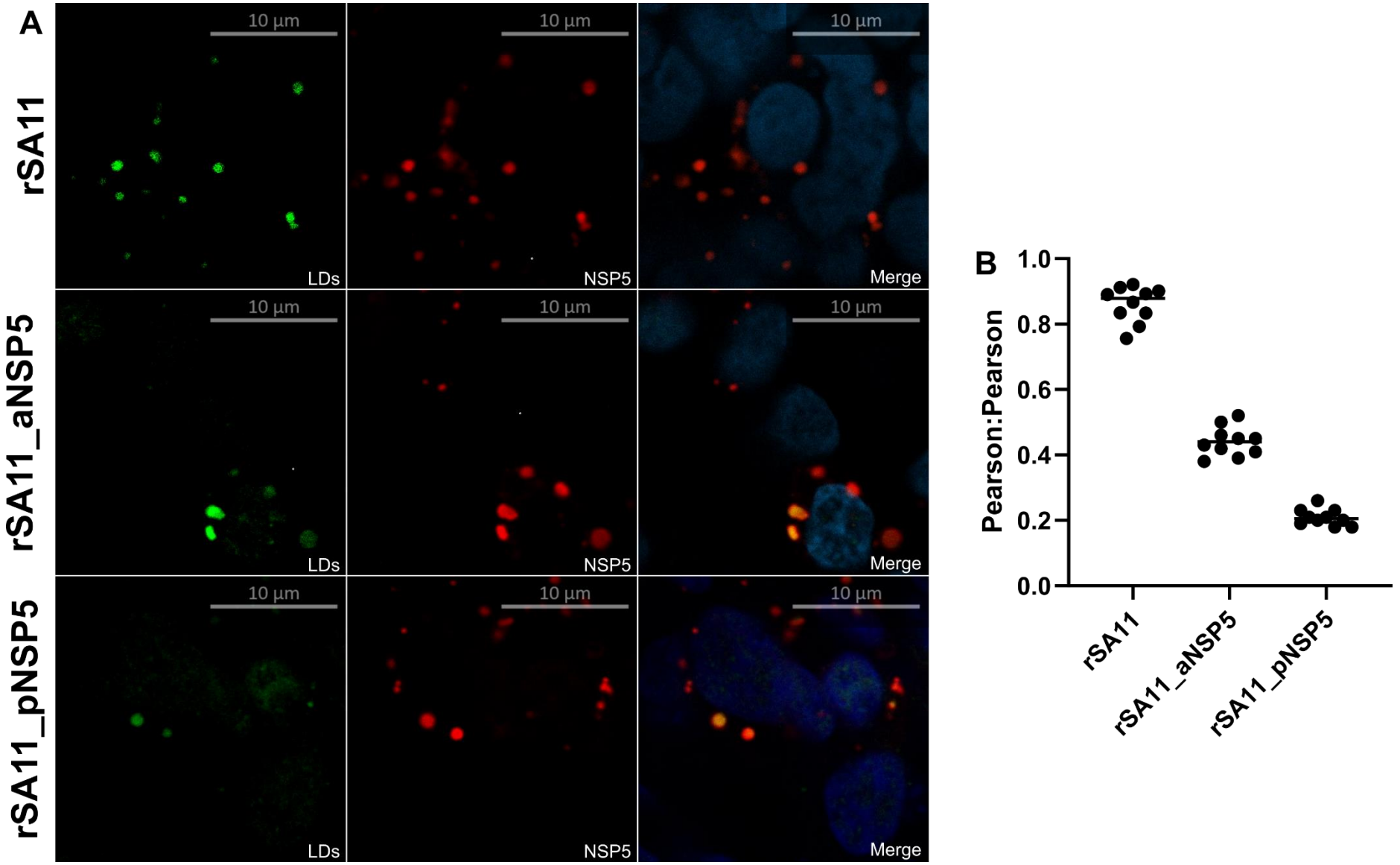

Figure 3. 11. Laser scanning microscopy images showing co-localisation with LDs. A) Infection of HEK293 with rSA11 shows co-localisation between viroplasms with LDs. Although co-localisation is observed between viroplasms in cells infected with rSA11_aNSP5 and SA11_pSP5, there appears to be a decrease in the amount of viroplasms observed. B) Pearson:Pearson correlation coefficients of confocal microscopy images as determined by ImageJ are shown in the adjacent graph (Schneider et al., 2012). Values close to -1 indicate no co-localisation with values close to 0 indicating random co-localisation, while values close to 1 indicate co-localisation with a (very) high degree of certainty. Scale bar 10 µm

3.3.7. NSP5 co-sediments with Perilipin-2 (PLIN2) during co-expression of NSP2 and during rotavirus infection

Confocal laser scanning microscopy is a powerful tool to visualise co-localisation but, in our case, did not provide the resolution required to determine localisation of NSP5 directly at the surface of LDs or in membranes that are near LDs. We thus purified LDs by density gradient centrifugation from HEK293 cells infected with rSA11, rSA11_aNSP5 or SA11_pNSP5 or transfected HEK293 cells and probed for the presence of viral proteins by immunoblotting. As expected, only the transfection of HEK293 with plasmids containing the ORF for both NSP2 and NSP5 showed co-sedimentation of NSP5 with PLIN2 (**Figure 3. 12A**). As expected, during rSA11 infection, viroplasms were enriched in the fractions that also contained the LD marker PLIN2 (**Figure 3. 12B**), confirming that viroplasms associate with LDs as has been shown before (Cheung et al., 2010). In contrast, rSA11_aNSP5 and SA11_pSP5 showed less association with the LD-enriched fraction and were present in fractions 4 to 5 and fraction 5, respectively (**Figure 3. 12 & D**). Interestingly, the phosphorylation state of NSP5 appears to be affected by the mutations as hyperphosphorylated NSP5 is observed in rSA11 infected cells as well as during dual expression (**Figure 3. 12B**), while less phosphorylation is observed for both rSA11_aNSP5 infections (**Figure 3. 12C**) rSA11_pNSP5 (**Figure 3. 12D**). Our results indicated that the mutations introduced in the C-terminal α-helix decreased the interaction between viroplasms and LDs.

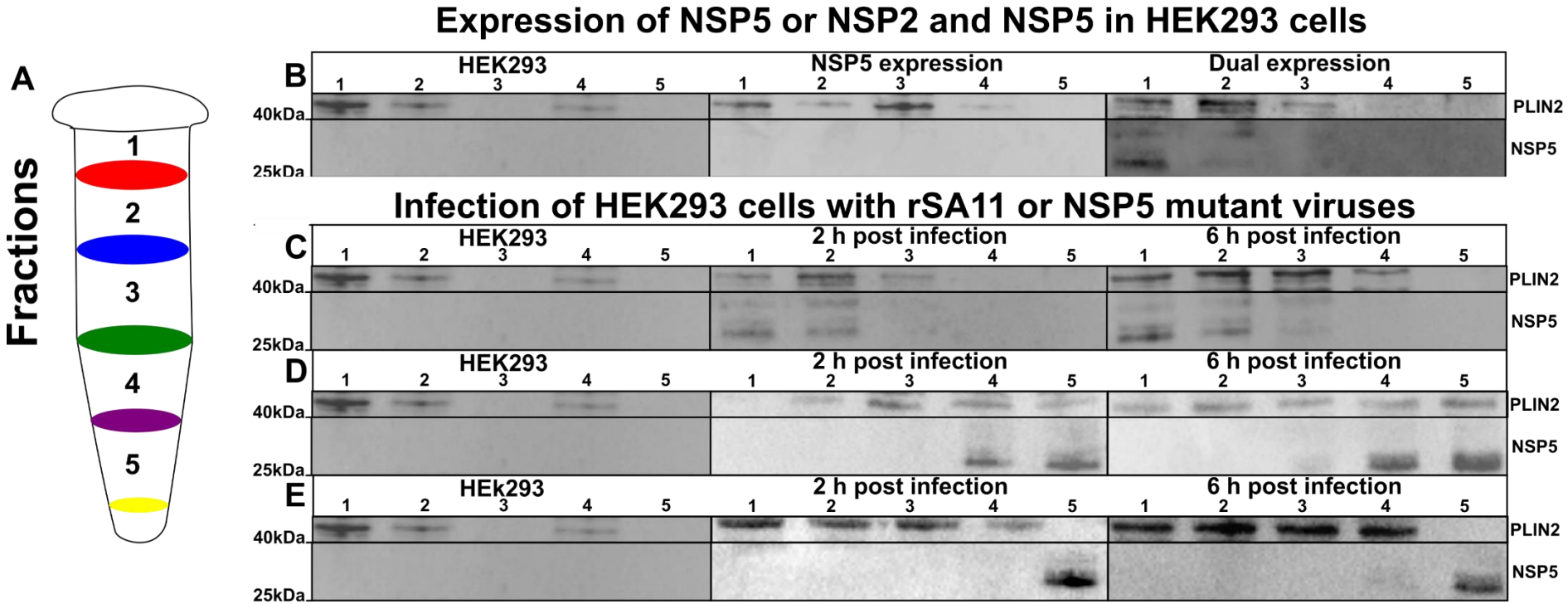

Figure 3. 12. Immunoblotting of NSP5 and perilipin-2 (PLIN2) after purification of LDs of RV-infected cells by floatation. A) Western blot was performed to analyse NSP5 in fractions 1–5 in transfected B) HEK293 cells and HEK293 cells infected with C) rSA11, D) rSA11_aNSP5 and E) rSA11_pNSP5 from fractions sampled from the top to the bottom of the gradient. PLIN2 was used as marker for interaction with LDs for lipid droplets (right panel).

3.4. Discussion

Viroplasms, consisting of both viral proteins and host LDs, have long been recognised as essential to supporting RV replication (Papa et al., 2021). Of the two non-structural proteins involved in viroplasm formation, NSP5 plays a critical role by potentially providing a scaffold for the recruitment of additional viral proteins (Contin et al., 2010). In addition to NSP5, host LDs are also essential for viroplasm formation and function, as the inhibition of their formation has deleterious effects on viral replication and subsequent yield (Cheung et al., 2010). Furthermore, in the previous chapter we showed that PGE_2 produced in LDs during RV infections enhanced the attachment and penetration of RV during early infection.

Because previous work by Fabbretti and co-workers (1999) showed that the dual expression of NSP5 and NSP2 leads to the formation of VLSs and that viroplasms closely associate with LDs (Cheung et al., 2010; Crawford and Desselberger, 2016), we wanted to determine the role of these proteins (NSP2 and NSP5) or viroplasm-like structures in the induction of PGE_2 production during RV replication. Using plasmids that express the single proteins NSP2/NSP5, or co-expressing of both NSP2 and NSP5, we showed that neither the proteins on their own, nor the formation of VLSs could induce the production of PGE_2 in transfected HEK293 cells. We thus hypothesized that at least the complete viroplasm (consisting of viral RNA and other viral proteins) (Papa et al., 2021) needs to be present for the induction of PGE_2 production.

Recent work by Papa and co-workers (2020) showed that removing the C-terminal region from NSP5 caused the formation of aberrant viroplasm structures, containing no other viral proteins or RNA, preventing viral replication. This C-terminal region has been predicted to contain an α-helix whose structure is essential in the formation of VLSs (Sen et al., 2007). Using a modified SA11-based reverse genetics system (Kanai et al., 2017), we provide evidence for the essential role for the predicted α-helix in the C-terminal region of NSP5 in the formation of viroplasms. To characterize the replication of the NSP5 mutants we established a *trans*-complementing system that provides NSP5 to the virus in the NSP5-producing MA104, enabling rescue of the mutant SA11 viruses lacking functional NSP5. By using both restriction digestion and NGS we showed the successful rescue of all mutant SA11 viruses. In addition, no additional changes in the protein coding regions were observed for the viral proteins

analysed. Modelling data generated shows that replacing hydrophobic amino acids with alanine decreases the overall hydrophobicity of the α-helix structure, while replacement with proline completely abolishes the structure. By using this approach, we showed that NSP5-deficient RV appeared to form fewer viroplasms in HEK293 cells, which subsequently impacted both viral RNA levels and viral yield. rSA11_aNSP5 replicated in HEK293 with both RNA level and viral yield increasing from two to six hours post infection. In contrast, no increase in RNA levels from 2 to 6 hours post infection is seen in the rSA11_pNSP5 mutant, while there is a decrease in viral yield over this time. This could suggest that the mutations introduced have no effect on the initial stages of viral replication, but impact later stages, such as assembly. The mutant viruses also affect the amount of PGE_2 produced in HEK293 cells. Although increases were observed when HEK293 cells were infected with rSA11_aNSP5 and rSA11_pNSP5 at 2 hours post infection, the increase was remarkably lower for the rSA11_aNSP5 with almost no change for the rSA11_pNSP5 at 6-hour post infection. The lack of PGE_2 production was also observed using confocal laser scanning microscopy. Using western blot analysis, we showed that rSA11-produced NSP5 co-sedimented with fractions containing the LD-associated PLIN2. This result agrees with Cheung and co-workers (2010) who showed that ultracentrifugation of rotavirus-infected cell extracts through iodixanol gradients contained perilipin 1/A (lipid droplet marker) in the same low-density fractions (1.11 to 1.15 g/ml) as NSP5.. In contrast while rSA11_aNSP5 showed some association, it appeared in lower fractions. As expected, rSA11_pNSP5 showed no co-sedimentation with fractions containing LD-associated PLIN2, indicating that the mutations do affect the interactions between LDs and NSP5 preventing the formation of viroplasms and affecting downstream viral replication.

In addition, we found that the mutations introduced in NSP5 affected the phosphorylation of NSP5. According to Eichwald and co-workers (2002) four serines (Ser^{153}, Ser^{155}, Ser^{163}, and Ser^{165}) are phosphor-acceptor sites. However, all the NSP5 mutations introduced in this study were between amino acids 180 to 198. In addition, Papa and co-workers (2020) showing that Ser^{67} and the C-terminal amino acids 176 to 180 was critical in initiating the phosphorylation cascade. Since Eichwald and co-workers (2002) showed that NSP5 (Ser mutated to Ala) formed viroplasms independent of phosphorylation state, we can conclude that the effect observed in the

mutant viruses were due to weakened/abolished α-helical structure in the C-terminus and not lack of phosphorylation.

In conclusion, we show that the individual expression of NSP2 or NPS5 as well as the formation of VLS in HEK293 cells is incapable of inducing the production of PGE_2. Furthermore, we show that mutations in the C-terminal α-helix of NSP5 affects PGE_2 production but most probably be due to slower viral replication rather than decreased viroplasm-LD interactions. Since it appears that decreased replication results in decreased PGE_2 production, it is quite possible that another mechanism is responsible for the induction of PGE_2 production. We show that both changing the hydrophobicity (rSA11_aNSP5) and completely abolishing the α-helix (rSA11_pNSP5) decrease viral yield and viral RNA levels, with the latter being more severe. Therefore, not only is the C-terminal region of NSP5 required for effective replication as shown by Papa co-workers (2020), but the secondary structure and hydrophobicity are critical for optimal viral replication. Since it is known that Ca^{2+} is required for the activation and translocation of the PLA_2 (Burke and Dennis, 2009), the rate-limiting step in PGE_2 production, and the role of NSP4 in the increase in cytoplasm Ca^{2+} levels is well described (Hyser et al., 2010), our focus shifted to the role of NSP4 in the induction of PGE_2.

4.1. Introduction

A hallmark of rotavirus (RV) infection is the increase in cytoplasmic Ca^{2+} (cyto[Ca^{2+}]) by both leakage from the endoplasmic reticulum (ER) and influx from the plasma membrane. The modulation of cyto[Ca^{2+}] levels is due to two different forms of NSP4 (Hyser et al., 2010). Extracellular NSP4 (eNSP4) is a secreted enterotoxin that triggers phospholipase C (PLC)-dependent Ca^{2+} flux via interactions with cellular receptors, while intracellular NSP4 (iNSP4) localises to the ER and elevates cyto[Ca^{2+}] through its viroporin activity. The increase in Ca^{2+} is essential for several processes during replication, including the nucleation of RV viroplasms and assembly of the outer capsid protein, VP7 (Pham et al., 2017). In addition to its role in replication, NSP4 is also crucial for viral morphogenesis, acting as an intracellular receptor for double-layered particles (DLP) (Silvestri et al., 2005). Binding of the NSP4 C-terminal to DLPs triggers rapid budding of DLPs into the ER, where they are briefly enveloped by a NSP4-ER membrane which is subsequently replaced by the outer capsid, VP4 and VP7 (Taylor et al., 1996).

Calcium is not only required for optimal RV replication but has also been shown to induce the production of PGE_2 by at least two different mechanisms. Firstly, cyto[Ca^{2+}] can lead to the activation of cytoplasmic phospholipase A_2 ($cPLA_2$), the rate-limiting enzyme during PGE_2 biosynthesis (Gijón and Leslie, 1999). Cytoplasmic phospholipase A_2 is the only known member of the phospholipase A_2 family with a specificity for sn-2 arachidonic acid and is thus essential to produce eicosanoids such as PGE_2. Calcium post-transcriptionally regulates $cPLA_2$ by binding to a calcium-phospholipid binding domain, allowing for the translocation of $cPLA_2$ from the cytosol to membranes, containing arachidonic acid, including those of lipid droplets (LDs). Although, $cPLA_2$ has been shown to associate with LDs, no direct evidence has yet shown that $cPLA_2$ is capable of directly hydrolysing AA-containing phospholipids in the LD monolayer (Bermúdez et al., 2021). Secondly, both intra- and extracellular Ca^{2+} has been shown to increase the expression of cyclooxyganse-2 (COX-2). Treatment of primary calvarial osteoblasts with Ca^{2+} increased the expression of COX-2 in a dose-dependent manner, leading to marked increases in PGE_2 production (Mellas, 2002). Furthermore, Liu and co-workers (2007) showed that the transient expression

of SARS-associated coronavirus (SARS-CoV) S protein, rapidly increased the levels of cyto[Ca^{2+}], and that the subsequent treatment of the cells with EDTA (a well-known Ca^{2+} chelator) affected COX-2 expression and extracellular signal-regulated kinase (ERK) phosphorylation. In chapter 2 we showed that inhibition of phospholipase A_2 significantly decreased the rate of viral replication, especially during early infection. Results in chapter 3 indicate that neither viroplasms nor their associated proteins are directly responsible for inducing PGE_2 production and that a different mechanism may be used by RV.

The aim of this chapter is to determine if NSP4-induced Ca^{2+} increases affect $cPLA_2$ activity and subsequently PGE_2 production. Therefore, we employed the RV reverse genetic system to engineer a recombinant RV with mutations in the viroporin domain of NSP4.

4.2. Materials and Methods

4.2.1. Cells, virus, inhibitors, and chemicals

Human embryonic kidney 293 (HEK293) cells and the rotavirus simian agent 11 strain (SA11) were maintained as described in Section 3.2.1

The calcium chelators, BAPTA-AM (Thermo Fisher Scientific) and ethylenediaminetetraacetic acid (EDTA) (Thermo Fisher Scientific), bromoenol lactone, and thioetheramide-PC were obtained from Cayman Chemicals and resuspended in 100% (v/v) dimethyl sulfoxide (DMSO; Sigma-Aldrich), while ratiometric Ca^{2+} dye, Fura dextran (Thermo Fisher Scientific), was dissolved in ddH_20.

4.2.2. Cytotoxicity of inhibitors and EDTA

Cytotoxicity testing was performed as in Section 2.2.2. BAPTA-AM concentrations ranged from 1 µM to 100 µM, while concentrations ranging from 0.5 mM to 25 mM were used for EDTA.

4.2.3. Generation of mutant virus

4.2.3.1. Construction of transcription plasmids pT7SA11_rNSP4

An overview of the unmodified SA11 viroporin domain sequence of NSP4 is provided in **Figure 4. 1A**. **Figure 4. 1B** indicates the exact location of the amino acid substitutions for the plasmid encoding rSA11_rNSP4 as shown by Pham and co-workers (2017).

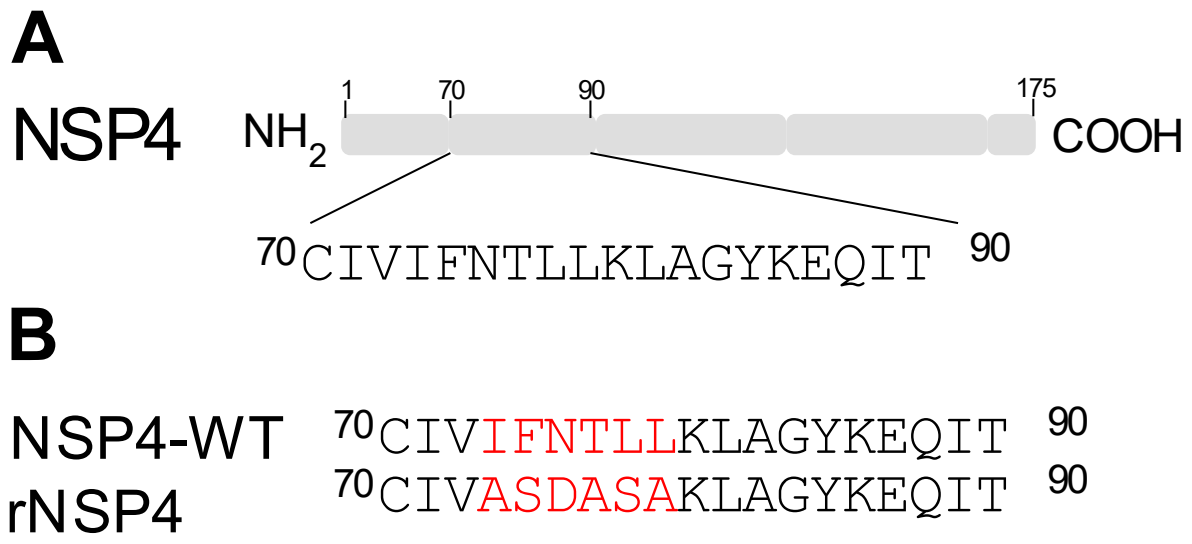

Figure 4. 1. Illustration of NSP4 and rNSP4. (A) Schematic representation of NSP4 and primary sequence of the viroporin region (T, aa70–90) (B) Alignment of the NSP4 proteins corresponding to wild-type (NSP4-WT) or recombinant (rNSP4) mutated sequences. The primary sequence of the NSP5-WT peptide details the mutations (in red) in the amphipathic domain.

The transcription plasmids encoding the eleven simian SA11 genome segments (Kanai et al., 2017)as well as the two helper plasmids (phCMVdream-C3P3 and pCAG-FAST-p10) were a kind gift from Prof. Albie van Djik (North-West University). The plasmid encoding mutant rSA11_rNSP4 was generated using NEBuilder® HiFi DNA Assembly Cloning Kit (NEB, USA). Briefly, fragments were amplified from their respective sources (**Appendix**) using the primers in **Table 4. 1** and Phusion DNA polymerase as previously described. The mutated viroporin region of NSP4 was amplified from plasmids purchased from GenScript (USA), while the backbone was amplified from the T7 plasmid, excluding the region for encoding NSP4 viroporin domain. After digestion with DpnI, the insert and vector fragments were added to the NEBuilder® HiFi DNA Assembly Master Mix and nuclease-free H_2O at a ratio of 2:1 and allowed to assemble for 30 min at 50°C. The assembled fractions were then transformed into competent DH5-α™ *Escherichia coli*. The integrity of the mutant

plasmids after cloning was confirmed by digestion with the corresponding restriction enzyme and Sanger sequencing.

Table 4. 1. List of primers used in the construction of pT7-rNSP4

	PRIMER	PRIMER SEQUENCE
Amplification of NSP4	pcDNANSP4_F	AATGTTCATATAAAGTGG
	pcDNANSP4_R	AGGTCCGATGGTGCTTAC
Amplification of pT7 vector backbone	rNSP4_F	GTAAGCACCATCGGAACCTGATGGCTGACTGAG
	rNSP4_R	CCACTTTATATGAACCATTTTGACGTTTTCAATGCAATTTTC

4.2.3.2. Transfection of pT7SA11 transcription plasmids

Transfection of pT7SA11 transcription plasmids was done as described in Section 3.2.3.3.

4.2.3.3. Passaging

Passaging of rescued viruses were done as described in Section 3.2.3.4.

4.2.3.4. Confirmation of rescued viruses

Confirmation of rescued viruses was done as described in Section 3.2.3.5.

4.2.4. Prostaglandin E_2 quantification

Quantification of PGE_2 production in MA104 cells infected with wildtype SA11 and SA11_rNSP4 was determined as previously described in section 2.2.3.

4.2.5. Calcium assay

Pinocytic loading of Fura dextran into cells was performed as described by Gilmore and co-workers (2001) with modifications. In brief, 1 x 10^4 HEK293 cells were seeded into 96-well black and clear bottom plates (Thermo Fisher Scientific) and grown to 90 % confluency at 37°C and 5 % CO_2. The media was removed, and the cells were incubated in hyper-osmotic buffer (10m M HEPES (Thermo Fisher Scientific), pH 7.4, 10 % (v/v) PEG1000 (Thermo Fisher Scientific), 0.5 M sucrose (Thermo Fisher Scientific)) containing either no addition or 10 µM Fura dextran for 10 min at 37°C. After incubation, the hyper-osmotic buffer was removed, and the cells were incubated in hypo-osmotic buffer (60 % DMEM: 40 % water (v/v)) for 2 min at 37°C. The cells were then allowed to recover in complete DMEM media for 10 min at 37°C. The cells were washed three times with phosphate buffer saline and infected at MOI of 20 for 1 h at 37°C. Thereafter, the virus was removed, and the media was replaced with FluoroBrite™ DMEM (Thermo Fisher Scientific) containing either no addition or 10 µM BAPTA-AM and incubated for 2:30 h at 37°C. Finally, readings were taken every 15

min for 1 h at alternate excitation wavelengths (340/380 nm) and filtering the emission at 530 nm using a microphotometer (Spectramax M2, Molecular Devices).

4.2.6. Cytoplasmic phospholipase A_2 activity

$cPLA_2$ activity in HEK293 cells was measured using a $cPLA_2$ assay kit (Cayman Chemical) following the manufacturer's instructions. Briefly, 7 x 10^5 MA104 cells were seeded in 6-well tissue culture plates and incubated overnight at 37°C and 5 % CO_2. The HEK293 cells were subsequently infected with SA11 or SA11_rNSP4 for 1 h at 37°C in the presence or absence of BAPTA-AM. After infection, the cells were washed once with serum free media and DMEM containing 1 µg/ml pancreatic porcine trypsin type IX was added to the cells. At 2 and 6 h post infection the cells were harvested and prepared in homogenization buffer (50 mM HEPES, pH 7.4, containing 1 mM EDTA). After a brief sonication, the lysed cells were centrifuged at 14 000 x g for 15 min at 4°C. The lysed cells were then incubated with arachidonoyl thio-phosphatidylcholine, a synthetic substrate of $cPLA_2$. Hydrolysis of arachidonoyl thio-phosphatidylcholine by $cPLA_2$ released free thiol, which was converted by 5,5′-dithiobis(2-nitrobenzoic acid) to give 2-nitro-5-thiobenzoic acid. The 2-nitro-5-thiobenzoic acid concentration was determined by spectrophotometric analysis at 405 nm on a Victor Nivo plate reader (PerkinElmer). To ensure that only $cPLA_2$ activity would be measured by the assay, samples were pre-treated with iPLA2-specific inhibitor (bromoenol lactone, 5 mM) and $sPLA_2$-specific inhibitor (thioetheramide-PC, 5 mM) for 20 min at 25°C as recommended by the manufacturer. $cPLA_2$ activity was calculated following the manufacturer's instructions and expressed in nmol/min/mL.

4.2.7. Replication kinetics, *RNA isolation and RT-qPCR*

The yield of GS6 in MA104 cells infected with rSA11 or SA11_rNSP4 was determined at 2 and 6 hours post infection as previously described in Section 2.2.5.

4.2.8. Statistical analysis

Each assay was carried out at least in triplicate (biological/independent replicates) on separate days. Each repeat was analysed in triplicate (n = 3). Data are presented as means ± standard error of the mean. For statistical analysis, two-way analysis of variance (ANOVA) was performed using a Tukey-Kramer test in R studio software (2022.7.1.554) for Windows (R studio, USA). In all tests, $p < 0.05$ was considered statistically significant.

4.3. Results

4.3.1. Toxicity of BAPTA-AM and EDTA in HEK293 cells

To determine the optimal concentration of inhibitors, XTT cell viability assays were performed. Data from the XTT viability assays showed that the highest concentrations to be used for the different inhibitors were as follows: EDTA 1 mM (viability: 96.67 %±3.51) and BAPTA-AM 25 µM (viability: 97 %±5.2) (**Figure 4. 2**).

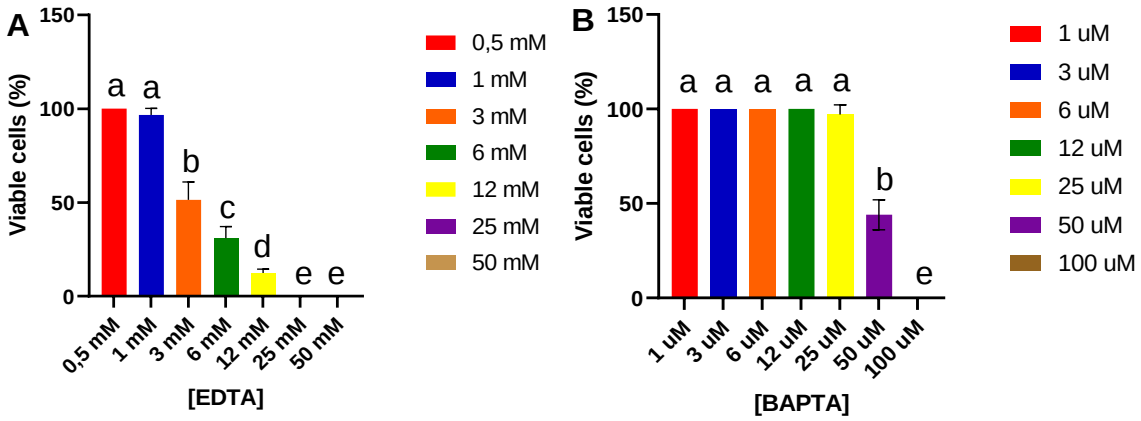

Figure 4. 2. Cellular toxicity of the inhibitors was evaluated with the XTT assay. HEK293 cells (4 x 10^4 cells/ml) were seeded into 96 well plates and allowed to grow to 100 % confluence. The inhibitors were added 1 h prior to infection and subsequently every 4 hours till the completion of the experiment. Data obtained from the toxicity assays of (A) EDTA and (B) BAPTA The following specific indices were calculated for the inhibitors:

	EDTA	BAPTA
CC_{50}	3 mM	50 uM
Conc used	1 mM	25 uM

4.3.2. Rescue and confirmation of SA11_rNSP4

After transfection and co-seeding (P0) the mutant and rescued viruses were freeze-thawed to release any possible virus and confluent monolayers of MA104 cells were infected. The subsequent viral supernatant was activated and added to fresh monolayers of MA104 cells (P1). As indicated in **Table 4. 2**, rSA11 first showed cytopathic effect (CPE) at day two post infection with complete CPE observed at 3 days post infection as seen in **Figure 4. 3.** In contrast rSA11_rNSP4 only started showing sign of CPE at 2 days post infection with partial CPE on 3 days post infection as seen in **Figure 4. 3.**

Table 4. 2. Cytopathic effect score chart of mutant viruses compared to rSA11 and associated controls.

		Day 1	Day 2	Day 3
P1	MA104	-	-	-
	w/o pT7-VP1SA11	-	-	-
	rSA11	-	+	+++
P3	rSA11_NSP4	-	+/-	+

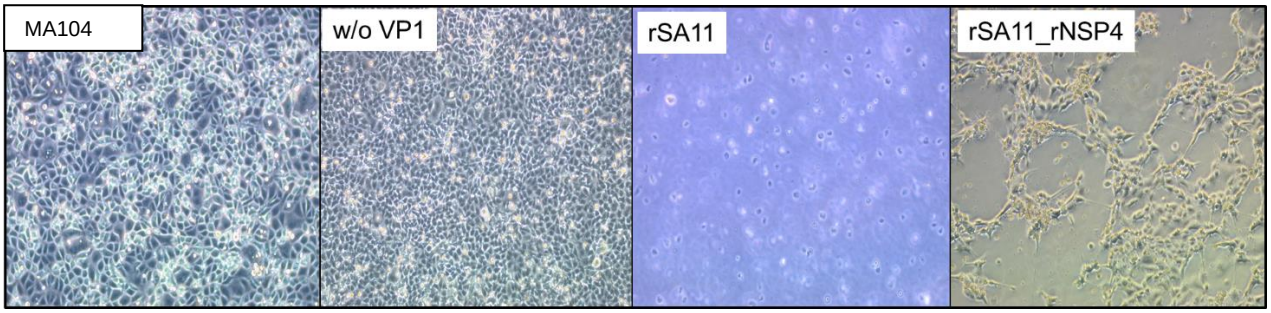

Figure 4. 3. Light microscope images showing cytopathic effect of rSA11, rSA11_NSP4 at three days post infection. MA104 cells were mocked infected, while w/o VP1 was infected with supernatant from HEK293 cells transfected with plasmids containing all the genome segments, except for the plasmid encoding VP1.

The viral RNA that was extracted from the viruses (**Figure 4. 4**), was subjected to cDNA synthesis and both restriction enzyme digestion and whole genome characterisation using Illumina MiSeq was used to ensure the viruses contained the inserted mutations.

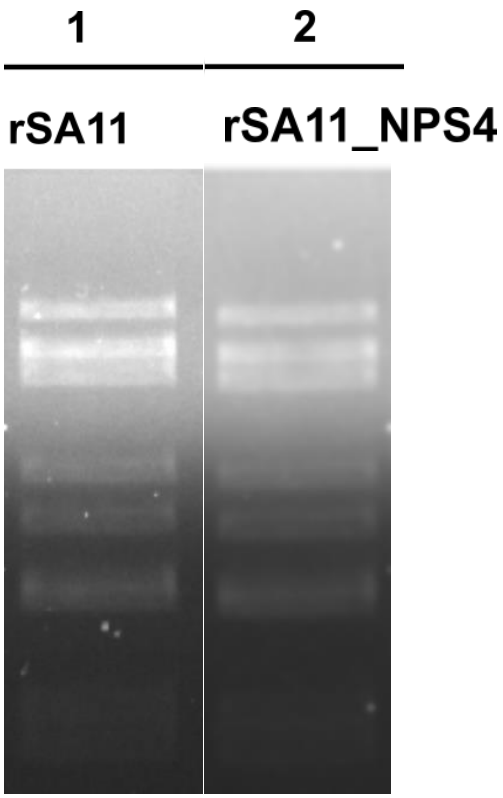

Figure 4. 4. Viral RNA extraction and analysis. RNA extraction from cellular pellets collected from the 75 cm^3 tissues cultures flasks infected with (lane 1) rSA11, (lane 2) rSA11_NSP4 on a 1.0 % TBE-Agarose gel.

Figure 4. 5 shows the successful digestion of the cDNA of genome segment 8 confirming the successful rescue of rSA11 and rSA11_rNSP4. Restriction enzyme digestion of the cDNA of genome segment 10 with XbaI is also shown in **Figure 4. 5**, confirming the successful rescue of rSA11 and rSA11_rNSP4. Next generation sequencing data can be seen in **Appendix** and shows that rSA11_rNSP4 was successfully rescued. However, the next generation sequencing data also indicates changes at T134A, M135A and T137S.

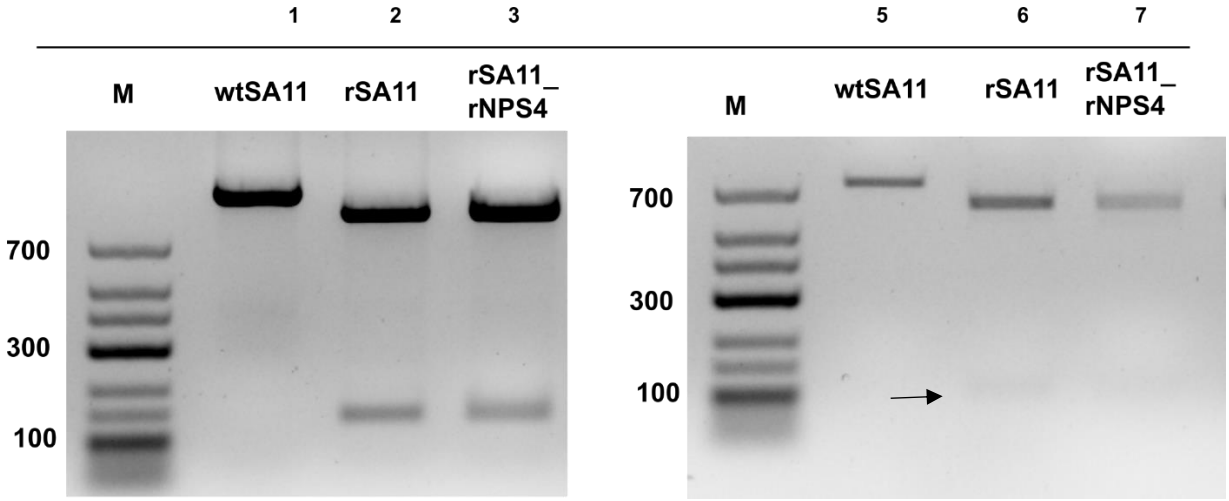

Figure 4. 5. Restriction enzyme digestion analysis for amplified genome segments 8 and 10. A 2.0 % agarose gel indicating the restriction enzyme digestion. Lane 1 shows an uncut genome segment 8 and lanes 2-3 shows the respective mutant genome segment 8 cut with BstUl resulting in two products – 800bp and 150bp. Lane 4 shows an uncut genome segment 10 and lanes 5 shows the respective mutant genome segment 10 cut with Xbal resulting in two products – 638bp and 100 bp (indicated by arrow) ,while lane 6 shows undigested recombinant genome segment 10 with a single product of 738 bp.

4.3.3. Prostaglandin E_2 production

There was a significant decrease ($p = 0.0003$, $p= 0.0003$) in the production of PGE_2 in HEK293 cells infected with rSA11+BAPTA (84.67±3.79 pg/ml) and rSA11_rNSP4 (43.67±20.50 pg/ml) when compared to rSA11 (1436.67± 255.41 pg/ml) at two hours post infection (**Figure 4. 6**). In addition, significant decreases ($p = 0.0004$, $p = 0.004$) in PGE_2 production were observed in HEK293 cells infected with rSA11+BAPTA (493.33±318.77 pg/ml) and rSA11_rNSP4 (186±82.50 pg/ml) when compared to rSA11 ($1.61x10^6$±$3.18x10^5$ pg/ml) at six hours post infection. The results indicate that the treatment of rSA11-infected HEK293 cells with BAPTA and the mutations introduced in the viroporin domain of NSP4 decrease the amount of PGE_2 produced during infection.

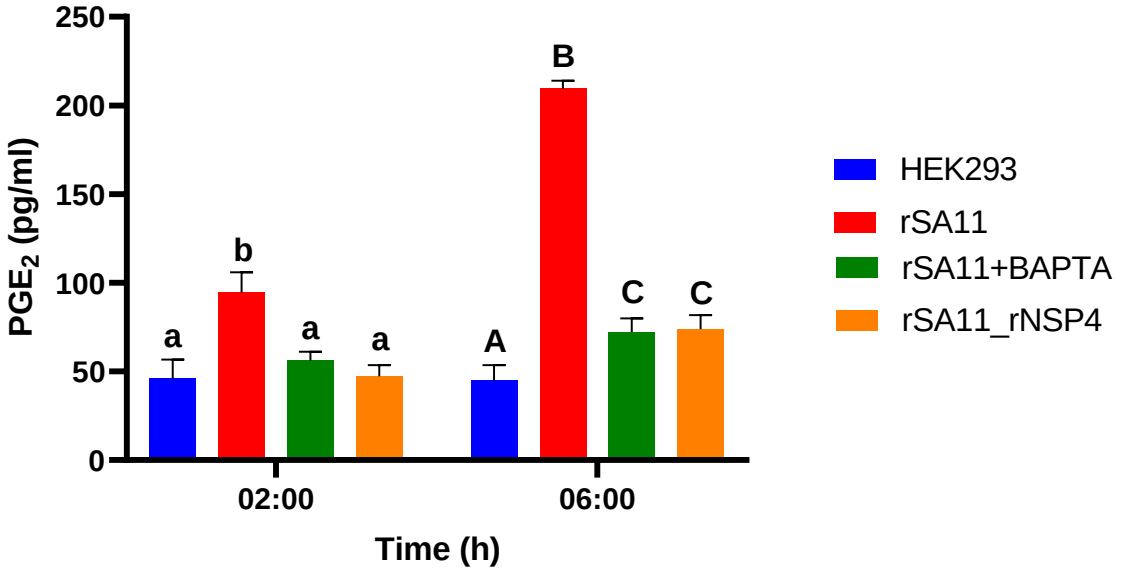

Figure 4. 6. Rotavirus increases the concentration of prostaglandin E_2 in HEK293. The amount of PGE_2 produced during rSA11+BAPTA and rSA11_rNSP4 infection (MOI = 5) as determined by ELISA was compared to rSA11 infected HEK293 cells at two and six hours post infection. Error bars indicate the standard error of the mean (n = 3). Lowercase and uppercase letters indicate a significant difference ($p<0.05$) compared to the control.

4.3.4. *Calcium activity*

To determine how the mutation within the viroporin domain of NSP4 affects calcium activity, we used Fura-dextran, a Ca^{2+} indicator. **Figure 4. 7** shows that the addition of lipopolysaccharides (LPS) to HEK293 cells immediately prior to reading the assay, increases the A340/A380 ratio indicating that the assay was successfully established, since the binding of cytosolic free Ca^{2+} to Fura-2, shifts the peak excitation wavelength from 380 to 340 nm. In addition, we used BAPTA (a cyto[Ca^{2+}] chelator) to lower the activity of Ca^{2+} which can be seen in **Figure 4. 7**. When comparing the Ca^{2+} activity of both rSA11_BAPTA and rSA11_rNSP4 to that of rSA11, at two hours post infection there is no significant difference (**Figure 4. 7A**). However, when looking at Ca^{2+} activity at six hours post infection there is a significant difference in activity when comparing both rSA11+BAPTA and rSA11_rNSP4 to that of rSA11.

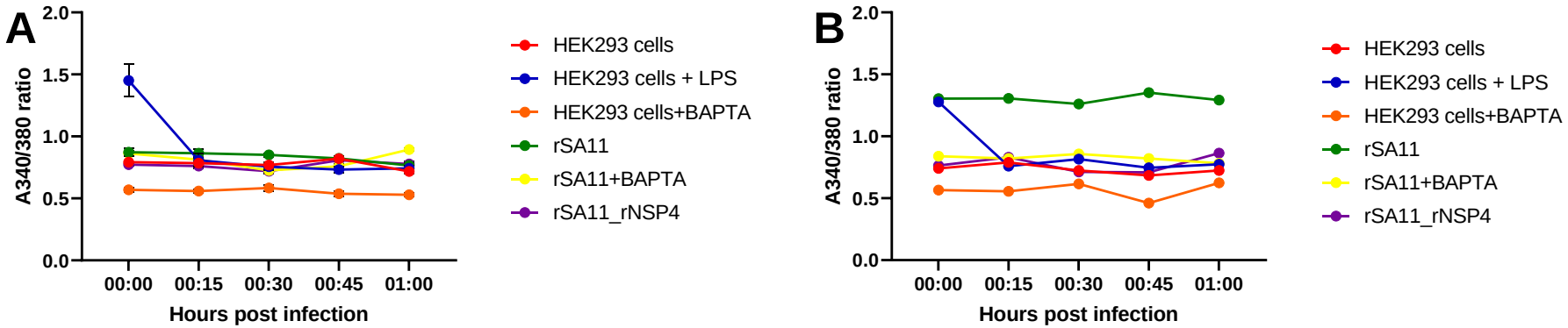

Figure 4. 7. Mutations in the viroporin domain of NSP4 affect Ca^{2+} activity in HEK293 cells. The activity of Ca^{2+} during rSA11+BAPTA and rSA11_rNSP4 infection (MOI = 5) as determined by Fura-dextran was compared to rSA11 infected HEK293 cells at (A) two and (B) six hours post infection. Error bars indicate the standard error of the mean (n = 3).

4.3.5. Cytoplasmic Phospholipase A_2 activity

By using a $cPLA_2$ activity kit we were able to determine the activity of $cPLA_2$ at two and six hours post infection **Figure 4. 8**. When the activity of rSA11+BAPTA (7.40±0.95 µmol/min/ml) and rSA11_NSP4 (5.86±1.03 µmol/min/ml) is compared to rSA11 (15.21±1.55 µmol/min/ml) at two hours post infection, there is a significant (p = 0.0008, p= 0.0005) decrease in activity observed. Furthermore, the ≈ fivefold to ninefold (p = 0.000004, p= 0.000005) reduction in $cPLA_2$ activity between rSA11 (35.94±1.43 µmol/min/ml) and rSA11_BAPTA (7.26±0.96 µmol/min/ml) and rSA11_NSP4 (4.99±1.30 µmol/min/ml) is also observed at six hours post infection. It should be noted that $cPLA_2$ has lower activity in uninfected HEK293 cells compared to HEK293 cells infected with rSA11_rNSP4, indicating a certain degree of NSP4 functionality. Interestingly, our data also shows that rSA11 is capable of activating $cPLA_2$ in a calcium-independent manner at two hours post infection, as cyto[Ca^{2+}] levels are comparable to the uninfected control at the same time point (**Figure 4. 7**).

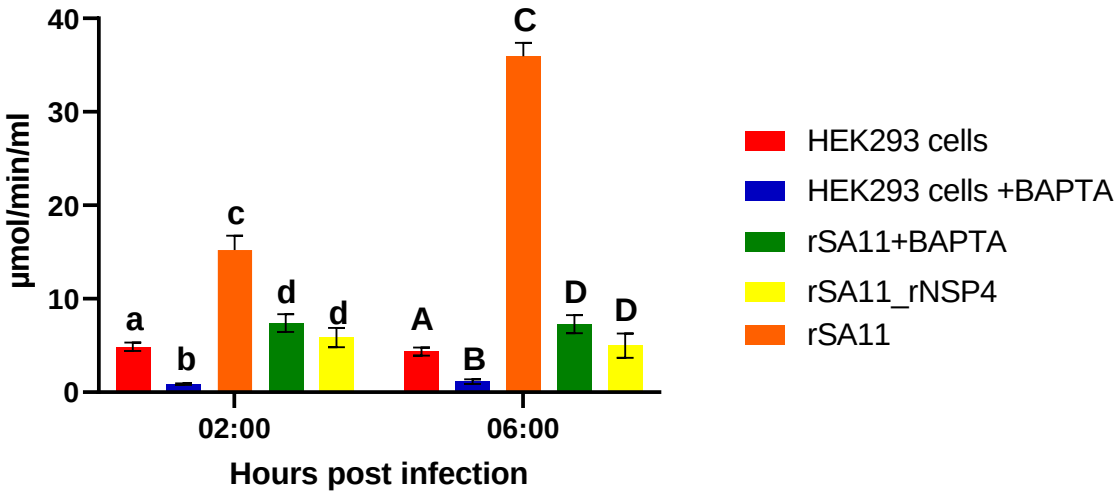

Figure 4. 8. Mutations in the viroporin domain of NSP4 affect phospholipase A_2 activity in HEK293 cells. The activity of phospholipase A_2 during rSA11+BAPTA and rSA11_rNSP4 infection (MOI = 5) as determined by phospholipase A_2 assay was compared to rSA11 infected HEK293 cells at (A) two and (B) six hours post infection. Error bars indicate the standard error of the mean (n = 3). Lowercase and uppercase letters indicate a significant difference ($p<0.05$) compared to the control.

4.3.6. Replication of rSA11_rNSP4

Here, we show the role of the NSP4 viroporin domain and cyto[Ca^{2+}] in RV replication, using an rSA11_rNSP4 and mutant virus and rSA11 infected cells treated with BAPTA. GS6 dsRNA synthesis appears significantly ($p = 0.0015$, $p = 0.0014$) affected at both two hours post infection [rSA11: $1.58x10^3 \pm 4.10x10^2$ molecules/g; rSA11+BAPTA: $5.60x10^1 \pm 3.00x10^1$ molecules/g; rSA11_rNSP4: $2.83x10^1 \pm 1.01x10^1$ molecules/g] and ($p = 0.0026$, $p = 0.0025$) six hours post infection [rSA11: $1.63x10^6 \pm 5.01x10^5$ molecules/g; rSA11+BAPTA: $1.85x10^4 \pm 7.32x10^3$ molecules/g; rSA11_rNSP4: $1.14x10^4 \pm 1.97x10^3$ molecules/g] (**Figure 4. 9A**). In addition, both mutant virus and treatment with BAPTA [rSA11+BAPTA: $3.80x10^1 \pm 3.82x10^1$ $TCID_{50}$/ml; rSA11_rNSP4: $2.70x10^1 \pm 2.62x10^1$ $TCID_{50}$/ml] showed significant ($p = 0.0003$, $p = 0.00034$) difference in viral yield at 2 h post infection compared to rSA11 ($1.44x10^3 \pm 2.55x10^2$ $TCID_{50}$/ml), and both rSA11+BAPTA: $4.93x10^2 \pm 3.19x10^2$ $TCID_{50}$/ml; rSA11_rNSP4: $1.86x10^2 \pm 8.25x10^1$ $TCID_{50}$/ml) showed significantly ($p = 0.00031$, $p = 0.00031$) lower yield at 6 h post infection compared to rSA11 ($1.26x10^6 \pm 9.45x10^5$ $TCID_{50}$/ml) (**Figure 4. 9B**).

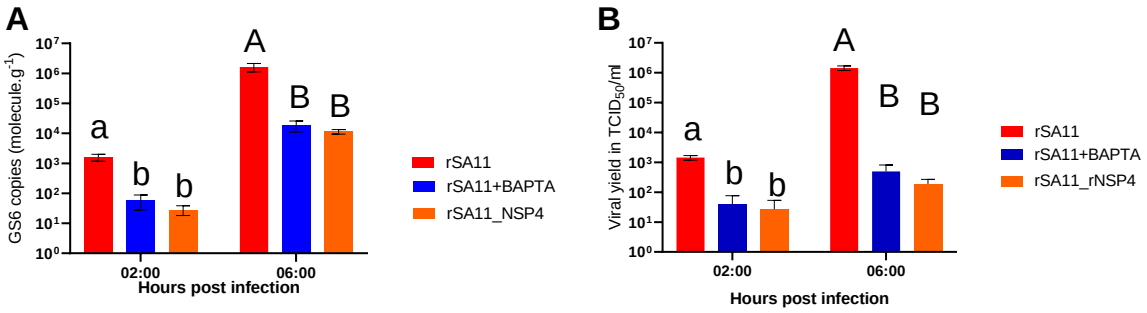

Figure 4. 9. Viral titre and copies of GS6 at 2 and 6 h post infection. A) Copy number of GS6 as determined by RT-qPCR was compared to rSA11-infected HEK293 cells and B) rotavirus yield as determined by $TCID_{50}$ at two and six hours post infection. Error bars indicate the standard error of the mean (n = 3). Lowercase and uppercase letters indicate significant difference ($p<0.05$) compared to the control. For further details see **Error! Reference source not found.**.

4.4. Discussion

The modulation of cyto[Ca^{2+}] is essential for viral replication and morphogenesis (Chang-Graham et al., 2019; 2020)(Chang-Graham et al., 2019; 2020)(Chang-Graham et al., 2019; 2020). The modulation in cyto[Ca^{2+}] is partly due to the viroporin domain, found within NSP4, which causes the flow of Ca^{2+} from ER stores into the cytoplasm (Pham et al., 2017). It has previously been shown that the chelation of cyto[Ca^{2+}] by BAPTA, significantly decreases the amount of RV progeny (Crawford et

al., 2012, 2020). In addition to cyto[Ca^{2+}] being critical for RV replication, it is also essential for the activation of cytoplasmic PLA_2, the rate-limiting enzyme in PGE_2 biosynthesis (Park et al., 2006). In the previous chapters we showed that inhibition of PGE_2 biosynthesis negatively affects RV replication, but that neither viroplasm associated proteins nor the formation of viroplasm-like structures were responsible for the induction of PGE_2.

Here we show that RV increases the activity of $cPLA_2$ during infection of HEK293 cells, subsequently affecting the production of PGE_2. By treating rSA11 infected-HEK293 cells with BAPTA, we showed a significant decrease in $cPLA_2$ activity which led to decreases in PGE_2 production, subsequently affecting both viral progeny and RNA synthesis. The decrease in viral yield is in concurrence with work by Crawford and co-workers (2012, 2020), which showed that treatment of SA11-infected MA104 cells with BAPTA lead to an 86 – 90 % decrease in viral progeny.

Using a modified reverse genetics system for SA11 (Kanai et al., 2017), we provide evidence for the essential role of the viroporin domain of NSP4 in the conduction of cytoplasmic Ca^{2+}, and subsequent increase in PGE_2 production during RV replication. Introduced mutations within the viroporin domain that limit the ability to conduct Ca^{2+} (Pham et al., 2017), significantly decreased the levels cyto[Ca2+], followed by decrease in cPLA2 activity, RNA yield and RV progeny. However, next generation sequencing data revealed additional amino acids changes at T134A, M135A and T137S (**Appendix**). These amino acids are found within the enterotoxin domain, which has been shown to have no effect in increasing cyto[Ca^{2+}] (Hyser et al., 2010; Hu et al., 2012b). While a protein alignment of several RV strains showed that the T137S mutation was quite common (results not shown), the effect of the other two mutations should be considered in future studies. No additional changes in the protein coding regions were observed for the viral proteins analysed.

Although no previous data has shown the importance of $cPLA_2$ during RV infection, several studies have shown its importance for other viruses. West Nile virus and human coronavirus 229E has been shown to require $cPLA_2$ activity for the formation of replication complexes (Liebscher et al., 2018; Müller et al., 2018). In addition, several viruses, including vaccinia virus, parvovirus and human cytomegalovirus, contain their own $cPLA_2$ which they use for enhancing egress, initiating viral replication

or at post entry steps (Baek et al., 1997; Zádori et al., 2001; Allal et al., 2004). The activity of $cPLA_2$ is also regulated by MAP kinase (Lin et al., 1993) and Menzel and co-workers (2012) showed that that hepatitis C virus infection activates the MAP kinase/ERK pathway subsequently modulating the activity of $cPLA_2$. Interestingly, we found that, although cyto[Ca2+] levels are close to basal during early infection, there is already an increase in the activity of $cPLA_2$. It, therefore, appears that rSA11 is able to increase $cPLA_2$ activity in a calcium-independent manner. We speculate that this could be due to the additional regulation of $cPLA_2$ by MAP kinase (Lin et al., 1993). It is therefore possible that NSP2, which has kinase-like activity (Taraporewala et al., 1999; Kumar et al., 2007) phosphorylates $cPLA_2$ early during infection, but this hypothesis needs to be further investigated.

In conclusion, we show that the NSP4 increased cyto[Ca^{2+}] levels, which lead to modulations in the activity of $cPLA_2$, increasing the production of PGE_2. Furthermore, we show that mutations in the viroporin domain of NSP4 affect PGE_2 production. We also show that the activity of $cPLA_2$ may be modulated independently of cytoplasmic Ca^{2+} levels during early infection.

5.1. Conclusions

Rotavirus (RV) increases the production of prostaglandin E_2 (PGE_2) during infection in MA104 cells, and this increase enhances the attachment and internalisation of RV. This supports work done by Rossen and co-workers (2004) who suggested that PGE_2 exerts its proviral effect during the early stages of RV replication. It also correlates with work done by Kim and co-workers (2020) who showed that, depending on when RV-cells are treated with genipin, PGE_2 inhibition either affects early stage (attachment and internalisation) or late stage (assembly and egress) viral replication. We also show that during replication, PGE_2 is produced in lipid droplets (LDs) that form part of viroplasms during viral replication. This aligns with previous data that showed during infection the relative percentages of both γ-linolenic and arachidonic acid is decreased (Sander, 2019).

To determine if viroplasms play a role in the induction of PGE_2 production during viral replication two approaches were employed. Firstly, we either expressed the proteins responsible for viroplasm formation (NSP2 and NSP5) separately or simultaneously so that viroplasm-like structures (VLS) could form. Neither of these conditions were sufficient to induce the production of PGE_2, suggesting that that RV might require at least a fully functioning viroplasm to induce PGE_2 production. Secondly, to verify this, we used the SA11-based reverse genetics system (Kanai et al., 2017) to introduce mutations in the C-terminal α-helix region of NSP5. All the hydrophobic amino acids were replaced with either alanine, to decrease the hydrophobicity, or proline, to completely abrogate the helical structure. Although both mutations lead to a decrease in PGE_2 production during replication, this was most likely due to a concurrent decrease in viral replication and not necessarily due to the decreased interaction between viroplasms and LDs, suggesting that PGE_2 production is induced by a mechanism not directly involving viroplasms **(Figure 5. 1)**. However, as RV can increase the number of LDs within infected cells(Gaunt et al., 2013b; Criglar et al., 2022) , which may increase the number of sites for PGE_2 biosynthesis (Jarc and Petan, 2020), decreased replication in the mutant rSA11_NSP5 viruses could indirectly contribute to lower PGE_2 levels. The rSA11_NSP5 mutant viruses decreased both, viral RNA yield and viral progeny, and we show that this is most likely due to weakened interactions of viroplasms with LDs. This is consistent with work done by Papa and co-

workers (2020) who showed that deleting the tail region of NSP5 severely hampers viral replication, while Sen and co-workers (2007) showed that replacing the hydrophobic amino acids with proline affects the formation of VLS during co-expression with NSP2. Interestingly, the mutation of hydrophobic amino acids to proline within the α-helix region also appears to be affected by the phosphorylation state of NSP5 based on the absence of hyperphosphorylated NSP5 on western blots. This observation, however, needs to be confirmed. Therefore, not only is the tail region required for the interaction of viroplasms with LDs, but the secondary structure (α-helix) and to a lesser extent the hydrophobic nature is also required.

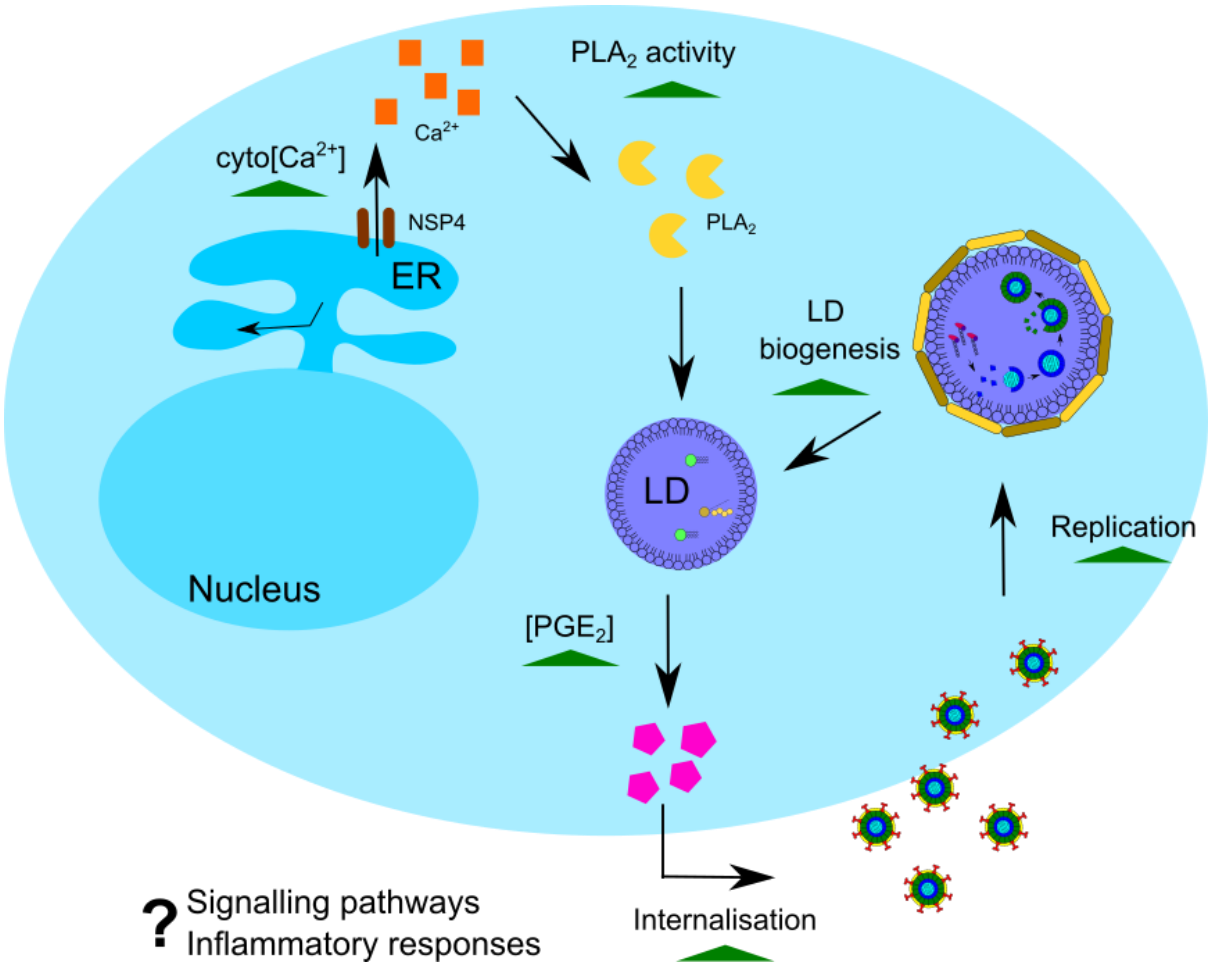

Figure 5. 1. Proposed model for the role of PGE_2 during RV infection. During viral replication cyto[Ca^{2+}] is increased due to the viroporin domain in NSP4 which increases the activity of $cPLA_2$ and subsequently increases the production PGE_2. Increased PGE_2 levels enhance viral attachment/internalisation which in turn increases viral replication and the number of LDs present in cells, resulting in more sites for PGE_2 production. If the pro-viral effect of PGE_2 is due to signalling pathways remain unknown.

After showing that the presence of viroplasms is most likely not directly involved in the induction of PGE_2 production during early infection, we shifted our focus to the role that NSP4-induced increased cytoplasmic Ca^{2+} (cyto[Ca^{2+}]) could have on PGE_2 production **(Figure 5. 1**). We show that during replication, the increase of cyto[Ca^{2+}] increases the activity of cytoplasmic phospholipase A_2 ($cPLA_2$), leading to increased production of PGE_2. Treatment of RV-infected cells with BAPTA-AM, a chelator of cyto[Ca^{2+}], significantly decreases the activity of $cPLA_2$ and consequently causes a decrease in PGE_2 production. A subsequent decrease in viral progeny and RNA yield was observed. This is in concurrence with work done by Crawford and co-workers (2012, 2020) showing that the treatment of RV-infected cells with BAPTA lead to decreases in viral progeny. To prove that NSP4 was responsible for the increase in $cPLA_2$, we introduced mutations in the viroporin domain that result in decreased conductivity of Ca^{2+} (Pham et al., 2017) and found that the introduced mutations limited the activity of $cPLA_2$, decreasing the amount of PGE_2 produced and having negative effects on viral progeny and RNA yield.

The direct or indirect induction of PGE_2 production enhances the internalisation of RV in a yet unknown manner. It is possible that PGE_2 promotes Ca^{2+}-mediated epithelial barrier disruption (Martién-Venegas et al., 2006; Rodríguez-Lagunas et al., 2010)Martién-Venegas et al., 2006; Rodríguez-Lagunas et al., 2010)Martién-Venegas et al., 2006; Rodríguez-Lagunas et al., 2010) or that PGE_2 creates a pro-inflammatory environment that benefits viral replication (Sander et al., 2017). Interestingly, Cheng and co-workers (2015) showed that the internalisation of bovine ephemeral fever virus (BEFV) through clathrin-mediated endocytosis required activation of several pathways, including COX-2-mediated PGE_2/Prostaglandin receptors receptor signalling. The binding of PGE_2 to G-protein-coupled E-(EP) prostanoid receptors stimulated Src-JNK-AP1 and PI3K-Akt-NF-κB signalling, promoting viral entry. In addition, Kaposi's sarcoma-associated herpesvirus, human immunodeficiency virus and human T-lymphotropic virus type 1 have all been shown to utilise PGE_2/EP receptor-mediated signalling (Dumais et al., 1998; Paul et al., 2013). Although no direct evidence links RV and PGE_2/EP signalling, it is known that RV activates both the JNK-AP1 and PI3K-Akt signalling pathways (Holloway and Coulson, 2006; Soliman et al., 2018). The phosphorylated pPI3K, pAkt and pERK interact with V-ATPase, increasing the proton gradient within endosomes resulting in their

acidification and release of RV into the cytoplasm. Furthermore, Holloway and Coulson (2006) showed that the activation of JNK and p38 leads to AP-1-driven transcriptional responses, which can influence RV mRNA levels and replication. It should be noted that the activation of JNK was only observed at two and six h post-infection in Caco-2 and MA104 cells, respectively. It could thus be possible that the increase in PGE_2, during RV infection enhances the internalisation of SA11 by clathrin-mediated endocytosis. Several RV strains use clathrin-mediated endocytosis for entry into host cells (Díaz-Salinas et al., 2013; Arias and López, 2021). This, however, brings up an interesting question of if and how PGE_2 affects clathrin-independent strains, such as the Rhesus rotavirus strain RRV (Gutiérrez et al., 2010; Arias and López, 2021). Furthermore, identifying the receptors involved for PGE_2-mediated internalisation could further enhance our understanding of RV internalisation.

5.2. Significance of study

To conclude, we have shown that PGE_2 enhances RV attachment and internalisation and is induced in a NSP4 viroporin-cyto[Ca^{2+}]-$cPLA_2$-dependent manner during replication. We show that reduced PGE_2 production, significantly affects viral replication and subsequently could limit the inflammatory response and duration of diarrhoea as was shown previously (Yamashiro et al., 1989; Kim et al., 2020). The viroporin domain of NSP4 is therefore a promising target for anti-viral treatment, and with viroporins found in several other viruses including influenza A virus, hepatitis C and HIV-1 (Luis Nieva et al., 2012) the possibility of viroporin inhibitors being used as a broad range anti-viral target is promising.

We also show that the α-helix within the C-terminal of NSP5 is essential for the interaction between viroplasms and LDs, with removal of the helical structure, nearly attenuating viral replication. In addition, the reduced production of PGE_2 observed for the rSA11_rNSP4 and the reduced replication of the rSA11_pNSP5 make combining these mutants an attractive next generation attenuated vaccine candidate with reduced proinflammatory responses.

Abdelhakim, A. H., Salgado, E. N., Fu, X., Pasham, M., Nicastro, D., Kirchhausen, T., et al. (2014). Structural Correlates of Rotavirus Cell Entry. *PLoS Pathog* 10, e1004355. doi: 10.1371/JOURNAL.PPAT.1004355.

Accioly, M. T., Pacheco, P., Maya-Monteiro, C. M., Carrossini, N., Robbs, B. K., Oliveira, S. S., et al. (2008). Lipid Bodies Are Reservoirs of Cyclooxygenase-2 and Sites of Prostaglandin-E 2 Synthesis in Colon Cancer Cells. *Cancer Res* 68, 1732–1740. doi: 10.1158/0008-5472.CAN-07-1999.

Afrikanova, I., Fabbretti, E., Miozzo, M. C., and Burrone, O. R. (1998). Rotavirus NSP5 phosphorylation is up-regulated by interaction with NSP2. *Journal of General Virology* 79, 2679–2686.

Afrikanova, I., Miozzo, M. C., Giambiagi, S., and Burrone, O. (1996). Phosphorylation Generates Different Forms of Rotavirus NSP5. *Journal of General Virology* 77, 2059–2065. doi: 10.1099/0022-1317-77-9-2059.

Allal, C., Buisson-Brenac, C., Marion, V., Claudel-Renard, C., Faraut, T., Dal Monte, P., et al. (2004). Human cytomegalovirus carries a cell-derived phospholipase A2 required for infectivity. *J Virol* 78, 7717–26. doi: 10.1128/JVI.78.14.7717-7726.2004.

Anthony, I. D., Bullivant, S., Dayal, S., Bellamy, A. R., and Berriman, J. A. (1991). Rotavirus spike structure and polypeptide composition. *J Virol* 65, 4334–40.

Arias, C. F., and López, S. (2021). Rotavirus cell entry: not so simple after all. *Curr Opin Virol* 48, 42–48. doi: 10.1016/j.coviro.2021.03.011.

Arias, C. F., Silva-Ayala, D., and López, S. (2015). Rotavirus Entry: a Deep Journey into the Cell with Several Exits. *J Virol* 89, 890. doi: 10.1128/JVI.01787-14.

Arnold, M. M., Sen, A., Greenberg, H. B., and Patton, J. T. (2013). The Battle between Rotavirus and Its Host for Control of the Interferon Signaling Pathway. *PLoS Pathog* 9, e1003064. doi: 10.1371/JOURNAL.PPAT.1003064.

Arnold, M., Patton, J. T., and Mcdonald, S. M. (2009). Culturing, Storage, and Quantification of Rotaviruses. *Current Protocols in Microcbioly*, 1–29. doi: 10.1002/9780471729259.mc15c03s15.

Asbóth, G., Phaneuf, S., Europe-Finner, G. N., Tóth, M., and Bernal, A. L. (1996). Prostaglandin E2 activates phospholipase C and elevates intracellular calcium in cultured myometrial cells: involvement of EP1 and EP3 receptor subtypes. *Endocrinology* 137, 2572–2579. doi: 10.1210/ENDO.137.6.8641211.

Au, K. S., Chan, W. K., Burns, J. W., and Estes, M. K. (1989). Receptor activity of rotavirus nonstructural glycoprotein NS28. *J Virol* 63, 4553–62.

Baek, S.-H., Kwak, J.-Y., Lee, S. H., Lee, T., Ryu, S. H., Uhlinger, D. J., et al. (1997). Lipase Activities of p37, the Major Envelope Protein of Vaccinia Virus. *Journal of Biological Chemistry* 272, 32042–32049. doi: 10.1074/jbc.272.51.32042.

Ball, J. M., Tian, P., Zeng, C. Q., Morris, A. P., and Estes, M. K. (1996). Age-dependent diarrhea induced by a rotaviral nonstructural glycoprotein. *Science* 272, 101–104. doi: 10.1126/science.272.5258.101.

Bandeira-Melo, C., Weller, P. F., and Bozza, P. T. (2011). EicosaCell - an immunofluorescent-based assay to localize newly synthesized eicosanoid lipid mediators at intracellular sites. *Methods Mol Biol* 689, 163–81. doi: 10.1007/978-1-60761-950-5_10.

Barbé, L., le Moullac-Vaidye, B., Echasserieau, K., Bernardeau, K., Carton, T., Bovin, N., et al. (2018). Histo-blood group antigen-binding specificities of human rotaviruses are associated with gastroenteritis but not with in vitro infection. *Sci Rep* 8. doi: 10.1038/S41598-018-31005-4.

Bartz, R., Li, W.-H., Venables, B., Zehmer, J. K., Roth, M. R., Welti, R., et al. (2007). Lipidomics reveals that adiposomes store ether lipids and mediate phospholipid traffic. *J Lipid Res* 48, 837–847. doi: 10.1194/jlr.M600413-JLR200.

Bermúdez, M. A., Balboa, M. A., and Balsinde, J. (2021). Lipid Droplets, Phospholipase A2, Arachidonic Acid, and Atherosclerosis. *Biomedicines* 9. doi: 10.3390/BIOMEDICINES9121891.

Berois, M., Sapin, C., Erk, I., Poncet, D., and Cohen, J. (2003). Rotavirus nonstructural protein NSP5 interacts with major core protein VP2. *J Virol* 77, 1757–1763. doi: 10.1128/JVI.77.3.1757-1763.2003.

Bican, P., Cohen, J., Charpilienne, A., and Scherrer, R. (1982). Purification and characterization of bovine rotavirus cores. *J Virol* 43, 1113–7.

Bingham, C. O., and Austen, K. F. (1999). Phospholipase A2 enzymes in eicosanoid generation. *Proc Assoc Am Physicians* 111, 516–524. doi: 10.1046/j.1525-1381.1999.99321.x.

Blackhall, J., Muñoz, M., Fuentes, A., and Magnusson, G. (1998). Analysis of rotavirus nonstructural protein NSP5 phosphorylation. *J Virol* 72, 6398–405.

Bonventre, J. v., and Swidler, M. (1988). Calcium dependency of prostaglandin E2 production in rat glomerular mesangial cells. Evidence that protein kinase C modulates the Ca2+-dependent activation of phospholipase A2. *J Clin Invest* 82, 168–176. doi: 10.1172/JCI113566.

Borodavka, A., Dykeman, E. C., Schrimpf, W., and Lamb, D. C. (2017). Protein-mediated RNA folding governs sequence-specific interactions between rotavirus genome segments. *Elife* 6. doi: 10.7554/ELIFE.27453.

Boshuizen, J. A., Reimerink, J. H. J., Korteland-van Male, A. M., van Ham, V. J. J., Koopmans, M. P. G., Büller, H. A., et al. (2003). Changes in Small Intestinal Homeostasis, Morphology,and Gene Expression during Rotavirus Infection of

InfantMice. *J Virol* 77, 13005–13016. doi: 10.1128/JVI.77.24.13005-13016.2003/ASSET/F2CAE9C9-64DA-4E93-BF7A-3AF5BB283754/ASSETS/GRAPHIC/JV2430909009.JPEG.

Boshuizen, J. A., Rossen, J. W. A., Sitaram, C. K., Kimenai, F. F. P., Simons-Oosterhuis, Y., Laffeber, C., et al. (2004). Rotavirus Enterotoxin NSP4 Binds to the Extracellular Matrix Proteins Laminin-β3 and Fibronectin. *J Virol* 78, 10045–10053. doi: 10.1128/JVI.78.18.10045-10053.2004/ASSET/F9B06B6D-FFB5-460C-895D-B87D599F3F6A/ASSETS/GRAPHIC/ZJV0180451200005.JPEG.

Boyle, J. F., and Holmes, K. V (1986). RNA-binding proteins of bovine rotavirus. *J Virol* 58, 561–8.

Bozza, P. T., Bakker-Abreu, I., Navarro-Xavier, R. A., and Bandeira-Melo, C. (2011). Lipid body function in eicosanoid synthesis: An update. *Prostaglandins Leukot Essent Fatty Acids* 85, 205–213. doi: 10.1016/j.plefa.2011.04.020.

Bravo, J. P. K., Borodavka, A., Barth, A., Calabrese, A. N., Mojzes, P., Cockburn, J. J. B., et al. (2018). Stability of local secondary structure determines selectivity of viral RNA chaperones. *Nucleic Acids Res* 46, 7924–7937. doi: 10.1093/NAR/GKY394.

Burke, J. E., and Dennis, E. A. (2009). Phospholipase A 2 structure/function, mechanism, and signaling 1. doi: 10.1194/jlr.R800033-JLR200.

Burke, R. M., Tate, J. E., Kirkwood, C. D., Steele, A. D., and Parashar, U. D. (2019). Current and new rotavirus vaccines. *Curr Opin Infect Dis* 32, 435–444. doi: 10.1097/QCO.0000000000000572.

Burnett, E., Parashar, U. D., and Tate, J. E. (2020). Real-world effectiveness of rotavirus vaccines, 2006–19: a literature review and meta-analysis. *Lancet Glob Health* 8, e1195–e1202. doi: 10.1016/S2214-109X(20)30262-X.

Burns, J. W., Siadat-Pajouh, M., Krishnaney, A. A., and Greenberg, H. B. (1996). Protective effect of rotavirus VP6-specific IgA monoclonal antibodies that lack neutralizing activity. *Science* 272, 104–7.

Buttafuoco, A., Michaelsen, K., Tobler, K., Ackermann, M., Fraefel, C., and Eichwald, C. (2020). Conserved Rotavirus NSP5 and VP2 Domains Interact and Affect Viroplasm. *J Virol* 94. doi: 10.1128/JVI.01965-19.

Campagna, M., Eichwald, C., Vascotto, F., and Burrone, O. R. (2005). RNA interference of rotavirus segment 11 mRNA reveals the essential role of NSP5 in the virus replicative cycle. *J Gen Virol* 86, 1481–1487. doi: 10.1099/VIR.0.80598-0.

Caoa, H., Xiaob, L., Park, G., Wang, X., Azimb, A. C., Christman, J. W., et al. (2008). An improved LC-MS-MS method for the quantification of prostaglandins E2 and D2 production in biological fluids. *Anal Biochem* 372, 41–51.

Carreño-Torres, J. J., Gutiérrez, M., Arias, C. F., López, S., and Isa, P. (2010). Characterization of viroplasm formation during the early stages of rotavirus infection. *Virol J* 7, 350. doi: 10.1186/1743-422X-7-350.

Cermelli, S., Guo, Y., Gross, S. P., and Welte, M. A. (2006). The Lipid-Droplet Proteome Reveals that Droplets Are a Protein-Storage Depot. *Current Biology* 16, 1783–1795. doi: 10.1016/j.cub.2006.07.062.

Chang-Graham, A. L., Perry, J. L., Engevik, M. A., Engevik, K. A., Scribano, F. J., Gebert, J. T., et al. (2020). Rotavirus induces intercellular calcium waves through ADP signaling. *Science (1979)* 370. doi: 10.1126/SCIENCE.ABC3621/SUPPL_FILE/ABC3621S9.MP4.

Chang-Graham, A. L., Perry, J. L., Strtak, A. C., Ramachandran, N. K., Criglar, J. M., Philip, A. A., et al. (2019). Rotavirus Calcium Dysregulation Manifests as Dynamic Calcium Signaling in the Cytoplasm and Endoplasmic Reticulum. *Sci Rep* 9, 10822. doi: 10.1038/s41598-019-46856-8.

Chen, D., Luongo, C. L., Nibert, M. L., and Patton, J. T. (1999). Rotavirus open cores catalyze 5'-capping and methylation of exogenous RNA: evidence that VP3 is a methyltransferase. *Virology* 265, 120–130. doi: 10.1006/viro.1999.0029.

Cheng, C. Y., Huang, W. R., Chi, P. I., Chiu, H. C., and Liu, H. J. (2015a). Cell entry of bovine ephemeral fever virus requires activation of Src-JNK-AP1 and PI3K-Akt-NF-κB pathways as well as Cox-2-mediated PGE2/EP receptor signalling to enhance clathrin-mediated virus endocytosis. *Cell Microbiol* 17, 967–987. doi: 10.1111/CMI.12414.

Cheng, C.-Y. Y., Huang, W.-R. R., Chi, P.-I. I., Chiu, H.-C. C., and Liu, H.-J. J. (2015b). Cell entry of bovine ephemeral fever virus requires activation of Src-JNK-AP1 and PI3K-Akt-NF-κB pathways as well as Cox-2-mediated PGE<inf>2</inf>/EP receptor signalling to enhance clathrin-mediated virus endocytosis. *Cell Microbiol* 17, 967–987. doi: 10.1111/cmi.12414.

Cheung, W., Gill, M., Esposito, A., Kaminski, C. F., Courousse, N., Chwetzoff, S., et al. (2010). Rotaviruses associate with cellular lipid droplet components to replicate in viroplasms, and compounds disrupting or blocking lipid droplets inhibit viroplasm formation and viral replication. *J Virol* 84, 6782–6798. doi: 10.1128/JVI.01757-09.

Chizhikov, V., and Patton, J. T. (2000). A four-nucleotide translation enhancer in the 3'-terminal consensus sequence of the nonpolyadenylated mRNAs of rotavirus. *RNA* 6, 814–25.

Choudhary, V., Golani, G., Joshi, A. S., Cottier, S., Schneiter, R., Prinz, W. A., et al. (2018). Architecture of lipid droplets in endoplasmic reticulum is determined by phospholipid intrinsic curvature. *Curr Biol* 28, 915. doi: 10.1016/J.CUB.2018.02.020.

Clark, B., and Desselberger, U. (1988). Myristylation of Rotavirus Proteins. *Journal of General Virology* 69, 2681–2686. doi: 10.1099/0022-1317-69-10-2681.

Clark, J. D., Schievella, A. R., Nalefski, E. A., and Lin, L. L. (1995). Cytosolic phospholipase A2. *J Lipid Mediat Cell Signal* 12, 83–117. doi: 10.1016/0929-7855(95)00012-F.

Cohen, S. (2018). “Lipid Droplets as Organelles,” in *International Review of Cell and Molecular Biology*, 83–110. doi: 10.1016/bs.ircmb.2017.12.007.

Contin, R., Arnoldi, F., Campagna, M., and Burrone, O. R. (2010). Rotavirus NSP5 orchestrates recruitment of viroplasmic proteins. *Journal of General Virology* 91, 1782–1793. doi: 10.1099/vir.0.019133-0.

Coulson, B. S., Londrigan, S. L., and Lee, D. J. (1997). Rotavirus contains integrin ligand sequences and a disintegrin-like domain that are implicated in virus entry into cells. *Proc Natl Acad Sci U S A* 94, 5389–5394. doi: 10.1073/pnas.94.10.5389.

Crawford, S. E., Criglar, J. M., Liu, Z., Broughman, J. R., Estes, M. K., and López, S. (2020). COPII Vesicle Transport Is Required for Rotavirus NSP4 Interaction with the Autophagy Protein LC3 II and Trafficking to Viroplasms. *jvi.asm.org 1 Journal of Virology* 94, 1341–1360. doi: 10.1128/JVI.01341-19.

Crawford, S. E., and Desselberger, U. (2016). Lipid droplets form complexes with viroplasms and are crucial for rotavirus replication. *Curr Opin Virol* 19, 11–15. doi: 10.1016/j.coviro.2016.05.008.

Crawford, S. E., Hyser, J. M., Utama, B., and Estes, M. K. (2012). Autophagy hijacked through viroporin-activated calcium/calmodulin-dependent kinase kinase-β signaling is required for rotavirus replication. *Proceedings of the National Academy of Sciences* 109. doi: 10.1073/pnas.1216539109.

Crawford, S. E., Ramani, S., Tate, J. E., Parashar, U. D., Svensson, L., Hagbom, M., et al. (2017). Rotavirus infection. *Nat Rev Dis Primers* 3, 17083. doi: 10.1038/nrdp.2017.83.

Criglar, J. M., Estes, M. K., and Crawford, S. E. (2022). Rotavirus-Induced Lipid Droplet Biogenesis Is Critical for Virus Replication. *Front Physiol* 13. doi: 10.3389/fphys.2022.836870.

Davidson, G. P., and Barnes, G. L. (1979). Structural and functional abnormalities of the small intestine in infants and young children with rotavirus enteritis. *Acta Paediatr* 68, 181–186. doi: 10.1111/j.1651-2227.1979.tb04986.x.

Denisova, E., Dowling, W., LaMonica, R., Shaw, R., Scarlata, S., Ruggeri, F., et al. (1999). Rotavirus capsid protein VP5* permeabilizes membranes. *J Virol* 73, 3147–53.

Deo, R. C., Groft, C. M., Rajashankar, K. R., and Burley, S. K. (2002). Recognition of the rotavirus mRNA 3’ consensus by an asymmetric NSP3 homodimer. *Cell* 108, 71–81.

Desselberger, U. (2017). Differences of Rotavirus Vaccine Effectiveness by Country: Likely Causes and Contributing Factors. *Pathogens* 6. doi: 10.3390/PATHOGENS6040065.

Díaz-Salinas, M. A., Romero, P., Espinosa, R., Hoshino, Y., López, S., and Arias, C. F. (2013). The Spike Protein VP4 Defines the Endocytic Pathway Used by Rotavirus To Enter MA104 Cells. *J Virol* 87, 1658–1663. doi: 10.1128/JVI.02086-12.

Ding, S., Zhu, S., Ren, L., Feng, N., Song, Y., Ge, X., et al. (2018). Rotavirus VP3 targets MAVS for degradation to inhibit type III interferon expression in intestinal epithelial cells. *Elife* 7. doi: 10.7554/eLife.39494.

Dormitzer, P. R., and Greenberg, H. B. (1992). Calcium chelation induces a conformational change in recombinant herpes simplex virus-1-expressed rotavirus VP7. *Virology* 189, 828–32.

Dormitzer, P. R., Sun, Z. Y. J., Wagner, G., and Harrison, S. C. (2002). The rhesus rotavirus VP4 sialic acid binding domain has a galectin fold with a novel carbohydrate binding site. *EMBO Journal* 21, 885–897. doi: 10.1093/emboj/21.5.885.

Dumais, N., Barbeau, B., Olivier, M., and Tremblay, M. J. (1998). Prostaglandin E2 Up-regulates HIV-1 Long Terminal Repeat-driven Gene Activity in T Cells via NF-κB-dependent and -Independent Signaling Pathways. *Journal of Biological Chemistry* 273, 27306–27314. doi: 10.1074/jbc.273.42.27306.

Duncan, R. (2019). Fusogenic Reoviruses and Their Fusion-Associated Small Transmembrane (FAST) Proteins. *https://doi.org/10.1146/annurev-virology-092818-015523* 6, 341–363. doi: 10.1146/ANNUREV-VIROLOGY-092818-015523.

Dunn, S. J., Cross, T. L., and Greenberg, H. B. (1994). Comparison of the Rotavirus Nonstructural Protein NSP1 (NS53) from Different Species by Sequence Analysis and Northern Blot Hybridization. *Virology* 203, 178–183. doi: 10.1006/viro.1994.1471.

Eichwald, C., Arnoldi, F., Laimbacher, A. S., Schraner, E. M., Fraefel, C., Wild, P., et al. (2012). Rotavirus Viroplasm Fusion and Perinuclear Localization Are Dynamic Processes Requiring Stabilized Microtubules. *PLoS One* 7, e47947. doi: 10.1371/journal.pone.0047947.

Eichwald, C., Rodriguez, J. F., and Burrone, O. R. (2004). Characterization of rotavirus NSP2/NSP5 interactions and the dynamics of viroplasm formation. *Journal of General Virology* 85, 625–634. doi: 10.1099/vir.0.19611-0.

Eichwald, C., Vascotto, F., Fabbretti, E., and Burrone, O. R. (2002). Rotavirus NSP5: Mapping Phosphorylation Sites and Kinase Activation and Viroplasm Localization Domains. *J Virol* 76, 3461–3470. doi: 10.1128/JVI.76.7.3461-3470.2002.

Ericson, B. L., Graham, D. Y., Mason, B. B., and Estes, M. K. (1982). Identification, synthesis, and modifications of simian rotavirus SA11 polypeptides in infected cells. *J Virol* 42, 825–39.

Ericson, B. L., Graham, D. Y., Mason, B. B., Hanssen, H. H., and Estes, M. K. (1983). Two types of glycoprotein precursors are produced by the simian rotavirus SA11. *Virology* 127, 320–32.

Estes, M. K., and Greenberg, H. B. (2013). "Rotaviruses," in *Fields in Virology*, eds. D. M. Knipe and P. M. Howley (Philadelphia: Lippincott Williams & Wilkins), 1347–1401.

Estes, M. K., Kang, G., Zeng, C. Q., Crawford, S. E., and Ciarlet, M. (2001). Pathogenesis of rotavirus gastroenteritis. *Novartis Found Symp* 238, 82–96; discussion 96-100.

Evans, J. H., Spencer, D. M., Zweifach, A., and Leslie, C. C. (2001). Intracellular Calcium Signals Regulating Cytosolic Phospholipase A 2 Translocation to Internal Membranes. *Journal of Biological Chemistry* 276, 30150–30160. doi: 10.1074/jbc.M100943200.

Exner, T., Beretta, C. A., Gao, Q., Afting, C., Romero-Brey, I., Bartenschlager, R., et al. (2019). Lipid droplet quantification based on iterative image processing. *J Lipid Res* 60, 1333–1344. doi: 10.1194/jlr.D092841.

Fabbretti, E., Afrikanova, I., Vascotto, F., and Burrone, O. R. (1999). Two non-structural rotavirus proteins, NSP2 and NSP5, form viroplasm-like structures in vivo. *Journal of General Virology* 80, 333–339.

Fiore, L., Greenberg, H. B., and Mackow, E. R. (1991). The VP8 fragment of VP4 is the rhesus rotavirus hemagglutinin. *Virology* 181, 553–63.

Funk, C. D. (2001). Prostaglandins and leukotrienes: advances in eicosanoid biology. *Science (1979)* 294, 1871–1875. doi: 10.1126/science.294.5548.1871.

Gaunt, E. R., Cheung, W., Richards, J. E., Lever, A., and Desselberger, U. (2013a). Inhibition of rotavirus replication by downregulation of fatty acid synthesis. *Journal of General Virology* 94, 1310–1317. doi: 10.1099/vir.0.050146-0.

Gaunt, E. R., Zhang, Q., Cheung, W., Wakelam, M. J. O., Lever, A. M. L., and Desselberger, U. (2013b). Lipidome analysis of rotavirus-infected cells confirms the close interaction of lipid droplets with viroplasms. *Journal of General Virology* 94, 1576–1586. doi: 10.1099/vir.0.049635-0.

Geiger, F., Acker, J., Papa, G., Wang, X., Arter, W. E., Saar, K. L., et al. (2021). Liquid–liquid phase separation underpins the formation of replication factories in rotaviruses. *EMBO J* 40, e107711. doi: 10.15252/EMBJ.2021107711.

Gijón, M. A., and Leslie, C. C. (1999). Regulation of arachidonic acid release and cytosolic Phospholipase A 2 activation. *J Leukoc Biol* 65, 330–336. doi: 10.1002/jlb.65.3.330.

Gilmore, K. J., Quinn, H. E., and Wilson, M. R. (2001). Pinocytic loading of cytochrome c into intact cells specifically induces caspase-dependent permeabilization of mitochondria: evidence for a cytochrome c feedback loop. *Cell Death Differ* 8, 631–639. doi: 10.1038/sj.cdd.4400858.

González, R. A., Torres-Vega, M. A., López, S., and Arias, C. F. (1998). In vivo interactions among rotavirus nonstructural proteins. *Arch Virol* 143, 981–996. doi: 10.1007/s007050050347.

González, S. A., and Burrone, O. R. (1991). Rotavirus NS26 is modified by addition of single O-linked residues of N-acetylglucosamine. *Virology* 182, 8–16.

Graff, J. W., Mitzel, D. N., Weisend, C. M., Flenniken, M. L., and Hardy, M. E. (2002). Interferon regulatory factor 3 is a cellular partner of rotavirus NSP1. *J Virol* 76, 9545–50. doi: 10.1128/JVI.76.18.9545.

Greenberg, H. B., Flores, J., Kalica, A. R., Wyatt, R. G., and Jones, R. (1983). Gene Coding Assignments for growth Restriction, Neutralization and Subgroup Specificities of the W and DS-1 Strains of Human Rotavirus. *Journal of General Virology* 64, 313–320. doi: 10.1099/0022-1317-64-2-313.

Groft, C. M., and Burley, S. K. (2002). Recognition of eIF4G by rotavirus NSP3 reveals a basis for mRNA circularization. *Mol Cell* 9, 1273–83.

Gubern, A., Casas, J., Barceló -Torns, M., Barneda, D., de la Rosa, X., Masgrau, R., et al. (2008). Group IVA Phospholipase A 2 Is Necessary for the Biogenesis of Lipid Droplets . *Journal of Biological Chemistry* 283, 27369–27382. doi: 10.1074/jbc.M800696200.

Guo, Y., Cordes, K. R., Farese, R. V, and Walther, T. C. (2009). Lipid droplets at a glance. *J Cell Sci* 122, 749–752. doi: 10.1242/jcs.037630.

Gutiérrez, M., Isa, P., Sánchez-San Martin, C., Pérez-Vargas, J., Espinosa, R., Arias, C. F., et al. (2010). Different rotavirus strains enter MA104 cells through different endocytic pathways: the role of clathrin-mediated endocytosis. *J Virol* 84, 9161–9169. doi: 10.1128/JVI.00731-10.

Hagbom, M., Istrate, C., Engblom, D., Karlsson, T., Rodriguez-Diaz, J., Buesa, J., et al. (2011). Rotavirus Stimulates Release of Serotonin (5-HT) from Human Enterochromaffin Cells and Activates Brain Structures Involved in Nausea and Vomiting. *PLoS Pathog* 7. doi: 10.1371/JOURNAL.PPAT.1002115.

Hagbom, M., Sharma, S., Lundgren, O., and Svensson, L. (2012). Towards a human rotavirus disease model. *Curr Opin Virol* 2, 408–418. doi: 10.1016/j.coviro.2012.05.006.

Hanna, V. S., and Hafez, E. A. A. (2018). Synopsis of arachidonic acid metabolism: A review. *J Adv Res* 11, 23–32. doi: 10.1016/j.jare.2018.03.005.

Harizi, H., Corcuff, J.-B., and Gualde, N. (2008). Arachidonic-acid-derived eicosanoids: roles in biology and immunopathology. *Trends Mol Med* 14, 461–9. doi: 10.1016/j.molmed.2008.08.005.

Henschke, N., Bergman, H., Hungerford, D., Cunliffe, N. A., Grais, R. F., Kang, G., et al. (2022). The efficacy and safety of rotavirus vaccines in countries in Africa and Asia with high child mortality. *Vaccine* 40, 1707–1711. doi: 10.1016/j.vaccine.2022.02.003.

Hodges, B. D. M., and Wu, C. C. (2010). Proteomic insights into an expanded cellular role for cytoplasmic lipid droplets. *J Lipid Res* 51, 262. doi: 10.1194/JLR.R003582.

Holloway, G., and Coulson, B. S. (2006). Rotavirus Activates JNK and p38 Signaling Pathways in Intestinal Cells, Leading to AP-1-Driven Transcriptional Responses and Enhanced Virus Replication. *J Virol* 80, 10624–10633. doi: 10.1128/JVI.00390-06.

Holloway, G., Johnson, R. I., Kang, Y., Dang, V. T., Stojanovski, D., Coulson, B. S., et al. (2015). Rotavirus NSP6 localizes to mitochondria via a predicted N-terminal α-helix. *Journal of General Virology* 96, 3519–3524. doi: 10.1099/jgv.0.000294.

Hoshino, Y., and Kapikian, A. Z. (1996). Classification of rotavirus VP4 and VP7 serotypes. *Arch Virol Suppl* 12, 99–111.

Hoshino, Y., Sereno, M. M., Midthun, K., Flores, J., Kapikian, A. Z., and Chanock, R. M. (1985). Independent segregation of two antigenic specificities (VP3 and VP7) involved in neutralization of rotavirus infectivity. *Proc Natl Acad Sci U S A* 82, 8701–4.

Hu, L., Crawford, S. E., Czako, R., Cortes-Penfield, N. W., Smith, D. F., le Pendu, J., et al. (2012a). Cell attachment protein VP8* of a human rotavirus specifically interacts with A-type histo-blood group antigen. *Nature* 485, 256–259. doi: 10.1038/nature10996.

Hu, L., Crawford, S. E., Hyser, J. M., Estes, M. K., and Prasad, B. V. V. (2012b). Rotavirus non-structural proteins: Structure and function. *Curr Opin Virol* 2, 380–388. doi: 10.1016/j.coviro.2012.06.003.

Hua, J., Chen, X., and Patton, J. T. (1994). Deletion mapping of the rotavirus metalloprotein NS53 (NSP1): the conserved cysteine-rich region is essential for virus-specific RNA binding. *J Virol* 68, 3990–4000.

Hyser, J. M., Collinson-Pautz, M. R., Utama, B., and Estes, M. K. (2010). Rotavirus disrupts calcium homeostasis by NSP4 viroporin activity. *mBio* 1. doi: 10.1128/mBio.00265-10.

International Committee on Taxonomy of Viruses (2021). ICTV Taxonomy Release. Available at: https://ictv.global/taxonomy [Accessed November 13, 2022].

Jackson, C. L., Walch, L., and Verbavatz, J.-M. (2016). Lipids and Their Trafficking: An Integral Part of Cellular Organization. *Dev Cell* 39, 139–153. doi: 10.1016/j.devcel.2016.09.030.

Jagannath, M. R., Vethanayagam, R. R., Reddy, B. S., Raman, S., and Rao, C. D. (2000). Characterization of human symptomatic rotavirus isolates MP409 and MP480 having “long” RNA electropherotype and subgroup I specificity, highly related to the P6[1],G8 type bovine rotavirus A5, from Mysore, India. *Arch Virol* 145, 1339–57.

Jarc, E., and Petan, T. (2020). A twist of FATe: Lipid droplets and inflammatory lipid mediators. *Biochimie* 169, 69–87. doi: 10.1016/J.BIOCHI.2019.11.016.

Jayaram, H., Taraporewala, Z., Patton, J. T., and Prasad, B. V. V. (2002). Rotavirus protein involved in genome replication and packaging exhibits a HIT-like fold. *Nature* 417, 311–315. doi: 10.1038/417311a.

Jiménez-Zaragoza, M., Yubero, M. P., Martín-Forero, E., Castón, J. R., Reguera, D., Luque, D., et al. (2018). Biophysical properties of single rotavirus particles account for the functions of protein shells in a multilayered virus. *Elife* 7. doi: 10.7554/eLife.37295.

Johne, R., Schilling-Loeffler, K., Ulrich, R. G., and Tausch, S. H. (2022). Whole Genome Sequence Analysis of a Prototype Strain of the Novel Putative Rotavirus Species L. *Viruses* 14. doi: 10.3390/V14030462/S1.

Kalica, A. R., Flores, J., and Greenberg, H. B. (1983). Identification of the rotaviral gene that codes for hemagglutination and protease-enhanced plaque formation. *Virology* 125, 194–205.

Kalica, A. R., Greenberg, H. B., Wyatt, R. G., Flores, J., Sereno, M. M., Kapikian, A. Z., et al. (1981). Genes of human (strain Wa) and bovine (strain UK) rotaviruses that code for neutralization and subgroup antigens. *Virology* 112, 385–90.

Kanai, Y., Komoto, S., Kawagishi, T., Nouda, R., Nagasawa, N., Onishi, M., et al. (2017). Entirely plasmid-based reverse genetics system for rotaviruses. *Proceedings of the National Academy of Sciences*, 201618424. doi: 10.1073/pnas.1618424114.

Kang, G. (2013). New-Generation Treatment? Targeted Antiviral Therapy for Rotavirus. doi: 10.1053/j.gastro.2013.08.023.

Kaplan, L., Weiss, J., and Elsbach, P. (1978). Low concentrations of indomethacin inhibit phospholipase A2 of rabbit polymorphonuclear leukocytes. *Proc Natl Acad Sci U S A* 75, 2955–2958. doi: 10.1073/pnas.75.6.2955.

Kattoura, M. D., Chen, X., and Patton, J. T. (1994). The Rotavirus RNA-Binding Protein NS35 (NSP2) Forms 10S Multimers and Interacts with the Viral RNA Polymerase. *Virology* 202, 803–813. doi: 10.1006/viro.1994.1402.

Kattoura, M. D., Clapp, L. L., and Patton, J. T. (1992). The rotavirus nonstructural protein, NS35, possesses RNA-binding activity in vitro and in vivo. *Virology* 191, 698–708. doi: 10.1016/0042-6822(92)90245-K.

Kelley, L. A., Mezulis, S., Yates, C. M., Wass, M. N., and Sternberg, M. J. E. (2015). The Phyre2 web portal for protein modeling, prediction and analysis. *Nature Protocols 2015 10:6* 10, 845–858. doi: 10.1038/nprot.2015.053.

Kim, J. H., Kim, K., and Kim, W. (2020). Genipin inhibits rotavirus-induced diarrhea by suppressing viral replication and regulating inflammatory responses. *Scientific Reports 2020 10:1* 10, 1–11. doi: 10.1038/s41598-020-72968-7.

Kim, Y., George, D., Prior, A. M., Prasain, K., Hao, S., Le, D. D., et al. (2012). Novel triacsin C analogs as potential antivirals against rotavirus infections. *Eur J Med Chem* 50, 311–318. doi: 10.1016/j.ejmech.2012.02.010.

Kojima, K., Taniguchi, K., and Kobayashi, N. (1996). Species-specific and interspecies relatedness of NSP1 sequences in human, porcine, bovine, feline, and equine rotavirus strains. *Arch Virol* 141, 1–12.

Kuda, O., Jenkins, C. M., Skinner, J. R., Moon, S. H., Su, X., Gross, R. W., et al. (2011). CD36 protein is involved in store-operated calcium flux, phospholipase A2 activation, and production of prostaglandin E2. *J Biol Chem* 286, 17785–17795. doi: 10.1074/JBC.M111.232975.

Kumar, D., Yu, X., Crawford, S. E., Moreno, R., Jakana, J., Sankaran, B., et al. (2020). 2.7 Å cryo-EM structure of rotavirus core protein VP3, a unique capping machine with a helicase activity. *Sci Adv* 6. doi: 10.1126/SCIADV.AAY6410.

Kumar, M., Jayaram, H., Vasquez-Del Carpio, R., Jiang, X., Taraporewala, Z. F., Jacobson, R. H., et al. (2007). Crystallographic and Biochemical Analysis of Rotavirus NSP2 with Nucleotides Reveals a Nucleoside Diphosphate Kinase-Like Activity. *J Virol* 81, 12272–12284. doi: 10.1128/JVI.00984-07.

Lawton, J. A., Estes, M. K., and Prasad, B. v (1997). Three-dimensional visualization of mRNA release from actively transcribing rotavirus particles. *Nat Struct Biol* 4, 118–21. Available at: http://www.ncbi.nlm.nih.gov/pubmed/9033591.

Leslie, C. C. (2015). Cytosolic phospholipase A2: physiological function and role in disease. *J Lipid Res* 56, 1386–1402. doi: 10.1194/JLR.R057588.

Li, Z., Baker, M. L., Jiang, W., Estes, M. K., and Prasad, B. V. V. (2009). Rotavirus architecture at subnanometer resolution. *J Virol* 83, 1754–66. doi: 10.1128/JVI.01855-08.

Liebscher, S., Ambrose, R. L., Aktepe, T. E., Mikulasova, A., Prier, J. E., Gillespie, L. K., et al. (2018). Phospholipase A2 activity during the replication cycle of the flavivirus West Nile virus. *PLoS Pathog* 14, e1007029. doi: 10.1371/journal.ppat.1007029.

Lin, L. L., Wartmann, M., Lin, A. Y., Knopf, J. L., Seth, A., and Davis, R. J. (1993). cPLA2 is phosphorylated and activated by MAP kinase. *Cell* 72, 269–278. doi: 10.1016/0092-8674(93)90666-E.

Liu, H., and Cheng, L. (2015). Cryo-EM shows the polymerase structures and a nonspooled genome within a dsRNA virus. *Science (1979)* 349, 1347–1350. doi: 10.1126/SCIENCE.AAA4938/SUPPL_FILE/LIU.SM.PDF.

Liu, M., and Estes, M. K. (1989). Nucleotide sequence of the simian rotavirus SA11 genome segment 3. *Nucleic Acids Res* 17, 7991–7991. doi: 10.1093/nar/17.19.7991.

Liu, M., Mattion, N. M., and Estes, M. K. (1992). Rotavirus VP3 expressed in insect cells possesses guanylyltransferase activity. *Virology* 188, 77–84. doi: 10.1016/0042-6822(92)90736-9.

Liu, M., Yang, Y., Gu, C., Yue, Y., Wu, K. K., Wu, J., et al. (2007). Spike protein of SARS-CoV stimulates cyclooxygenase-2 expression via both calcium-dependent and calcium-independent protein kinase C pathways . *The FASEB Journal* 21, 1586–1596. doi: 10.1096/FJ.06-6589COM.

Long, C. P., and McDonald, S. M. (2017). Rotavirus genome replication: Some assembly required. *PLoS Pathog* 13, e1006242. doi: 10.1371/journal.ppat.1006242.

López, S., Arias, C. F., Bell, J. R., Strauss, J. H., and Espejo, R. T. (1985). Primary structure of the cleavage site associated with trypsin enhancement of rotavirus SA11 infectivity. *Virology* 144, 11–9. Available at: http://www.ncbi.nlm.nih.gov/pubmed/2998038 [Accessed October 24, 2018].

Lorrot, M., and Vasseur, M. (2007). How do the rotavirus NSP4 and bacterial enterotoxins lead differently to diarrhea? *Virol J* 4, 1–6. doi: 10.1186/1743-422X-4-31/TABLES/1.

Ludert, J. E., Feng, N., Yu, J. H., Broome, R. L., Hoshino, Y., and Greenberg, H. B. (1996). Genetic mapping indicates that VP4 is the rotavirus cell attachment protein in vitro and in vivo. *J Virol* 70, 487–93.

Ludwig, J., Bovens, S., Brauch, C., Elfringhoff, A. S., and Lehr, M. (2006). Design and synthesis of 1-indol-1-yl-propan-2-ones as inhibitors of human cytosolic phospholipase A2α. *J Med Chem* 49, 2611–2620. doi: 10.1021/JM051243A/SUPPL_FILE/JM051243ASI20060301_113316.PDF.

Luis Nieva, J., Madan, V., and Carrasco, L. (2012). Viroporins: structure and biological functions. doi: 10.1038/nrmicro2820.

Mansell, E. A., Ramig, R. F., and Patton, J. T. (1994). Temperature-sensitive lesions in the capsid proteins of the rotavirus mutants tsF and tsG that affect virion assembly. *Virology* 204, 69–81.

Martién-Venegas, R., Roig-Peérez, S., Ferrer, R., and Moreno, J. J. (2006). Arachidonic acid cascade and epithelial barrier function during Caco-2 cell differentiation. *J Lipid Res* 47, 1416–1423. doi: 10.1194/jlr.M500564-JLR200.

Martínez, J. L., Eichwald, C., Schraner, E. M., López, S., and Arias, C. F. (2022). Lipid metabolism is involved in the association of rotavirus viroplasms with

endoplasmic reticulum membranes. *Virology* 569, 29–36. doi: 10.1016/J.VIROL.2022.02.005.

Martínez, M. A., López, S., Arias, C. F., and Isa, P. (2013). Gangliosides Have a Functional Role during Rotavirus Cell Entry. *J Virol* 87, 1115–1122. doi: 10.1128/JVI.01964-12.

Mason, B. B., Graham, D. Y., and Estes, M. K. (1980). In vitro transcription and translation of simian rotavirus SA11 gene products. *J Virol* 33, 1111–21.

Matthijnssens, J., Attoui, H., Bányai, K., Brussaard, C. P. D., Danthi, P., del Vas, M., et al. (2022). ICTV Virus Taxonomy Profile: Sedoreoviridae 2022. *J Gen Virol* 103, 001782. doi: 10.1099/JGV.0.001782/CITE/REFWORKS.

Mattion, N. M., Cohen, J., Aponte, C., and Estes, M. K. (1992). Characterization of an oligomerization domain and RNA-binding properties on rotavirus nonstructural protein NS34. *Virology* 190, 68–83.

Mattion, N. M., Mitchell, D. B., Both, G. W., and Estes, M. K. (1991). Expression of rotavirus proteins encoded by alternative open reading frames of genome segment 11. *Virology* 181, 295–304. doi: 10.1016/0042-6822(91)90495-W.

Mellas, S. P. (2002). Extracellular Calcium Regulation of COX-2 Expression. Available at: https://opencommons.uconn.edu/sodm_masters/90 [Accessed November 17, 2022].

Menzel, N., Fischl, W., Hueging, K., Bankwitz, D., and Frentzen, A. (2012). MAP-Kinase Regulated Cytosolic Phospholipase A2 Activity Is Essential for Production of Infectious Hepatitis C Virus Particles. *PLoS Pathog* 8, 1002829. doi: 10.1371/journal.ppat.1002829.

Meyer, J. C., Bergmann, C. C., and Bellamy, A. R. (1989). Interaction of rotavirus cores with the nonstructural glycoprotein NS28. *Virology* 171, 98–107.

Michelangeli, F., Abad, M. J., Ruiz, M. C., Cohen, J., Charpilienne, A., Vasseur, M., et al. (1997). Solubilized and cleaved VP7, the outer glycoprotein of rotavirus, induces permeabilization of cell membrane vesicles. *Journal of General Virology* 78, 1367–1371. doi: 10.1099/0022-1317-78-6-1367.

Mitchell, D. B., and Both, G. W. (1990a). Completion of the genomic sequence of the simian rotavirus SA11: nucleotide sequences of segments 1, 2, and 3. *Virology* 177, 324–31.

Mitchell, D. B., and Both, G. W. (1990b). Conservation of a potential metal binding motif despite extensive sequence diversity in the rotavirus nonstructural protein NS53. *Virology* 174, 618–21.

Mitchell, J. A., Akarasereenont, P., Thiemermann, C., Flower, R. J., and Vane, J. R. (1993). Selectivity of nonsteroidal antiinflammatory drugs as inhibitors of constitutive and inducible cyclooxygenase. *Proceedings of the National Academy of Sciences* 90, 11693–11697. doi: 10.1073/pnas.90.24.11693.

Mlera, L., O'Neill, H. G., Jere, K. C., and van Dijk, A. a. (2013). Whole-genome consensus sequence analysis of a South African rotavirus SA11 sample reveals a mixed infection with two close derivatives of the SA11-H96 strain. *Arch Virol* 158, 1021–1030. doi: 10.1007/s00705-012-1559-5.

Monson, E. A., Trenerry, A. M., Laws, J. L., Mackenzie, J. M., and Helbig, K. J. (2021). Lipid droplets and lipid mediators in viral infection and immunity. *FEMS Microbiol Rev* 45, 1–20. doi: 10.1093/femsre/fuaa066.

Müller, C., Hardt, M., Schwudke, D., Neuman, B. W., Pleschka, S., and Ziebuhr, J. (2018). Inhibition of Cytosolic Phospholipase A 2 α Impairs an Early Step of Coronavirus Replication in Cell Culture . *J Virol* 92. doi: 10.1128/JVI.01463-17/SUPPL_FILE/ZJV004183282S1.PDF.

Murakami, M., Sato, H., and Taketomi, Y. (2020). Updating Phospholipase A2 Biology. *Biomolecules* 10, 1457. doi: 10.3390/biom10101457.

Nalefski, E. A., and Falke, J. J. (1996). The C2 domain calcium-binding motif: Structural and functional diversity. *Protein Science* 5, 2375–2390.

Offit, P. A., and Blavat, G. (1986). Identification of the two rotavirus genes determining neutralization specificities. *J Virol* 57, 376–8.

Papa, G., Borodavka, A., and Desselberger, U. (2021). Viroplasms: Assembly and Functions of Rotavirus Replication Factories. *Viruses* 13, 1349. doi: 10.3390/v13071349.

Papa, G., Venditti, L., Arnoldi, F., Schraner, E. M., Potgieter, C., Borodavka, A., et al. (2020). Recombinant rotaviruses rescued by reverse genetics reveal the role of NSP5 hyperphosphorylation in the assembly of viral factories. *J Virol* 94. doi: 10.1101/660217.

Park, J. Y., Pillinger, M. H., and Abramson, S. B. (2006). Prostaglandin E_2 synthesis and secretion: The role of PGE_2 synthases. *Clinical Immunology* 119, 229–240. doi: 10.1016/j.clim.2006.01.016.

Patton, J. T. (1995). Structure and function of the rotavirus RNA-binding proteins. *Journal of General Virology* 76, 2633–2644. doi: 10.1099/0022-1317-76-11-2633.

Patton, J. T. (1996). Rotavirus VP1 alone specifically binds to the 3' end of viral mRNA, but the interaction is not sufficient to initiate minus-strand synthesis. *J Virol* 70, 7940–7.

Patton, J. T. (2001). Rotavirus RNA replication and gene expression. *Novartis Found Symp* 238, 64–77; discussion 77-81.

Patton, J. T., Jones, M. T., Kalbach, A. N., He, Y. W., and Xiaobo, J. (1997). Rotavirus RNA polymerase requires the core shell protein to synthesize the double-stranded RNA genome. *J Virol* 71, 9618–9626.

Paul, A. G., Chandran, B., and Sharma-Walia, N. (2013). Cyclooxygenase-2-prostaglandin e2-eicosanoid receptor inflammatory axis: A key player in Kaposi's sarcoma-associated herpes virus associated malignancies. *Translational Research* 162, 77–92. doi: 10.1016/j.trsl.2013.03.004.

Petrie, B. L., Greenberg, H. B., Graham, D. Y., and Estes, M. K. (1984). Ultrastructural localization of rotavirus antigens using colloidal gold. *Virus Res* 1, 133–52.

Pham, T., Perry, J. L., Dosey, T. L., Delcour, A. H., and Hyser, J. M. (2017). The Rotavirus NSP4 Viroporin Domain is a Calcium-conducting Ion Channel. *Sci Rep* 7, 43487. doi: 10.1038/srep43487.

Phipps, R. P., Stein, S. H., and Roper, R. L. (1991). A new view of prostaglandin E regulation of the immune response. *Immunol Today* 12, 349–352. doi: 10.1016/0167-5699(91)90064-Z.

Piron, M. (1998). Rotavirus RNA-binding protein NSP3 interacts with eIF4GI and evicts the poly(A) binding protein from eIF4F. *EMBO J* 17, 5811–5821. doi: 10.1093/emboj/17.19.5811.

Pizarro, J. L., Sandino, A. M., Pizarro, J. M., Fernández, J., and Spencer, E. (1991). Characterization of rotavirus guanylyltransferase activity associated with polypeptide VP3. *J Gen Virol* 72 (Pt 2), 325–32. doi: 10.1099/0022-1317-72-2-325.

Pohl, M. O., and Stertz, S. (2015). Measuring Attachment and Internalization of Influenza A Virus in A549 Cells by Flow Cytometry. *Journal of Visualized Experiments*, 53372. doi: 10.3791/53372.

Poncet, D., Duarte, M., Arias, C. F., González, R. A., López, S., and Torres-Vega, M. A. (2000). The C-terminal domain of rotavirus NSP5 is essential for its multimerization, hyperphosphorylation and interaction with NSP6. *Journal of General Virology* 81, 821–830. doi: 10.1099/0022-1317-81-3-821.

Poncet, D., Laurent, S., and Cohen, J. (1994). Four nucleotides are the minimal requirement for RNA recognition by rotavirus non-structural protein NSP3. *EMBO J* 13, 4165–73.

Poncet, D., Lindenbaum, P., L'Haridon, R., and Cohen, J. (1997). In vivo and in vitro phosphorylation of rotavirus NSP5 correlates with its localization in viroplasms. *J Virol* 71, 34–41.

Potgieter, A. C., Page, N. A., Liebenberg, J., Wright, I. M., Landt, O., and van Dijk, A. A. (2009). Improved strategies for sequence-independent amplification and sequencing of viral double-stranded RNA genomes. *Journal of General Virology* 90, 1423–1432. doi: 10.1099/VIR.0.009381-0/CITE/REFWORKS.

Prasad, B. V. V., Wang, G. J., Clerx, J. P. M., and Chiu, W. (1988). Three-dimensional structure of rotavirus. *J Mol Biol* 199, 269–275. doi: 10.1016/0022-2836(88)90313-0.

Prasad, B. v, Rothnagel, R., Zeng, C. Q.-Y., Jakana, J., Lawton, J. A., Chiu, W., et al. (1996). Visualization of ordered genomic RNA and localization of transcriptional complexes in rotavirus. *Nature* 382, 471–3. doi: 10.1038/382471a0.

Rainsford, E. W., and McCrae, M. A. (2007). Characterization of the NSP6 protein product of rotavirus gene 11. *Virus Res* 130, 193–201. doi: 10.1016/J.VIRUSRES.2007.06.011.

Ramani, S., Hu, L., Venkataram Prasad, B. V., and Estes, M. K. (2016). Diversity in Rotavirus–Host Glycan Interactions: A “Sweet” Spectrum. *Cell Mol Gastroenterol Hepatol* 2, 263–273. doi: 10.1016/j.jcmgh.2016.03.002.

Ramig, R. F. (2004). Pathogenesis of intestinal and systemic rotavirus infection. *J Virol* 78, 10213–10220. doi: 10.1128/JVI.78.19.10213-10220.2004.

Reed, L. J., and Muench, H. (1938). A simple method of estimating fifty per cent endpoints. *THE AMERICAN JOURNAL OF HYGIENE VOL.* 27, 493–497.

Ricciotti, E., and FitzGerald, G. A. (2011). Prostaglandins and Inflammation. *Arterioscler Thromb Vasc Biol* 31, 986–1000. doi: 10.1161/ATVBAHA.110.207449.

Robb, C. T., Goepp, M., Rossi, A. G., and Yao, C. (2020). Non-steroidal anti-inflammatory drugs, prostaglandins, and COVID-19. *Br J Pharmacol* 177, 4899–4920. doi: 10.1111/BPH.15206.

Rodríguez-Lagunas, M. J., Martín-Venegas, R., Moreno, J. J., and Ferrer, R. (2010). PGE 2 promotes Ca 2+ -mediated epithelial barrier disruption through EP 1 and EP 4 receptors in Caco-2 cell monolayers. *American Journal of Physiology-Cell Physiology* 299, C324–C334. doi: 10.1152/ajpcell.00397.2009.

Rossen, J. W. A., Bouma, J., Raatgeep, R. H. C., Büller, H. A., and Einerhand, A. W. C. (2004). Inhibition of cyclooxygenase activity reduces rotavirus infection at a postbinding step. *J Virol* 78, 9721–9730. doi: 10.1128/JVI.78.18.9721–9730.2004.

Ruggeri, F. M., and Greenberg, H. B. (1991). Antibodies to the trypsin cleavage peptide VP8 neutralize rotavirus by inhibiting binding of virions to target cells in culture. *J Virol* 65, 2211–9.

Sander, W. J. (2019). Investigation into the effect of fatty acids on the yield and replication of rotavirus in cell culture. MSc Dissertation, University of the Free State.

Sander, W. J., O’Neill, H. G., and Pohl, C. H. (2017). Prostaglandin E_2 as a modulator of viral infections. *Front Physiol* 8, 89. doi: 10.3389/fphys.2017.00089.

Schneider, C. A., Rasband, W. S., and Eliceiri, K. W. (2012). NIH Image to ImageJ: 25 years of image analysis. *Nat Methods* 9, 671–675. doi: 10.1038/nmeth.2089.

Schönthal, A. H. (2007). Direct non-cyclooxygenase-2 targets of celecoxib and their potential relevance for cancer therapy. *Br J Cancer* 97, 1465–1468. doi: 10.1038/sj.bjc.6604049.

Sen, A., Sen, N., and Mackow, E. R. (2007). The Formation of Viroplasm-Like Structures by the Rotavirus NSP5 Protein Is Calcium Regulated and Directed by a C-Terminal Helical Domain. *J Virol* 81, 11758–11767. doi: 10.1128/JVI.01124-07.

Settembre, E. C., Chen, J. Z., Dormitzer, P. R., Grigorieff, N., and Harrison, S. C. (2011). Atomic model of an infectious rotavirus particle. *EMBO J* 30, 408–416. doi: 10.1038/emboj.2010.322.

Shaw, A. L., Rothnagel, R., Chen, D., Ramig, R. F., Chiu, W., and Prasad, B. V (1993). Three-dimensional visualization of the rotavirus hemagglutinin structure. *Cell* 74, 693–701.

Silvestri, L. S., Alejandra Tortorici, M., Vasquez-Del Carpio, R., and Patton, J. T. (2005). Rotavirus Glycoprotein NSP4 Is a Modulator of Viral Transcription in the Infected Cell. *J Virol* 79, 15165–15174. doi: 10.1128/JVI.79.24.15165-15174.2005.

Silvestri, L. S., Taraporewala, Z. F., and Patton, J. T. (2004). Rotavirus Replication: Plus-Sense Templates for Double-Stranded RNA Synthesis Are Made in Viroplasms. *J Virol* 78, 7763–7774. doi: 10.1128/JVI.78.14.7763.

Smith, C. J., Zhang, Y., Koboldt, C. M., Muhammad, J., Zweifel, B. S., Shaffer, A., et al. (1998). Pharmacological analysis of cyclooxygenase-1 in inflammation. *Proc Natl Acad Sci U S A* 95, 13313–13318. doi: 10.1073/pnas.95.22.13313.

Smith, R. E., Kister, S. E., and Carozzi, N. B. (1989). Cloning and expression of the major inner capsid protein of SA-11 simian rotavirus in Escherichia coli. *Gene* 79, 239–248. doi: 10.1016/0378-1119(89)90206-0.

Soliman, M., Seo, J.-Y., Kim, D.-S., Kim, J.-Y., Park, J.-G., Alfajaro, M. M., et al. (2018). Activation of PI3K, Akt, and ERK during early rotavirus infection leads to V-ATPase-dependent endosomal acidification required for uncoating. *PLoS Pathog* 14, e1006820. doi: 10.1371/journal.ppat.1006820.

Steer, S. A., and Corbett, J. A. (2003). The Role and Regulation of COX-2 during Viral Infection. *Viral Immunol* 16, 447–460. doi: 10.1089/088282403771926283.

Strydom, A., João, E. D., Motanyane, L., Nyaga, M. M., Christiaan Potgieter, A., Cuamba, A., et al. (2019). Whole genome analyses of DS-1-like Rotavirus A strains detected in children with acute diarrhoea in southern Mozambique suggest several reassortment events. *Infection, Genetics and Evolution* 69, 68–75. doi: 10.1016/J.MEEGID.2019.01.011.

Suárez, Y. G., Martínez, J. L., Hernández, D. T., Hernández, H. O., Pérez-Delgado, A., Méndez, M., et al. (2019). Nanoscale organization of rotavirus replication machineries. *Elife* 8. doi: 10.7554/ELIFE.42906.

Superti, F., Marziano, M. L., Donelli, G., Marchetti, M., and Seganti, L. (1995). Enhancement of rotavirus infectivity by saturated fatty acids. *Comp Immunol Microbiol Infect Dis* 18, 129–135. doi: 10.1016/0147-9571(95)98854-B.

Svensson, L., Desselberger, U., Estes, M. K., and Greenberg, H. B. (2016). *Viral Gastroenteritis*. Elsevier doi: 10.1016/C2014-0-03000-6.

Tafazoli, F., Zeng, C. Q., Estes, M. K., Magnusson, K.-E., and Svensson, L. (2001). NSP4 Enterotoxin of Rotavirus Induces Paracellular Leakage in Polarized Epithelial Cells. *J Virol* 75, 1540. doi: 10.1128/JVI.75.3.1540-1546.2001.

Tanaka, T., Morishige, J. I., Takimoto, T., Takai, Y., and Satouchi, K. (2001). Metabolic characterization of sciadonic acid (5c,11c,14c-eicosatrienoic acid) as an effective substitute for arachidonate of phosphatidylinositol. *Eur J Biochem* 268, 4928–4939. doi: 10.1046/j.0014-2956.2001.02423.x.

Taraporewala, Z., Chen, D., and Patton, J. T. (1999). Multimers formed by the rotavirus nonstructural protein NSP2 bind to RNA and have nucleoside triphosphatase activity. *J Virol* 73, 9934–43. Available at: http://www.ncbi.nlm.nih.gov/pubmed/10559306 [Accessed October 24, 2018].

Taraporewala, Z. F., and Patton, J. T. (2001). Identification and Characterization of the Helix-Destabilizing Activity of Rotavirus Nonstructural Protein NSP2. *J Virol* 75, 4519–4527. doi: 10.1128/JVI.75.10.4519-4527.2001.

Taraporewala, Z. F., Schuck, P., Ramig, R. F., Silvestri, L., and Patton, J. T. (2002). Analysis of a Temperature-Sensitive Mutant Rotavirus Indicates that NSP2 Octamers Are the Functional Form of the Protein. *J Virol* 76, 7082–7093. doi: 10.1128/JVI.76.14.7082–7093.2002.

Taylor, J. A., O'Brien, J. A., and Yeager, M. (1996). The cytoplasmic tail of NSP4, the endoplasmic reticulum-localized non-structural glycoprotein of rotavirus, contains distinct virus binding and coiled coil domains. *EMBO J* 15, 4469. doi: 10.1002/j.1460-2075.1996.tb00824.x.

Tian, P., Hu, Y., Schilling, W. P., Lindsay, D. A., Eiden, J., and Estes, M. K. (1994). The nonstructural glycoprotein of rotavirus affects intracellular calcium levels. *J Virol* 68, 251–7.

Tithof, P. K., Roberts, M. P., Guan, W., Elgayyar, M., and Godkin, J. D. (2007). Distinct phospholipase A2 enzymes regulate prostaglandin E2 and F2alpha production by bovine endometrial epithelial cells. doi: 10.1186/1477-7827-5-16.

Tompkins, C. V., Sonksen, P. H., and Jones, R. H. (1975). Structural modifications to the insulin molecule and their effects on glucose metabolism. *Journal of Endocrinology* 65, 1485–1497. doi: 10.1093/emboj/20.7.1485.

Torres-Flores, J. M., Silva-Ayala, D., Espinoza, M. A., López, S., and Arias, C. F. (2014). The tight junction protein JAM-A functions as coreceptor for rotavirus entry into MA104 cells. doi: 10.1016/j.virol.2014.11.016.

Trask, S. D., and Dormitzer, P. R. (2006). Assembly of highly infectious rotavirus particles recoated with recombinant outer capsid proteins. *J Virol* 80, 11293–11304. doi: 10.1128/JVI.01346-06.

Troeger, C., Khalil, I. A., Rao, P. C., Cao, S., Blacker, B. F., Ahmed, T., et al. (2018). Rotavirus vaccination and the global burden of rotavirus diarrhea among children younger than 5 years. *JAMA Pediatr* 98121, 1–8. doi: 10.1001/jamapediatrics.2018.1960.

Uddin, M. J., Rao, P. N. P., and Knaus, E. E. (2003). Design and synthesis of novel celecoxib analogues as selective cyclooxygenase-2 (COX-2) inhibitors: Replacement of the sulfonamide pharmacophore by a sulfonylazide bioisostere. *Bioorg Med Chem* 11, 5273–5280. doi: 10.1016/j.bmc.2003.07.005.

van der Schyff, S. S. (2021). An investigation into the molecular basis of the reassortment of rotavirus VP7, encoded by genome segment 9. MSc Dissertation, University of the Free State.

Vascotto, F., Campagna, M., Visintin, M., Cattaneo, A., and Burrone, O. R. (2004). Effects of intrabodies specific for rotavirus NSP5 during the virus replicative cycle. *J Gen Virol* 85, 3285–3290. doi: 10.1099/VIR.0.80075-0.

Velasquez, D. E., Parashar, U., and Jiang, B. (2018). Decreased performance of live attenuated, oral rotavirus vaccines in low-income settings: causes and contributing factors. *Expert Rev Vaccines* 17, 145. doi: 10.1080/14760584.2018.1418665.

Vende, P., Piron, M., Castagné, N., and Poncet, D. (2000). Efficient translation of rotavirus mRNA requires simultaneous interaction of NSP3 with the eukaryotic translation initiation factor eIF4G and the mRNA 3’ end. *J Virol* 74, 7064–71.

Venkataram Prasad, B., Shanker, S., Hu, L., Choi, J.-M., Crawford, S. E., Ramani, S., et al. (2014). Structural basis of glycan interaction in gastroenteric viral pathogens. *Curr Opin Virol* 7, 119–127. doi: 10.1016/j.coviro.2014.05.008.

Walther, T. C., Chung, J., and Farese, R. V. (2017). Lipid Droplet Biogenesis. *Annu Rev Cell Dev Biol* 33, 491–510. doi: 10.1146/annurev-cellbio-100616-060608.

Ward, K. E., Ropa, J. P., Adu-Gyamfi, E., and Stahelin, R. v. (2012). C2 domain membrane penetration by group IVA cytosolic phospholipase A2 induces membrane curvature changes. *J Lipid Res* 53, 2656–2666. doi: 10.1194/jlr.M030718.

Yamashiro, Y., Shimizu, T., Oguchi, T., and Sato, M. (1989). Prostaglandins in the plasma and stool of children with rotavirus gastroenteritis. *J Pediatr Gastroenterol Nutr* 9, 322–327.

Yang, K., Wang, S., Chang, K. O., Lu, S., Saif, L. J., Greenberg, H. B., et al. (2001). Immune responses and protection obtained with rotavirus VP6 DNA vaccines given by intramuscular injection. *Vaccine* 19, 3285–91.

Zádori, Z., Szelei, J., Lacoste, M.-C., Li, Y., Gariépy, S., Raymond, P., et al. (2001). A Viral Phospholipase A2 Is Required for Parvovirus Infectivity. *Dev Cell* 1, 291–302. doi: 10.1016/S1534-5807(01)00031-4.

Zarate, S., Espinosa, R., Romero, P., Mendez, E., Arias, C. F., and Lopez, S. (2000). The VP5 Domain of VP4 Can Mediate Attachment of Rotaviruses to Cells. *J Virol* 74, 593–599. doi: 10.1128/JVI.74.2.593-599.2000.

Zeng, C. Q., Wentz, M. J., Cohen, J., Estes, M. K., and Ramig, R. F. (1996). Characterization and replicase activity of double-layered and single-layered rotavirus-like particles expressed from baculovirus recombinants. *J Virol* 70, 2736–42.

Zeng, C. Q.-Y., Labbé, M., Cohen, J., Prasad, B. V. V., Chen, D., Ramig, R. F., et al. (1994). Characterization of Rotavirus VP2 Particles. *Virology* 201, 55–65. doi: 10.1006/viro.1994.1265.

Zijlstra, R. T., McCracken, B. A., Odle, J., Donovan, S. M., Gelberg, H. B., Petschow, B. W., et al. (1999). Malnutrition modifies pig small intestinal inflammatory responses to rotavirus. *J Nutr* 129, 838–843.

Appendix A

UNIVERSITY OF THE FREE STATE
UNIVERSITEIT VAN DIE VRYSTAAT
YUNIVESITHI YA FREISTATA

UFS·UV
RESEARCH DEVELOPMENT
NAVORSINGSONTWIKKELING

Environment & Biosafety Research Ethics Committee

29-Nov-2022

Dear Mr Willem Sander

Project Title: **Investigating the role and mechanism of the inflammatory eicosanoid,PGE2, during rotavirus infection**

Department: **Microbiology and Biochemistry Department (Bloemfontein Campus)**

APPLICATION APPROVED

This letter confirms that this research proposal was given ethical clearance by the Environment & Biosafety Research Ethics Committee of the University of the Free State.

Your ethical clearance number, to be used in all correspondence is: **UFS-ESD2019/0170**

Please note the following:

1. **This ethical clearance is granted for data collection for this project for the duration of 03 Year/s from the issuance of this letter.**
2. **If the duration of the data colection indicated above is less than one year, your ethics clearance will be valid for 12 months from the issuance of this letter. Please submit a Continuation Report to the Ethics Committee if your data collection takes longer than a year, or longer than the alloted time indicated above if it is longer than one year .**
3. **Please note that the maximum amount of time that ethical clearance will be granted is 5 years, and that a Continuation Report must be submitted for any projects where data is collected for longer.**
4. **If any changes are made during the research process (including a change in investigators), please inform the Ethics Committee by submitting an Amendment.**
5. **When the research is concluded, please submit a Final Report to the Ethics Committee.**

Thank you for your application and we wish you well in all of your research endeavours.

Yours Sincerely

Appendix B

Major parts of Chapter 2 have been published in:

Sander WJ, Kemp G, Hugo A, Pohl CH and O'Neill HG (2022) Rotavirus-Mediated Prostaglandin E_2 Production in MA104 Cells Promotes Virus Attachment and Internalisation, Resulting in an Increased Viral Load. Frontiers in Physiology, 13:805565. doi: 10.3389/fphys.2022.805565

- For the purpose of the thesis, the introduction of Chapter 2 was slightly modified and the data describing lipid analysis was excluded.
- A section in the conclusion of the published paper has now also been included in Chapter 5.

Author contributions:

WJ Sander, CH Pohl, HG O'Neill – conceptualisation of study

WJ Sander – performed most of experimental work and data analysis and interpretation of data (G. Kemp assisted with LC-MS/MS analysis; A. Hugo assisted with lipid analysis – not included in PhD thesis)

WJ Sander – wrote original draft

All authors reviewed and edited submitted version.

Appendix C

Table 2. 1. Effects of host cell treatment with GLA (50 µM) or compounds Indomethacin (25 µM), celecoxib (5uM), SC-560 (2.5 uM), CAY10502 (25 nM) and PGE_2 (0.1 µM) on RV infectivity and RV RNA production.

	Infectivity		Viral RNA	
Compound	Fold Change	*P*	Fold Change	*P*
GLA	0.90 increase	0.018	0.92 increase	0.012
Indomethacin	1.31 decrease	0.005	1.22 decrease	0.005
Celecoxib	0.95 decrease	0.006	1.01 decrease	0.005
SC-560	0.95 decrease	0.002	0.92 decrease	0.006
CAY10502	1.13 decrease	0.003	1.09 decrease	0.008
Indomethacin+ PGE_2	0.83 decrease	0.17	0.88 decrease	0.44
CAY10502+ PGE_2	0.99 decrease	0.49	1 decrease	0.44

Table 2. 2 Effects of host cell treatment with GLA (50 µM) or compounds Indomethacin (25 µM), CAY10502 (25 nM) and PGE_2 (0.1 µM) on RV attachment and relative internalisation.

	Attachment		Relative internalisation	
Compound	Fold Change	*P*	Fold Change	*P*
GLA	0.94 increase	0.008	1.00 increase	0.0.46
Indomethacin	1.18 decrease	0.008	1.43 decrease	<0.001
Indomethacin+GLA	0.90 decrease	0.26	0.81 decrease	0.002
I Indomethacin+ PGE_2	0.94 decrease	0.017	0.85 decrease	0.20
CAY10502	1.20 decrease	0.003	1.55 decrease	<0.001
CAY10502+GLA	0.89 decrease	0.20	0.73 decrease	0.022
CAY10502+ PGE_2	0.94 decrease	0.22	0.87 decrease	0.22

Table 3. 6 Effects of alanine and proline mutations in the C-terminal tail region of NSP5 on RV infectivity and RV RNA production.

	Viral Yield				**Viral RNA**			
Compound	**2 hours post infection**		**6 hours post infection**		**2 hours post infection**		**6 hours post infection**	
	Fold Change	*P*	Fold Change	*P*	Fold Change	*P*	Fold Change	*P*
rSA11_aNSP5	0.99 decrease	0.39	1.27 decrease	0.005	1.02 decrease	0.31	1.51 decrease	0.015
rSA11_pNSP5	1.01 decrease	0.49	1.69 decrease	0.005	1.00 decrease	0.19	1.34 decrease	0.015

Table 4. 3. Effects of BAPTA treatment and mutations in the viroporin of NSP4 on RV infectivity and RV RNA production.

	Viral Yield				Viral RNA			
Compound	**2 hours post infection**		**6 hours post infection**		**2 hours post infection**		**6 hours post infection**	
	Fold Change	*P*	Fold Change	*P*	Fold Change	*P*	Fold Change	*P*
rSA11+BAPTA	2.0 decrease	0.005	2.29 decrease	0.005	1.81 decrease	0.012	1.46 decrease	0.015
rSA11_rNSP5	1.10 decrease	0.004	1.19 decrease	0.005	1.21 decrease	0.011	1.05 decrease	0.015

Appendix D

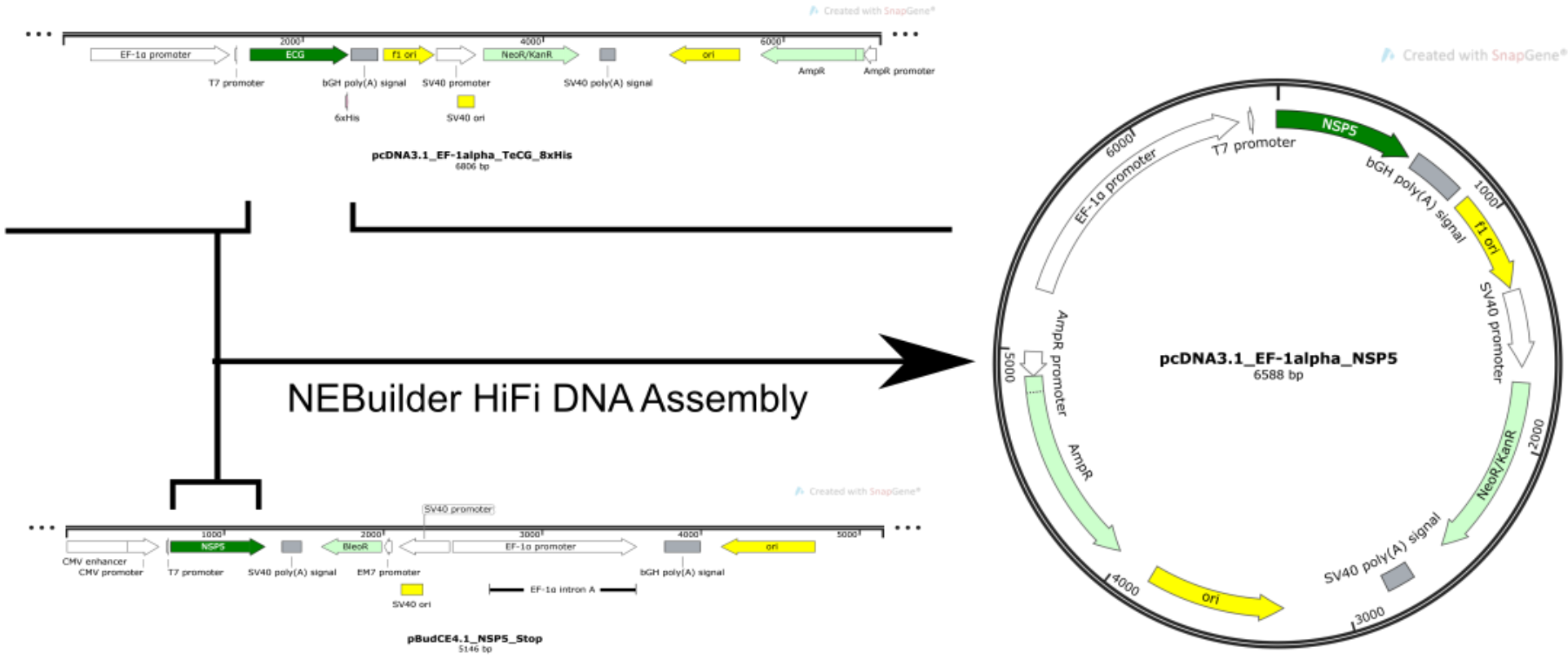

Figure 3. 13 *In silico* representation of the construction of pcDNA.3.1_EF-1alpha-NSP5 plasmid. NSP5 is amplified from pBudCE4.1 vector with overhangs that is complementary to the **of** pcDNA.3.1_EF-1alpha_ECG construct. The pcDNA3.1-NSP5 backbone is amplified using primers that produce overhangs that is complementary to NSP5.

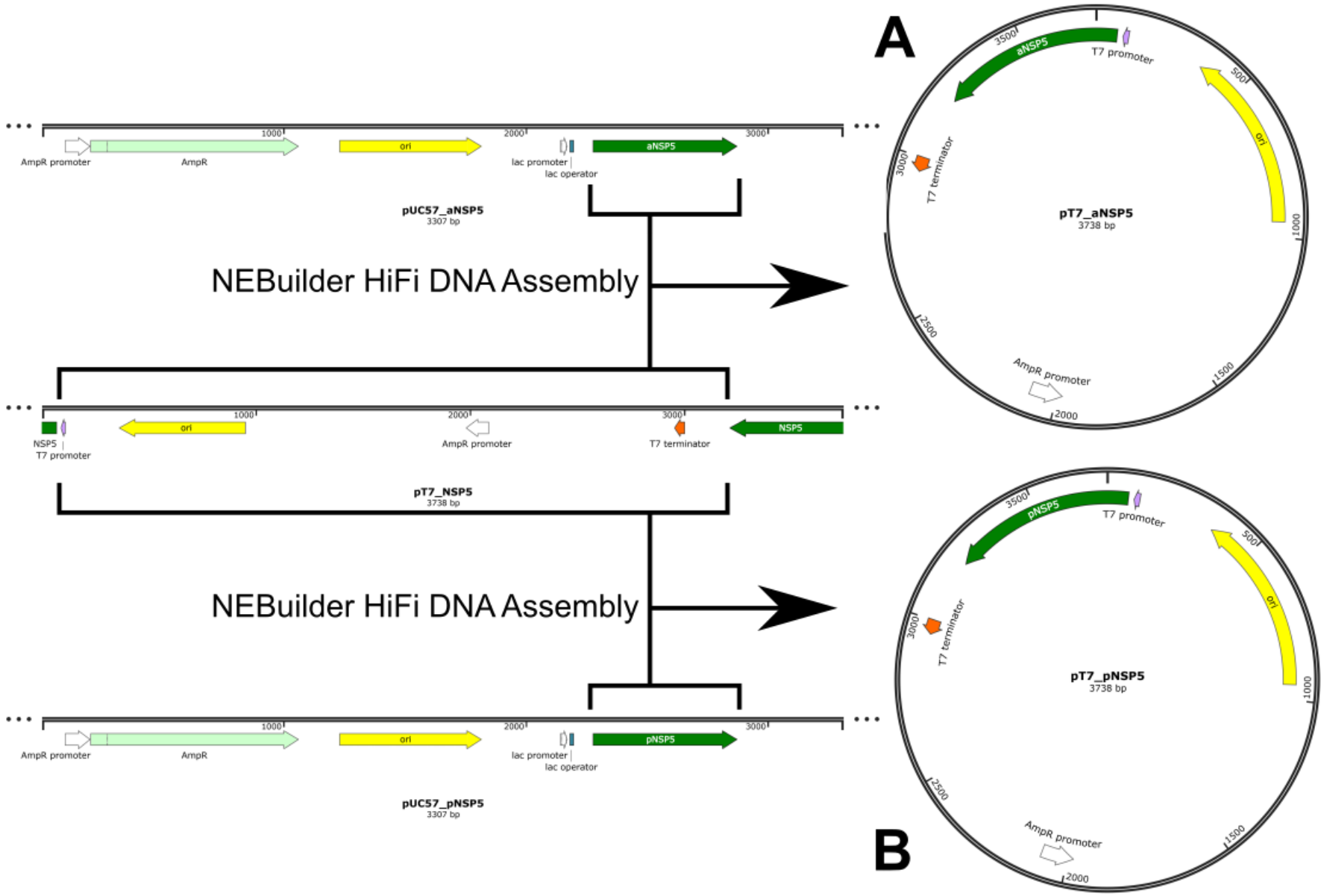

Figure 3. 14. *In silico* representation of the construction of pT7-NSP5 mutant plasmids. (A) aNSP5 and (B) pNSP5 is amplified from pUC57 vectors with overhangs that is complementary to the pT7-NSP5 construct. The pT7-NSP5 backbone is amplified using primers that produce overhangs that is complementary to the either aNSP5 or pNSP5.

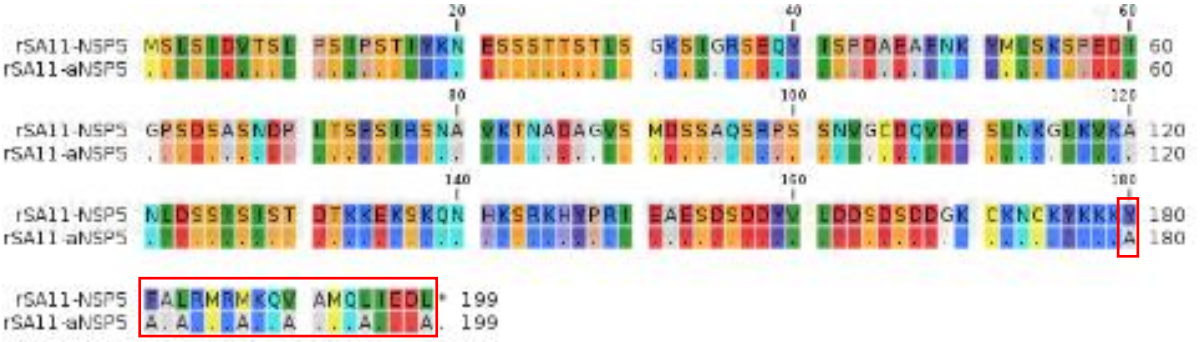

Figure 3. 15. Protein alignment of rSA11 with rSA11_aNSP5. Similar nucleic acids are indicated by dots. Change in the C-terminal of rSA11_aNSP5 can be seen from amino acid 179 to 199 (underlined), which encodes for the α-helix.

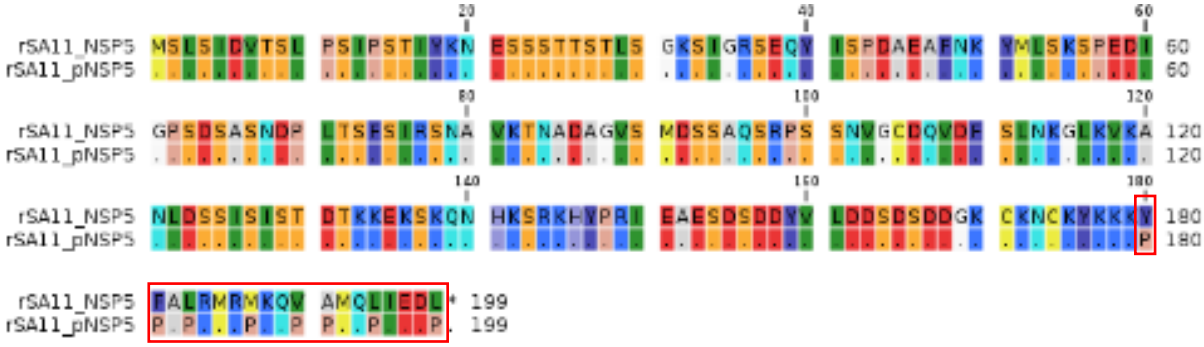

Figure 3. 16. Protein alignment of rSA11 with rSA11_pNSP5. Similar nucleic acids are indicated by dots. Change in the C-terminal of rSA11_pNSP5 can be seen from amino acid 179 to 199 (underlined), which encodes for the α-helix.

Appendix E

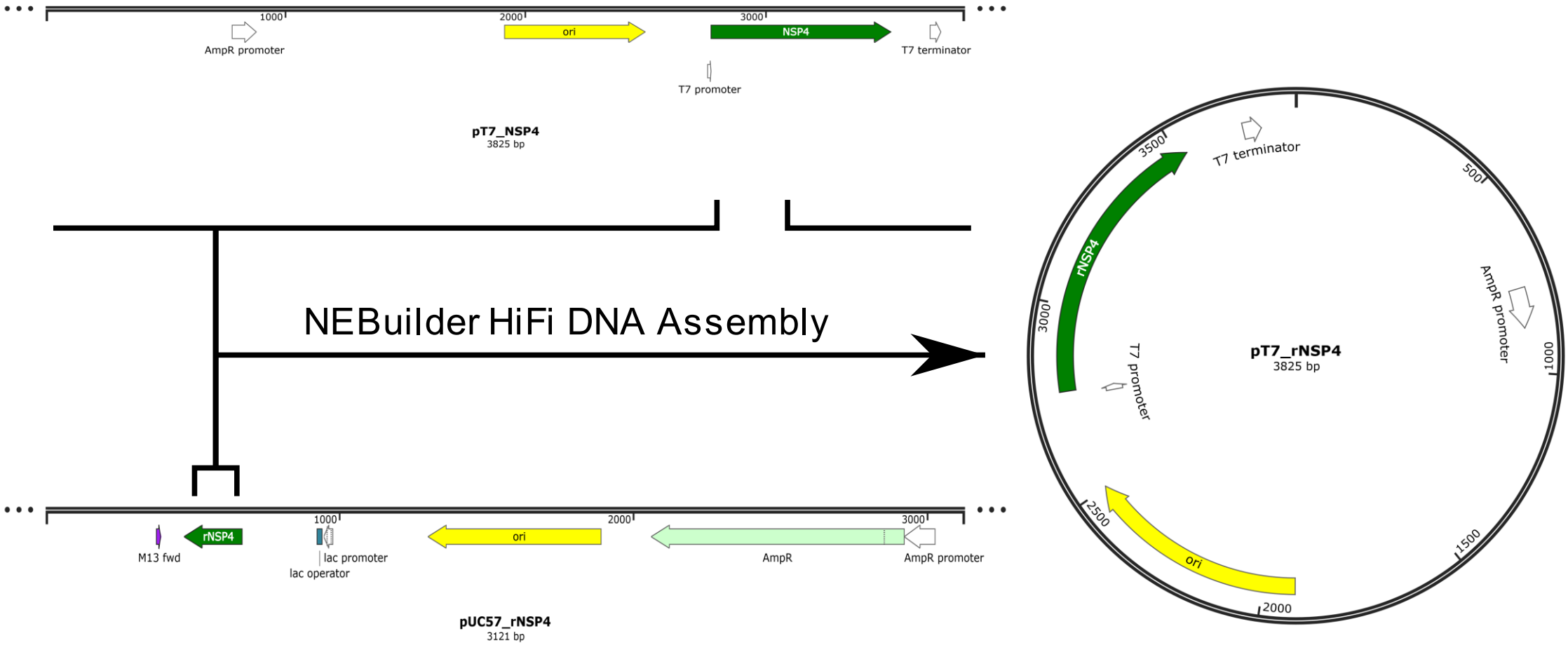

Figure 4. 10. ***In silico*** **representation of the construction of pT7-NSP4 mutant plasmid.** rNSP4 amplified from pUC57 vectors with overhangs that is complementary to the pT7_rNSP4 construct. The pT7- NSP4backbone is amplified using primers that produce overhangs that is complementary to the rNSP4.

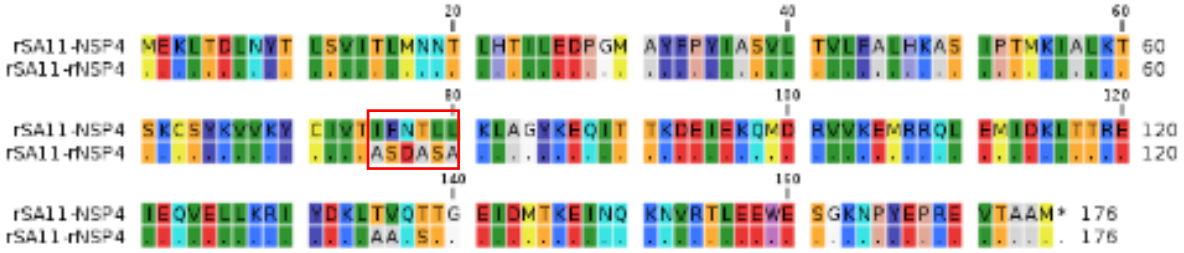

Figure 4. 11. Protein alignment of rSA11 with rSA11_rNSP4. Similar nucleic acids are indicated by dots. Change in the C-terminal of rSA11_rNSP4 can be seen from amino acid 75 to 80 (boxed), which encodes for the α-helix.

Appendix F

SPRINGER NATURE LICENSE TERMS AND CONDITIONS

Nov 30, 2022

This Agreement between WJ Sander ("You") and Springer Nature ("Springer Nature") consists of your license details and the terms and conditions provided by Springer Nature and Copyright Clearance Center.

License Number	5430090188258
License date	Nov 15, 2022
Licensed Content Publisher	Springer Nature
Licensed Content Publication	Springer eBook
Licensed Content Title	ElcosaCell – An Immunofluorescent-Based Assay to Localize Newly Synthesized Eicosanoid Lipid Mediators at Intracellular Sites
Licensed Content Author	Christianne Bandeira-Melo, Peter F. Weller, Patricia T. Bozza
Licensed Content Date	Jan 1, 2011
Type of Use	Thesis/Dissertation
Requestor type	academic/university or research institute
Format	electronic
Portion	figures/tables/illustrations
Number of figures/tables/illustrations	1
Will you be translating?	no
Circulation/distribution	1 - 29
Author of this Springer Nature content	no
Title	Prostaglandin E2 and the rotavirus conundrum
Institution name	University of the Free State
Expected presentation date	Nov 2022
Portions	Figure 10.2
Requestor Location	WJ Sander 205 Nelson Mandela Drive Parkwest Bloemfontein, Free State 9301 South Africa Attn: WJ Sander
Total	**0.00 USD**

ELSEVIER LICENSE TERMS AND CONDITIONS

Nov 30, 2022

This Agreement between WJ Sander ("You") and Elsevier ("Elsevier") consists of your license details and the terms and conditions provided by Elsevier and Copyright Clearance Center.

License Number	5430081013387
License date	Nov 15, 2022
Licensed Content Publisher	Elsevier
Licensed Content Publication	Biochimie
Licensed Content Title	A twist of FATe: Lipid droplets and inflammatory lipid mediators
Licensed Content Author	Eva Jarc,Toni Petan
Licensed Content Date	Feb 1, 2020
Licensed Content Volume	169
Licensed Content Issue	n/a
Licensed Content Pages	19
Start Page	69
End Page	87
Type of Use	reuse in a thesis/dissertation
Portion	figures/tables/illustrations
Number of figures/tables/illustrations	1
Format	electronic
Are you the author of this Elsevier article?	No
Title	Prostaglandin E2 and the rotavirus conundrum
Institution name	University of the Free State
Expected presentation date	Nov 2022
Portions	Figure 3
Requestor Location	WJ Sander 205 Nelson Mandela Drive Parkwest Bloemfontein, Free State 9301 South Africa Attn: WJ Sander
Publisher Tax ID	ZA 4110266048
Total	**0.00 USD**

ELSEVIER LICENSE TERMS AND CONDITIONS

Nov 30, 2022

This Agreement between WJ Sander ("You") and Elsevier ("Elsevier") consists of your license details and the terms and conditions provided by Elsevier and Copyright Clearance Center.

License Number	5430070778947
License date	Nov 15, 2022
Licensed Content Publisher	Elsevier
Licensed Content Publication	Current Opinion in Virology
Licensed Content Title	Rotavirus cell entry: not so simple after all
Licensed Content Author	Carlos F Arias,Susana López
Licensed Content Date	Jun 1, 2021
Licensed Content Volume	48
Licensed Content Issue	n/a
Licensed Content Pages	7
Start Page	42
End Page	48
Type of Use	reuse in a thesis/dissertation
Portion	figures/tables/illustrations
Number of figures/tables/illustrations	1
Format	electronic
Are you the author of this Elsevier article?	No
Will you be translating?	No
Title	Prostaglandin E2 and the rotavirus conundrum
Institution name	University of the Free State
Expected presentation date	Nov 2022
Portions	Figure 2. Models for RV cell entry.
Requestor Location	WJ Sander 205 Nelson Mandela Drive Parkwest Bloemfontein, Free State 9301 South Africa Attn: WJ Sander
Publisher Tax ID	ZA 4110256048
Total	**0.00 USD**

ELSEVIER LICENSE TERMS AND CONDITIONS

Nov 30, 2022

This Agreement between WJ Sander ("You") and Elsevier ("Elsevier") consists of your license details and the terms and conditions provided by Elsevier and Copyright Clearance Center.

License Number	5430090624229
License date	Nov 15, 2022
Licensed Content Publisher	Elsevier
Licensed Content Publication	Microbes and Infection
Licensed Content Title	Pathogenesis of Rotavirus diarrhea
Licensed Content Author	Ove Lundgren,Lennart Svensson
Licensed Content Date	Nov 1, 2001
Licensed Content Volume	3
Licensed Content Issue	13
Licensed Content Pages	12
Start Page	1145
End Page	1156
Type of Use	reuse in a thesis/dissertation
Portion	figures/tables/illustrations
Number of figures/tables/illustrations	1
Format	electronic
Are you the author of this Elsevier article?	No
Will you be translating?	No
Title	Prostaglandin E2 and the rotavirus conundrum
Institution name	University of the Free State
Expected presentation date	Nov 2022
Portions	Figure 1
Requestor Location	WJ Sander 205 Nelson Mandela Drive Parkwest Bloemfontein, Free State 9301 South Africa Attn: WJ Sander
Publisher Tax ID	ZA 4110256048
Total	**0.00 USD**